(1)

EFFECT OF SURFACE SHIP INTERNAL FLUID CONTAINERS ON EXTERNAL ACOUSTIC INTENSITY MEASUREMENTS

by

AMY RUTH SMITH

B.A. Chemistry
St Olaf College (1980)

M.S. Systems Management
University of Southern California (1986)

Submitted to the Departments of
Ocean Engineering and Mechanical Engineering
In Partial Fulfillment of the Requirements
For the Degrees of
NAVAL ENGINEER
and
MASTER OF SCIENCE IN MECHANICAL ENGINEERING
at the
MASSACHUSETTS INSTITUTE OF TECHNOLOGY
May 1990

NPS

N00123-89-G-0580

Signature of Author: Amy Ruth Smith
Department of Ocean Engineering, May 1990

Certified by: Richard H Lyon
Richard H. Lyon, Thesis Supervisor
Professor of Mechanical Engineering

Certified by: Ira Dyer
Ira Dyer, Thesis Reader
Professor of Ocean Engineering

Accepted by: A Douglas Carmichael
A. Douglas Carmichael, Chairman
Department of Ocean Engineering Graduate Committee

Accepted by:
Ain A. Sonin, Chairman
Department of Mechanical Engineering Graduate Committee

EFFECT OF SURFACE SHIP INTERNAL FLUID CONTAINERS ON EXTERNAL ACOUSTIC INTENSITY MEASUREMENTS

by

Amy Smith

Submitted to the Departments of
Ocean Engineering and Mechanical Engineering
on May 1990, in partial fulfillment of the requirements
For the Degrees of Naval Engineer and Masters of Science

ABSTRACT

The nearfield acoustic intensity resulting from vibration transmitted from a main machinery foundation through supporting structure and fluid containing tanks into the hull structure, and then into the surrounding fluid has been studied for a scale model of a frigate ship. The scale model is 1:10 and the scaled frequency range is 640 Hz to 15 kHz. Acoustic pressure is measured on adjacent cylindrical contours close to the surface of the underwater vibrating surface with the fluid-containing tank first empty and then full. The time-averaged acoustic intensity is then calculated from the pressure cross-spectrum. The resulting sound intensity patterns over the surface of the vibrating structure are studied to obtain an insight as to which parts of the structure are primarily responsible for the radiated noise. The spatial characteristics of the acoustic intensity patterns are indicators of the energy exchange between the structure and the acoustic medium. Additionally, the total radiated power has been calculated from the local acoustic intensity measurements and these experimental results have been compared with sound radiation measurements from a comparable model of scale 1:6.25.

Thesis Supervisor: Professor Richard H. Lyon
Professor of Mechanical Engineering

ACKNOWLEDGEMENTS

I want to express my sincere appreciation to the many individuals and organizations who have provided me assistance, guidance and cooperation with this educational project.

Foremost, I want to say thank you to the United States Navy for granting me the opportunity and financial support to study here at MIT.

I would especially like to express my thanks to my advisor Professor Lyon. He provided much-needed guidance and support from the inception of this research project through to its completion.

I am also grateful to the many members of the Physical Acoustics Branch at the Naval Research Laboratory (NRL) and associated contractors from Sachs Freeman Associates, Inc (SFA) in Washington D.C. Without their efforts, facilities, and advice, the experimental portion of this work would not have been possible. Specifically, the following individuals deserve special mention:

Dr. Earl Williams, Acoustics Interactions Section Head, NRL - for his advice on theoretical portions of this work and experimental setup.

Dr. Brian Houston, Target Facility Section Head, NRL - for his overall coordination of tank measurements and data tape preparation.

Mr. Roger Volk, Senior Acoustic Technician and Acoustic Pool Facility Manager (SFA) and Mr. Norman Dale, Electronics Engineer (SFA) - for their many hours of work in model alignment, measurement equipment setup, drive signal preparation, and model scans.

Mr. Philip Frank, Electrical Engineer; Mr. Tim Christian, Hardware/ Software Designer; and Ms. Kelly Gygax, Systems Manager (all SFA) - for their work in providing computer programming and support for the acoustic scans, and advice for data processing.

I wish to acknowledge the contributions of Mr. Bob Brackett with his efforts in building the model used in this research and the assistance of the VAX Computer Staff at the Whitaker College of Health Sciences and Technology in data post-processing.

Last, but far from least, I am deeply indebted to my family for their support throughout all the frustations that go hand in hand with any research project. To my husband Patrick for his love, understanding, patience, and willingness to undertake the "non-traditional" duties in the home which allowed me the time to complete this project. To my daughter Jessica for keeping a smile on my face. And to my unborn child for ever reminding me of the miracle of life.

TABLE OF CONTENTS

LIST OF FIGURES

LIST OF TABLES

NOMENCLATURE

English Capitals

E	Young's modulus of elasticity
$G_{12}(f)$	cross-spectral pressure density
$\vec{I}$	time averaged acoustic intensity
$I_r(f)$	radial component of acoustic intensity as function of frequency
L_F	approximation error level
L_{model}	axial length of model engineroom section
$L_{prototype}$	axial length of full scale engineroom section
$P_1(f)$, $P_2(f)$	frequency spectrum of sound pressure at measurement planes 1 and 2 respectively
T	time period

English Lower-Case Letters

c_f	sound speed in a fluid media
c_L	longitudinal wave speed
e	normalized standard error
f	frequency
f_c	critical frequency
f_r	ring frequency
h	plate thickness of model structure
j	$\sqrt{-1}$
k	wavenumber
k_B	bending wavenumber of a plate *in vacuo*
k_f	wavenumber in a fluid media

English Lower-Case Letters continued

p	sound pressure
p_1, p_2	sound pressure at measurement planes 1 and 2 respectively
p_1^*, p_2^*	complex conjugate of sound pressure at measurement planes 1 and 2 respectively
r	model radius or radial direction
Δr	separation between measurement planes for acoustic intensity calculations
t	plate thickness of model structure
$\vec{v}$	particle velocity vector
v_r	radial component of particle velocity vector
v_r^*	complex conjugate of particle velocity radial component
$< >_t$	time average

Greek Lower-Case Letters

λ	wavelength
λ_B	bending wavelength of a plate *in vacuo*
λ_f	wavelength in a fluid media
ν	Poisson's ratio
ρ	material density per unit volume
ρ_o	mean density of acoustic medium
ω	radian frequency

CHAPTER 1
INTRODUCTION

1.1 Background

Noise control on ships is a subject of increasing importance to naval architects. Three major reasons can be cited for the need to control noise on Navy ships.

(1) Farfield radiated noise must be limited in order to minimize chances of detection by passive sonar systems. Control of radiated sound is particularly important in the marine environment due to the small spatial attenuation of sound in water.

(2) Nearfield radiated noise control is important to avoid performance limitations on the ship's own sonar system.

(3) Finally, to avoid habitability problems, ship internal air-borne noise needs to be maintained within current design, occupational, and environmental standards.

There are numerous sources for ship radiated noise. Hydrodynamic sources such as flow over the hull tend to dominant at higher speeds. This flow noise can include hull or sonar dome cavitation, boundary layer turbulence, wake turbulence, and control-surface oscillating forces. Other hydrodynamic sources include propulsor cavitation and propulsor blade oscillating forces. At lower speeds, machinery sources tend to dominate. Propulsion machinery sources may include diesel engines, steam system noises, propulsion motor gears, and propulsion turbines. Auxiliary machinery sources can include diesel generators, pumps, compressors, hydraulic systems and ventilation systems. The typical frequency distribution for important sources of ship radiated noise is shown by figure 1.1.

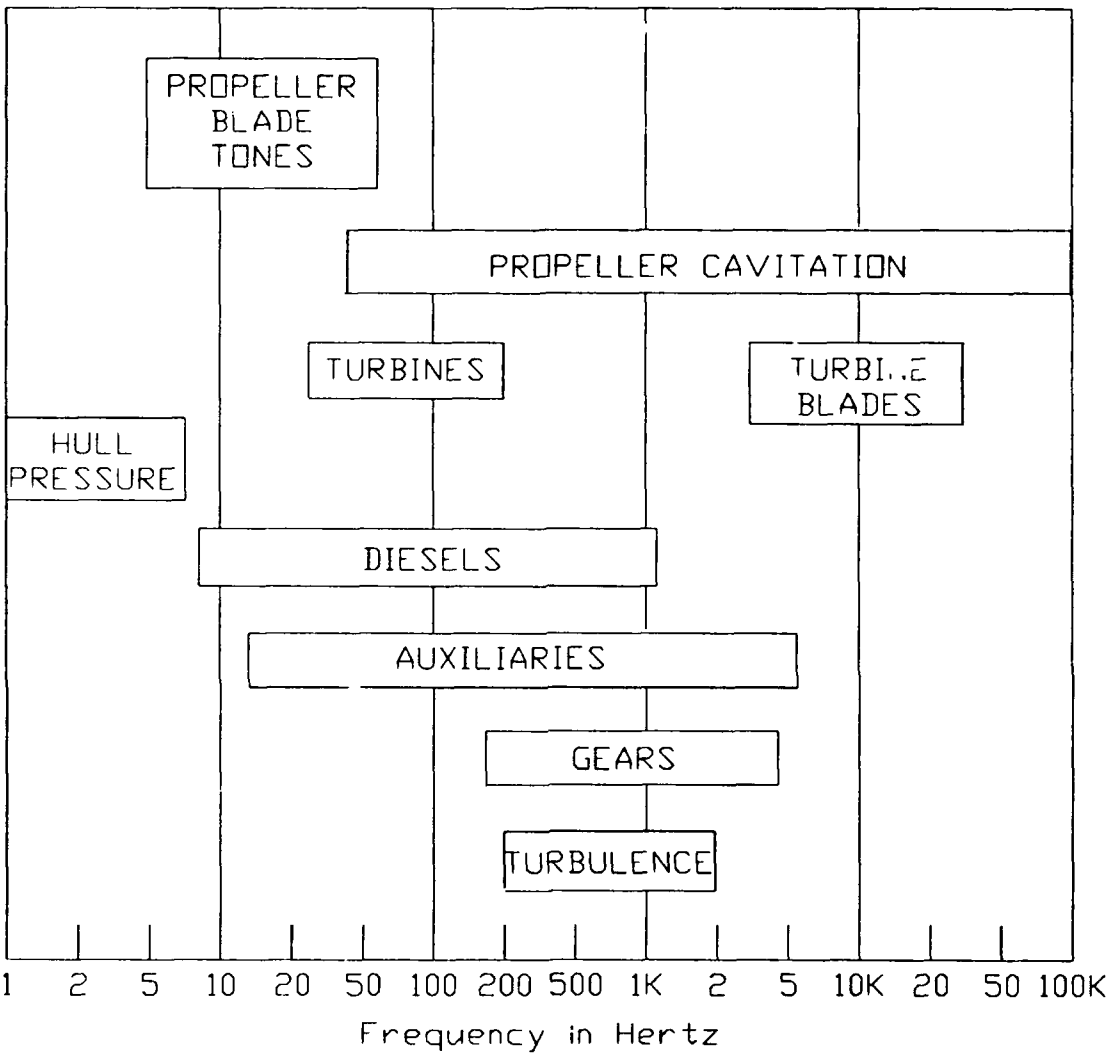

Figure 1.1 Frequency Distribution of Important Sources of Ship Radiated Noise

(from [1])

Machinery sources transmit vibration into their supporting structures as well as radiate sound into the surrounding air. The resulting structure-borne vibration, which is the primary focus of this thesis, may remain local to the vicinity of the machine, or it can be transmitted along the ship's hull and radiate as noise into the surrounding fluid. This underwater radiated noise can become significant when the vibrating surface is large or the vibrating levels are high.

There are several other factors which influence the level and location of radiated noise. Periodic rib stiffeners along the ship's hull (frames), hull inserts with thicknesses varying from the adjacent hull structure, and other structural discontinuities cause scattering of energy and thus affect vibration transmission. If the vibration transmission path includes internal fluid containers such as water, fuel, oil or ballast storage tanks, one may expect that varying tank-loading conditions will alter the transmission path and subsequent vibration levels. When all of these factors are combined, the ship designer's task of predicting and controlling underwater radiated noise from a ship structure becomes very complex.

1.2 Thesis Objective and Motivation

This thesis studies the effect of surface ship internal fluid containers, such as the water, fuel, oil, or ballast storage tanks mentioned above, on external acoustic intensity measurements resulting from machinery-generated vibration in a scaled frigate engineroom section. The purpose of this thesis is to obtain insight as to which parts of the ship structure are primarily responsible for the machinery-generated radiated sound under two different tank-loading conditions, empty and full. The spatial acoustic intensity patterns are expected to indicate the nature of the energy

exchange between the structure and the acoustic medium.

The motivation for this thesis is derived from work accomplished by Levi [2]. In his thesis, Levi studied the effects of surface ship internal fluid containers on external radiated sound power resulting from machinery vibration. Based on experimental results obtained from a 1:6.25 scale model of a frigate engineroom and from statistical energy analysis (SEA) calculations, Levi concluded that surface ship water storage tanks have the effect of increasing the sound power radiated externally in the frequency range of 63 Hz to 3.15 kHz for the prototype ship. From SEA, he showed that the dominant contributions to the total radiated power when the storage tanks are filled with water resulted from the underwater hull subsystems and the acoustical water spaces. From this, he concluded that filling the storage tanks with water added a highly conductive sound path through the hull structure.

This thesis attempts to verify Levi's conclusions by mapping the nearfield acoustic intensity (acoustic power/unit area) over the hull surface of a similar model. Due to size restrictions in the tank facility used to conduct experimental work, the scale model in this thesis is 1:10. The scaled frequency range is 640 Hz to 15 kHz. This correlates to a frequency range of 64 Hz to 1.5 kHz for full scale. Acoustic pressure is measured on adjacent cylindrical contours close to the surface of the underwater vibrating surface with the fluid-containing tank first empty and then full. The time-averaged acoustic intensity is then calculated from the pressure cross-spectrum. The resulting sound intensity patterns over the surface of the vibrating structure are indicators as to which parts of the structure are primarily responsible for the radiated noise. When the storage tank is empty, one expects that the hull structural members are primarily responsible for transmitting and radiating

the external sound power. In this case, one expects the intensity patterns to show localized "hot points" where structural members connect and apply forces to the hull. On the other hand, if the water-filled tank is indeed a transmission path for sound energy, then one expects a more uniform intensity pattern over the hull surface outboard of the tank.

1.3 Supporting Work

The effect of a water storage tank on vibration transmission through a ship structure has also been studied by Shimomura [3]. His primary concern was structure-borne noise and the effect of liquid loading on sound transmission internal to the ship structure. His goal was to assess the applicability of utilizing the liquid storage tank as an effective noise damper for sound transmission. If so, ship designers could use "strategic placement" of tanks for damping the sound transmitted from noisy spaces such as the main machinery plant into habitability spaces. His work, based on SEA and experimental results from a 1:10 scale model, concluded that at low frequencies sound radiation from the structural plates to the water spaces was negligibly small, and that the water was not important as a sound transmission path. However, as frequency increased, the water did serve as an important transmission path, dominating over transmission due to plate-coupling. At all frequencies, filling the tank with water resulted in decreasing the vibration energy level of the upper deck. This reduction was more than 8 dB at 2 kHz and gradually decreased to 1 dB as frequency increased to 20 kHz. Shimomura did not investigate energy levels external to (radiation from) the ship structure.

In addition to previous works dealing with the effects of water storage tanks on sound transmission, experimental and theoretical efforts concerned with nearfield acoustic measurements are directly applicable to this thesis. There are numerous references of interest (see references [4]-[10]), particularly the experimental results reported by Clark and Watkinson [11]. Their work is the most closely related to this thesis in that they mapped the underwater nearfield acoustic intensity for a periodically ribbed cylinder. Their intent was to show the effects of periodic ribs on sound radiation and how the sound energy radiates to the far field. In their work, ship machinery was represented by an electrodynamic shaker mounted on a rib. They measured both radial and axial components of intensity over a grid of points, and from this produced intensity vector maps and energy flux line plots.

Clark and Watkinson presented their results for the frequency range of 2 to 20 kHz. At low frequency (2 kHz), radiation from the drive point to the far field was most evident in the region closest to the drive point. Moving away from the drive point, they showed regions where the energy circulated from the fluid to the structure.

As frequency increased up to 10 kHz, their plots showed a decrease in the area of significant intensity magnitude. Above 10 kHz, their plots showed more complex interference patterns with the energy circulation directly above the drive point.

As stated previously, one of the primary concerns in Clark and Watkinson's studies was to show the effects of periodic ribs on sound radiation. The model used in this thesis work extends their work by including both periodic ribs and internal fluid storage tanks.

1.4 Thesis Outline

The thesis is organized into six chapters. Chapter 1 provides a background regarding the importance of understanding, predicting, and minimizing ship radiated noise. The motivation and objectives of the thesis are then discussed, as well as previous work accomplished by others which supports this thesis.

Chapter 2 discusses sound intensity measurements. The basic theory of sound intensity, methods of intensity measurement, and an analysis of error inherent in intensity measurements are discussed.

Chapter 3 presents the structural and acoustical modeling. Scaling parameters are summarized, and a complete description of the structural model and its structural wave characteristics are provided.

Chapter 4 outlines the experimental procedures and the test facilities used to conduct the experimental work. Descriptions of signal generation, data acquisition procedures, and data post-processing are included.

Chapter 5 presents contour and 3-dimensional plots of the intensity patterns over the model surface. Discussion of the similarities and differences between the two different tank-loading conditions is provided.

Finally, the thesis work is summarized in Chapter 6. Overall conclusions regarding the effect of internal fluid containers on external acoustic intensity measurements are drawn, and suggestions for further work are provided.

CHAPTER 2
SOUND INTENSITY MEASUREMENTS

2.1 Introduction

Sound intensity, or sound power per unit area, is a fundamental concept in acoustics. Sound intensity was defined by Lord Rayleigh in his well-known work Theory of Sound [12] published in 1877. However, despite the well-established theory, the first patented means of measuring acoustic intensity did not appear until 1932. This patent was issued to H.F. Olson for an acoustic wattmeter [13]. Early attempts at measuring acoustic intensity required complex, specialized instrumentation and the results were not very accurate.

With the development of digital instrumentation, methods for measuring acoustic intensity were significantly improved. In 1977, Fahy [14] introduced a means of measuring intensity which used the cross-spectral density of two microphone signals. His method allowed common acoustic instrumentation to be used for intensity measurement and produced more accurate results. Since then, the two microphone measurement technique has become a well-accepted method for measuring acoustic intensity.

2.2 Acoustic Intensity Formulation

For a directional sound source, power flow varies over a control surface enclosing the source. Measurements of the average power flow per unit area or local average acoustic intensity provides insight into the directive properties of the sound source. (However, this does not imply that nearfield variations in acoustic intensity

are the same as source directivity.) Mathematically average acoustic intensity is defined [15] as:

$$\vec{I} = \frac{1}{T}\int_0^T (p\vec{v})dt = \langle p\vec{v} \rangle_t \qquad (2.1)$$

Intensity is a vector quantity with magnitude and direction. Equation 2.1 is the time-averaged value of intensity, which gives only the net energy flux across the boundary. This value does not represent the absolute total of energy which may be flowing back and forth across the boundary.

As shown in equation 2.1, sound intensity is the product of particle velocity and pressure. When the particle is displaced, there is a temporary increase in pressure. This pressure acts to restore the displaced particle to its original position and passes the disturbance on to the next particle. In this manner, the pressure disturbances propagate through the acoustic medium as a sound wave.

The difficulty in using equation 2.1 directly is that it requires knowledge of the local particle velocity. To obtain a more useful equation for computing intensity, a relationship between pressure and velocity must be incorporated. This relationship is then used to develop an equation for calculating acoustic intensity from the pressure sensed at two microphones separated by a small radial distance of Δr.

The linearized form of the conservation of momentum equation for zero mean flow and no viscous dissipation relates particle acceleration to the pressure gradient:

$$\rho_o \frac{\partial \vec{v}}{\partial t} + \nabla p = 0 \qquad (2.2)$$

Consider now a steady sound source with time dependence $e^{j\omega t}$. This sound source creates a harmonically reciprocating boundary. For the radial velocity component of this source, equation 2.2 leads to:

$$\rho_o \frac{\partial v_r}{\partial t} = j\omega\rho_o v_r = -\frac{\partial p}{\partial r} \tag{2.3}$$

A finite difference approximation can be used for the pressure gradient:

$$\frac{\partial p}{\partial r} \approx \left[\frac{p_2 - p_1}{\Delta r} \right] \tag{2.4}$$

This notation assumes that the direction from sensor 1 to sensor 2 is in the positive r direction. By definition of the finite difference approximation, the resulting value for $\partial p/\partial r$ is valid for the point midway between the two sensor locations. Subsequently, when computing intensity, the pressure at the same point can be approximated as:

$$p \approx \frac{1}{2}(p_1 + p_2) \tag{2.5}$$

Substitution of equation 2.4 into equation 2.3 gives an equation for approximating the particle velocity from the pressures at two adjacent surfaces:

$$v_r \approx \left[\frac{j}{\omega\rho_o \Delta r}(p_2 - p_1) \right] \tag{2.6}$$

The complex conjugate for the particle velocity can then be approximated as:

$$v_r^* = \left[-\frac{j}{\omega\rho_o \Delta r}(p_2^* - p_1^*) \right] \tag{2.7}$$

Equations 2.5 and 2.7 can now be used to determine the value for the radial component of average acoustic intensity:

$$I_r = \langle pv_r \rangle_t = \frac{1}{2}\mathrm{Re}(pv_r^*) = \frac{1}{2}\mathrm{Im}(jpv_r^*)$$

$$\approx \frac{1}{2}\mathrm{Im}\left[\frac{1}{2}(p_1 + p_2)\frac{1}{\omega\rho_o\Delta r}(p_2^* - p_1^*)\right]$$

$$\approx \frac{1}{4\omega\rho_o\Delta r}\mathrm{Im}[|p_2|^2 - |p_1|^2 + p_1p_2^* - p_1^*p_2]$$

$$\approx \frac{1}{4\omega\rho_o\Delta r}\mathrm{Im}[p_1p_2^* - p_1^*p_2]$$

$$\approx \frac{1}{2\omega\rho_o\Delta r}\mathrm{Im}[p_1p_2^*]$$

$$I_r \approx -\frac{1}{\omega\rho_o\Delta r}\mathrm{Im}\left[\frac{1}{2}p_1^*p_2\right] \tag{2.8}$$

We can also interpret this result in terms of Fourier transforms. The desired equation for acoustic intensity in terms of the cross-spectral density between the two microphone pressures is then:

$$I_r(f) \approx -\frac{1}{\omega\rho_o\Delta r}\mathrm{Im}\left[\frac{1}{2}P_1^*(f)P_2(f)\right] \approx -\frac{1}{\omega\rho_o\Delta r}\mathrm{Im}G_{12}(f) \tag{2.9}$$

where:

$$G_{12}(f) = \frac{1}{2}[P_1^*(f)P_2(f)]$$

is the cross-spectral density as defined by [15].

2.3 Sources of Error in Acoustic Intensity Measurements

Although the two microphone technique yields more accurate results for acoustic intensity measurements than earlier methods, there are still limitations and sources for error in this technique. Several publications describe the limitations and error sources in depth ([16]-[22]). A summary of the major concerns is provided by this section.

Relative phase shifts between the two microphone signals can be a major source of error in intensity measurements. As the two signals are multiplied and time averaged, the result is unaffected by phase shifts in the signal so long as the signals undergo the same shift. However, if there is relative phase shift between the signals, substantial errors can occur. Measurement accuracy is particularly sensitive to instrument phase mismatch at low frequencies, when there is relatively small actual phase shift between the two measured signals.

To minimize pha e shift errors, phase matching of the two measurement channels becomes crucial. A technique has been developed by Chung [16] to eliminate errors resulting from phase mismatch. His technique is based on taking the geometric mean of the cross spectral estimates with the microphones in the forward and reversed positions. The phase error may also be estimated by using separate calibration experiments to determine the magnitude of the mismatch.

Another source of phase deviation results from interference effects due to the physical presence of the microphones in the acoustic field. There is also error due to diffraction around each of the two closely spaced microphones. The magnitude of error resulting from these effects is difficult to measure, but it is thought to be small

for the normal frequency range of the microphones [17].

Another major source of error is due to the finite difference approximation for the pressure gradient in equation 2.4. This source of error is analyzed by [17]-[19]. The underlying cause for error is that the spatial derivative of pressure cannot be accurately specified by only two pressure measurements; higher order terms in the Taylor series expansion used to approximate $\partial p/\partial r$ have some significance. Yet to include higher order terms, additional microphone positions would be required and data processing would be greatly complicated.

In analyzing the error associated with finite difference approximation, Thompson and Tree [19] use two non-dimensional parameters to define optimum ranges for obtaining accurate estimates of acoustic intensity from nearfield measurements. These parameters are $k\Delta r$ and $\Delta r/r$. In general, finite difference errors are minimized by selecting the smallest possible values of $k\Delta r$ and $\Delta r/r$. In practice, Δr must be large enough to obtain a useful difference in signal phases. If the level of approximation error is given by:

$$L_E = \log_{10}\left(\frac{I_{APPROXIMATE}}{I_{EXACT}}\right) \tag{2.10}$$

then the parameter ranges suggested by [18] and [20] for minimizing the approximation error to ± 1.5 dB are[1]:

---

1 Reference [19] suggests a lower limit of 0.1 for $k\Delta r$, and cites other experimental studies which would support this lower limit. However, [17] states that the low frequency limits are most probably caused by instrumentation errors and not a result of the finite difference approximation.

$$0 \le k\Delta r \le 1.3 \tag{2.11}$$

$$0 \le \frac{\Delta r}{r} \le 0.5 \tag{2.12}$$

Other potential sources for error include uncorrelated random noise from secondary acoustic sources. Random noise reduces the coherence between the measured acoustic pressure, thus increasing the random error in the acoustic intensity estimate. Reference [20] develops an expression for the normalized standard error of the acoustic intensity estimate. This error is shown to be a strong function of the coherence function and the phase angle spectrum. Maximum error occurs at low frequency and low coherence. At high frequency, this random error is not usually significant. The normalized standard error can be reduced by averaging the results from N neighboring sets of data. In this case the error is reduced to [23]:

$$e = \frac{1}{\sqrt{N}}$$

2.4 Measurement Technique

In the experimental work described by this thesis, the technique used to measure acoustic intensity varies slightly from the two hydrophone technique, but the principles are the same. Rather than use two hydrophones to simultaneously measure the underwater pressure field, a single hydrophone was used. This single hydrophone first sampled the pressure field along the inner plane of grid points, and then was mechanically moved radially outward to sample along the outer plane. Processing of the pressure data is then the same as the two hydrophone technique. (Further details on sound signal generation and data acquisition are provided by Chapter 4.)

There are several advantages to using a single hydrophone for measuring the pressure field [9]. With a single probe, phase mismatch between two separate hydrophones is avoided. Furthermore, mutual diffraction errors are eliminated. Interference effects are limited to just the disturbance of a single small hydrophone in the acoustic field.

The primary disadvantage to the single hydrophone technique concerns signal repeatability and phase stability. With digital signal formation, signal repeatability can be achieved with a high degree of confidence. However, as discussed previously, any deviation in phase can severely limit the accuracy of the resulting intensity measurements. With the single hydrophone technique, phase deviations can result from stray currents in the tank and/or background noise present at the time one sample is collected and not the other.

CHAPTER 3
MODELING

3.1 Scaling

To understand how vibrational energy from a machinery source propagates along structural members, through the hull, and then into the surrounding fluid, experimental measurements are taken using a representative model of the prototype structure. To be able to predict the vibrational characteristics of the prototype ship from those measured with the model, one must know how the applicable parameters scale.

In general, for a meaningful quantitative estimate of the prototype vibrational characteristics, the model must be exactly geometrically similar to the prototype. Furthermore, the following non-dimensional parameters must be identical in the model and prototype [24]:

$$\rho(\omega L)2/E \text{ and } \nu$$

where ρ is the material density per unit volume

E is Young's modulus

ω is radian frequency

L is length (of model or prototype)

ν is Poisson's ratio.

When the same material is used in both the model and the prototype, then E, ρ, and ν are also the same. In this case, the non-dimensional parameters reduce to

$$(\omega L)_{model} = (\omega L)_{prototype}$$

Subsequently, if the length scaling is 1:10, then the vibration frequency for the model must be ten times greater than that in the prototype.

From Figure 1.1, the frequency range for main and auxiliary machinery is seen to be in the range of 10 Hz to 5 kHz. It follows then, that for 1:10 scaling, the scaled frequency range for the model is 100 Hz to 50 kHz.

3.2 Structural Model

Due to the complexity of the prototype ship structure, it is not practical to make the model exactly geometrically similar. Approximations to the ship's hull and internal structure are used for ease of model construction. However, by using a representative model structure constructed for material with E, ρ, and ν nearly similar to the prototype, qualitative conclusions regarding the prototype vibrational characteristics can be made.

In this experiment, the structural model used to study the effects of internal fluid containers on external sound radiation is a $(L_{model}/L_{prototype})$=1/10 scale-model of the reference surface ship. The model is a smaller, simplified version of the 1/6.25 scale-model used by Levi [2]. As much as possible, the models were kept similar to ease comparison of experimental results. The 1/10 scaling for this experiment was determined by size limitations of the test facility.

The primary attributes of the model used in this experiment are listed below. The model is shown by figures 3.1 - 3.4 and a comparison of with Levi's model is shown by figure 3.5.

- The model hull is a half-cylindrical shell which is an idealized approximation of the reference ship.
- The model is fabricated from 0.8mm thick galvanized steel plate.
- There are five transverse stiffeners (frames) reinforcing the model shell.
- There is one central bottom tank with about 30-liter capacity. (There are no side tanks as in Levi's model [2].)
- There are cutouts in the structural supports within the tank to allow free communication of tank liquid throughout the entire tank.
- The junctions between the model tank top and outer hull are riveted and soldered.
- All other model junctions are soldered to minimize deformations. (Deformations caused by welding increase as plate thickness decreases.)
- To more closely approximate the level of damping in the reference ship, damping layer material was attached randomly to about 50% of the model's interior. Since trapped air bubbles underneath the damping strips could affect resulting pressure measurements, damping strips were not applied on any exterior surface.
- The shaker used to model broad-band excitation of shipboard machinery is mounted centrally on one of the engine foundation plates. The experimental frequency range is limited to 640 Hz to 15 kHz.

- To minimize bubbles from corrosion reactions (which could affect nearfield pressure measurements) when the model is in the chlorinated tank, the model exterior was primed and painted.

Model specifications are summarized in Table 3.1.

Table 3.1 lists the ring frequency for the model. This frequency is defined [2] as:

$$f_r = \frac{c_L}{2\pi r} \tag{3.1}$$

where $c_L \approx 5100$m/sec in steel and r=0.42m. As discussed by Levi [2], curvature effects may be neglected for frequencies above the ring frequency. This is the case for most of the frequency range of interest in this experiment.

To achieve the desired waterline when the model is in the tank facility, ten 25 lb lead blocks were mounted across the top of the model, supported by two metal channels. The model was then suspended by its four corner mounted lifting bolts by turnbuckles connected to metal channel supports running above the submerged workspace. The turnbuckles allowed precise model alignment, which is necessary for the robotic nearfield scans. This setup can be seen clearly in Figures 3.6 and 3.7.

Table 3.1 Model Specifications

Parameter	Units	Value
ν		0.3
E	N/m^2	$2.1*10^{11}$
ρ	kg/mm^3	7850
t	mm	0.8
f_{model}	kHz	0.64-15
$f_{prototype}$	Hz	64-1500
f_{ring}	Hz	1933

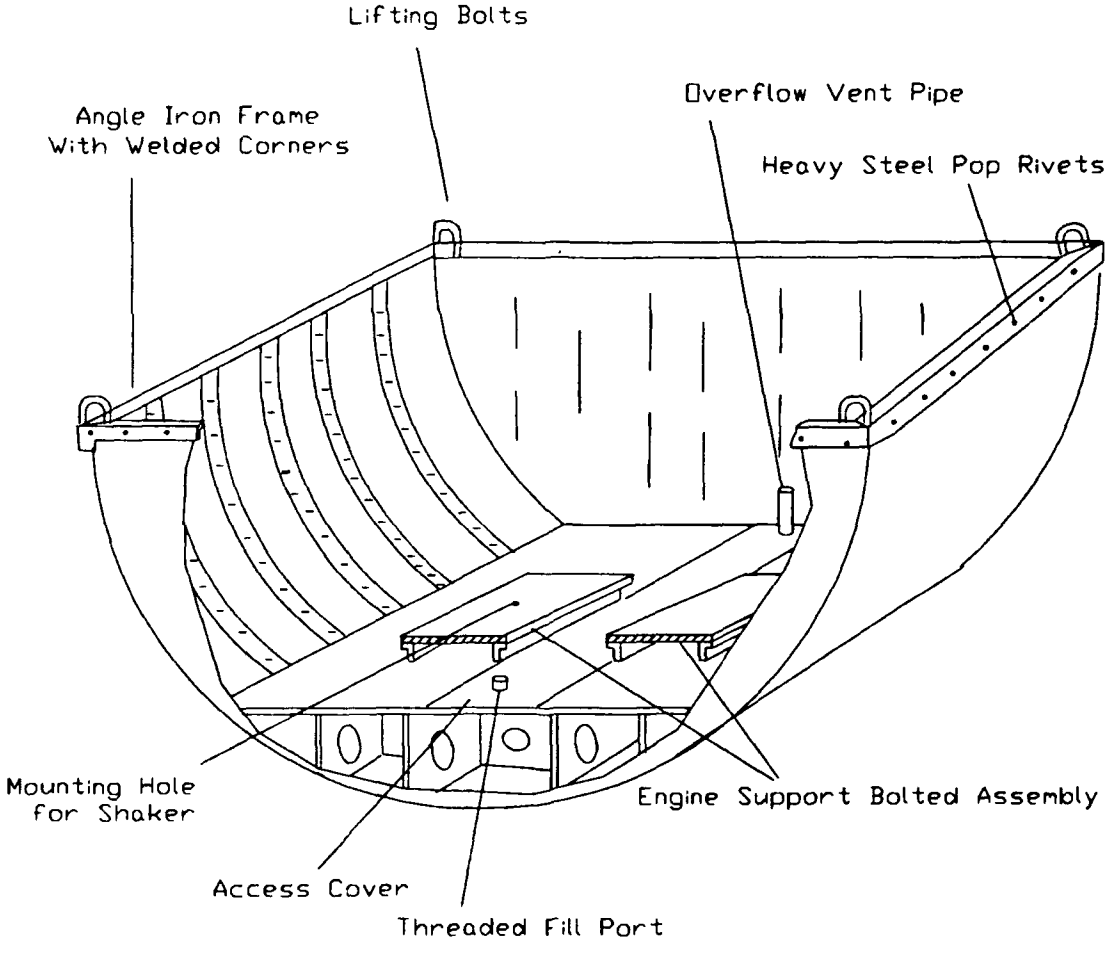

Figure 3.1 Model General View

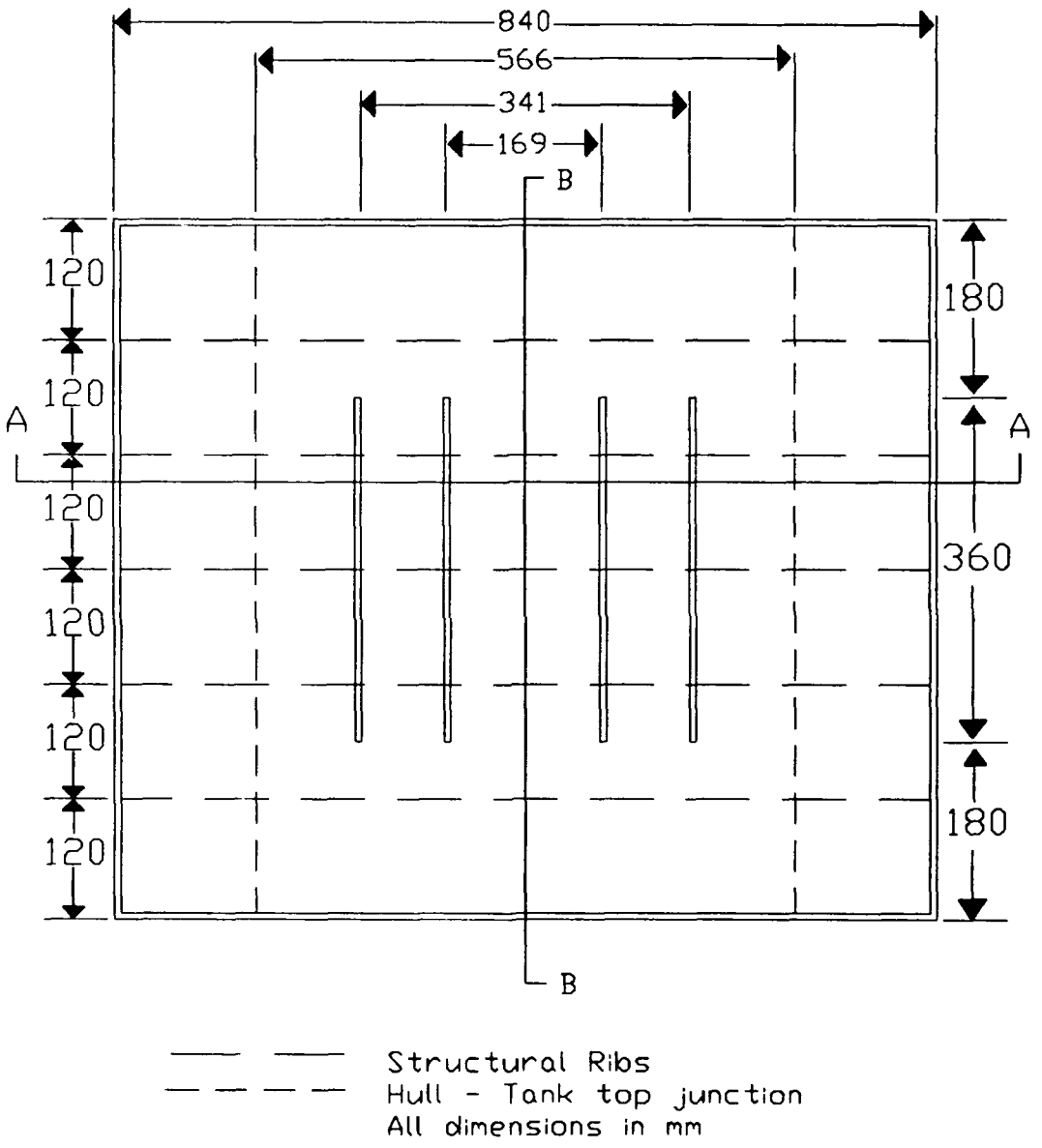

Figure 3.2 Model Topview

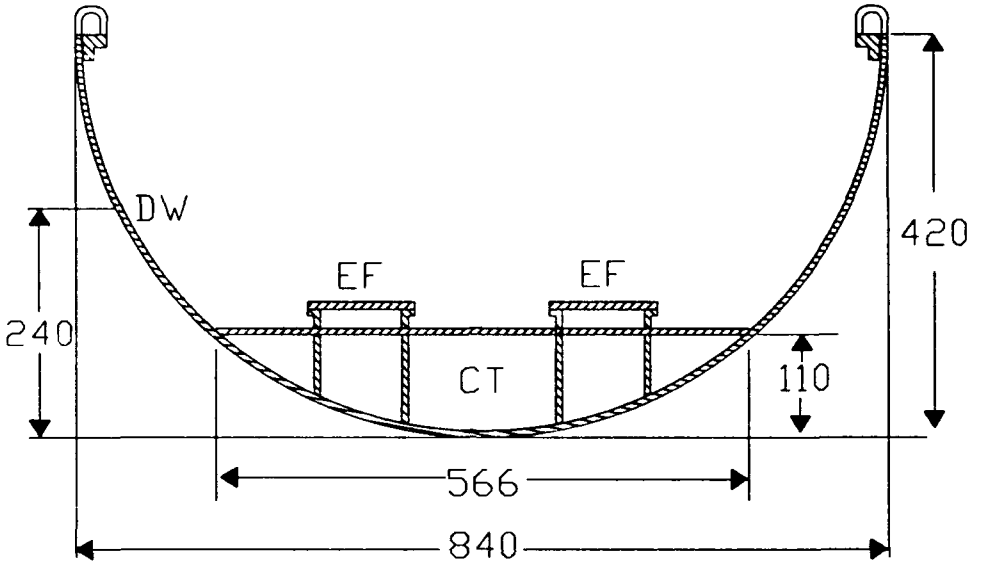

DW = Design Waterline
EF = Engine Foundation
CT = Center Tank
All dimensions in mm

Figure 3.3 Model Section A-A

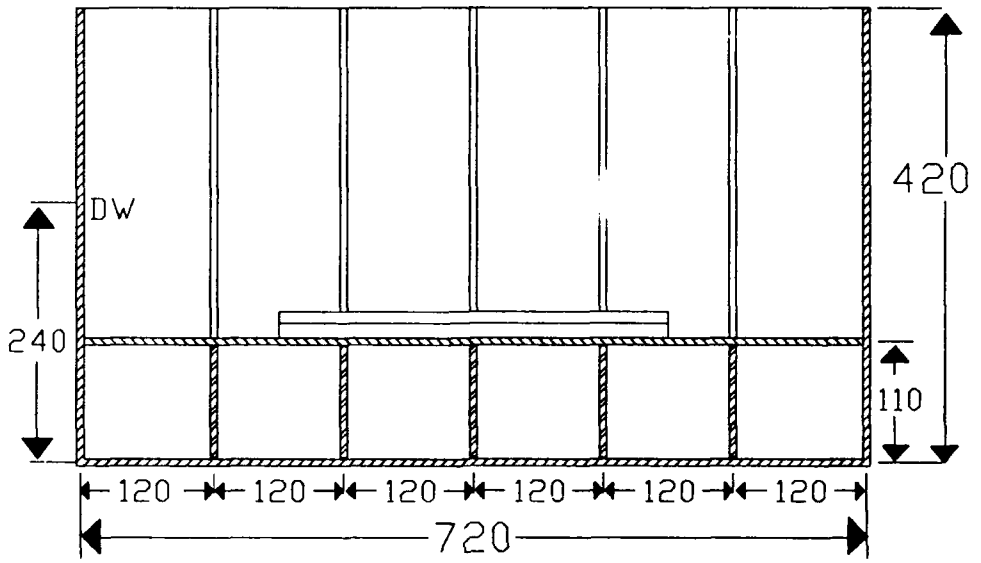

DW = Design Waterline
All dimensions in mm

Figure 3.4 Model Section B-B

LEVI'S
MODEL SECTION A-A

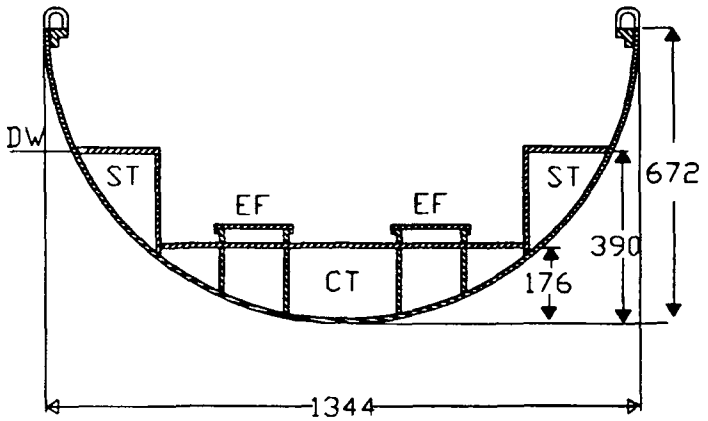

DW = Design Waterline
EF = Engine Foundation
CT = Center Tank
ST = Side Tank
All dimensions in mm

LEVI'S
MODEL SECTION B-B

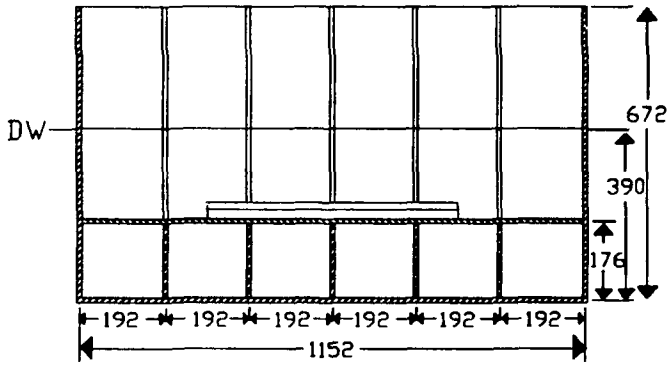

All dimensions in mm

Figure 3.5 Levi's Model Sections A-A and B-B

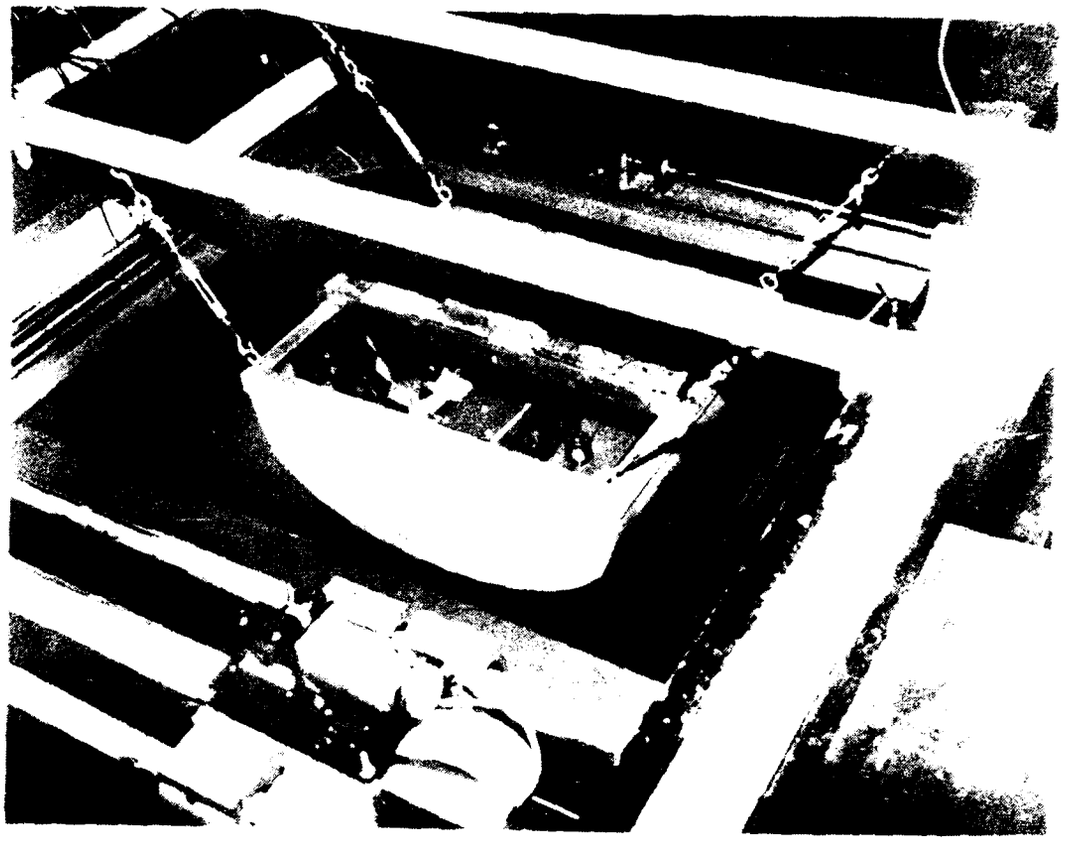

Figure 3.6 Ship Model in Acoustic Tank at NRL

(Photograph courtesy of NRL)

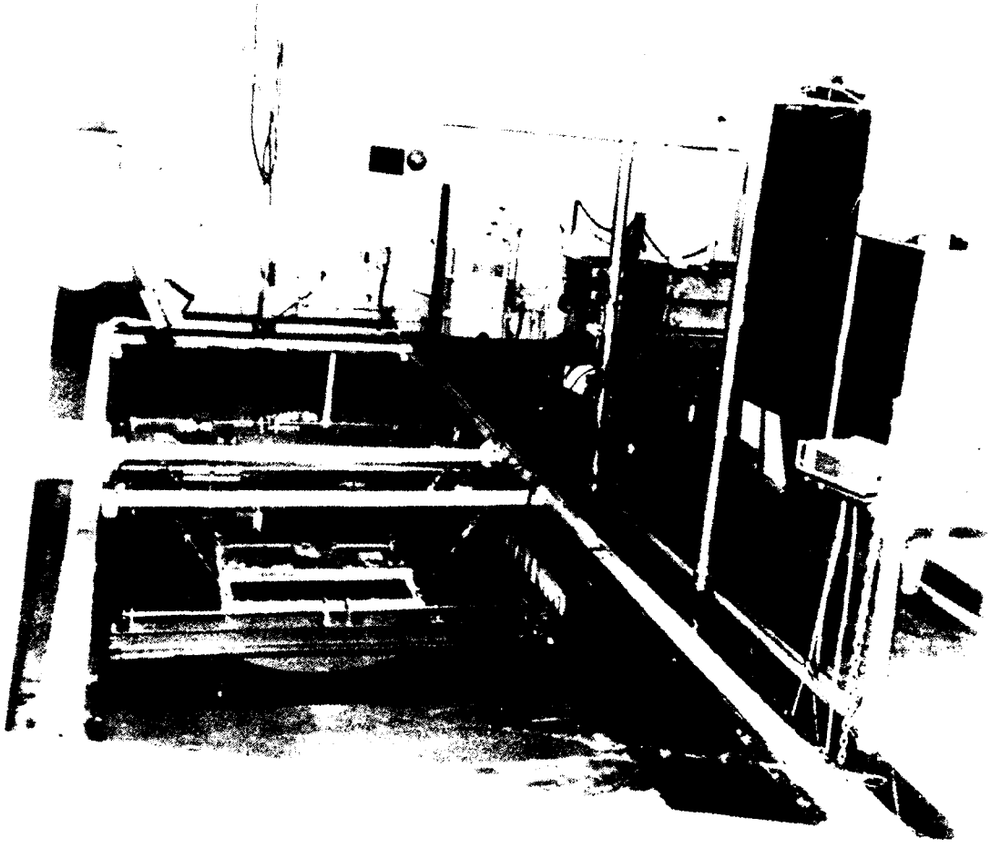

Figure 3.7 Acoustic Tank Scan Workspace with Model

(Photograph courtesy of NRL)

3.3 Model Structural Wave Characteristics

In [2], Levi developed equations describing structural wave motions in thin plates. These equations were used to determine the model's bending wave characteristics. These characteristic values and the equations from which they are derived are tabulated in Table 3.2. Table 3.3 provides corresponding wave characteristics of the external fluid for comparison. In these calculations, the following values were used: h = 0.0008 m (plate thickness), $c_L \approx 5100$m/sec in steel, and $c_f \approx 1475$m/sec for tank water at 17.9°C.

The critical frequency, or that frequency at which the plate bending speed in absence of fluid loading coincides with the sound speed of the ambient fluid, is defined [2] mathematically as:

$$f_c = \frac{\sqrt{3}\, c_f^2}{\pi h c_L} = 294 \text{ kHz} \tag{3.2}$$

By definition, λ_B equals λ_f at the critical frequency. Above the critical frequency, the model bending wave speed is supersonic and strong radiation by the structure occurs in the surrounding fluid medium.

Table 3.2 indicates that $\lambda_B < \lambda_f$. This implies that the plate bending wave speed is less than the fluid sound speed. For this case, the disturbance of the fluid decays exponentially with distance normal to the model structure.

The axial and circumferential modes (n and m respectively) can be determined from the bending wavenumber by:

$$k_B = (k_{axial}^2 + k_{circum}^2)^{1/2} \tag{3.3}$$

where:

$$k_{axial} = \frac{n\pi}{l} \qquad \text{and} \qquad l = 72\text{cm}$$

$$k_{circum} = \frac{m\pi}{\pi r} \qquad \text{and} \qquad r = 42\text{cm}$$

Table 3.2 Model Structural Wave Characteristics

Bending Wavenumber	$k_B = 2\left(\frac{\pi\sqrt{3}}{c_L}\right)^{1/2}\left(\frac{f}{h}\right)^{1/2}$
640 Hz	$k_B = 58.4\text{meters}^{-1}$
15,000 Hz	$k_B = 283\text{meters}^{-1}$
Bending Wavelength	$\lambda_B = \frac{2\pi}{k_B}$
640 Hz	$\lambda_B = 0.1076\text{meters}$
15,000 Hz	$\lambda_B = 0.0222\text{meters}$

Table 3.3 Acoustic Wave Characteristics

Acoustic Wavenumber	$k_f = \frac{2\pi f}{c_f}$
640 Hz	$k_f = 2.77\text{meters}^{-1}$
15,000 Hz	$k_f = 64.96\text{meters}^{-1}$
Acoustic Wavelength	$\lambda_f = \frac{c_f}{f}$
640 Hz	$\lambda_f = 2.266\text{meters}$
15,000 Hz	$\lambda_f = 0.0967\text{meters}$

CHAPTER 4
TEST FACILITIES AND EXPERIMENTAL PROCEDURES

4.1 Description of Test Facilities

The experimental work done in this thesis was carried out at the Physical Acoustics Branch of the Naval Research Laboratory in Washington, D.C. Their facilities include an automated scanning facility constructed to support work being done by Dr. Earl Williams and his associates in Nearfield Acoustical Holography. Descriptions of the NRL acoustic research tank facility are given by [8] and [9] . Key features of the facility, paraphrased from [9], are provided below.

A robotic manipulator (also called Automated Nearfield Acoustic Scanner) moves a piezoelectric hydrophone along the three Cartesian axes in the acoustic nearfield of the source being studied. The scanner operates in a 9.1-m-diameter x 6.7-m-deep, cypress-walled pool. The horizontal submerged workspace of the scanner is approximately 2.3-m x 1.2-m, while vertical travel is about 2.6-m. The hydrophone is positioned at the end of a thin boom. The hydrophone mounting fixtures and scanner mechanical parts are carefully arranged so as to limit errors in the measured data resulting through diffraction or reflection of the sound field.

Three motors under computer command are used to control scanner motion in the X, Y, and Z directions along preprogrammed paths. Stepping motors with optical encoder and analog tachometer feedback drive the horizontal axes. These axes are each controlled by dedicated microprocessor with independent interfaces to the VAX 8250 host computer. Vertically, the scanner is driven using a dc stepper motor in an

open loop fashion. It is controlled by a stepper motor translator with speed adjustment and switch-selectable index distance. The translator is interfaced to the host computer through microprocessor-controlled indexing switches which control direction, speed and length of travel.

The host computer is used for several functions. It sends motion commands to each of the scanner axes, triggers a two channel signal averager which digitizes the output of the hydrophones and reference source, applies a Fourier transform to the digitized data, and controls the graphic display. Major computations are performed on the Physical Acoustics Branch VAX 8250 computer, located in an adjacent building.

To minimize transient vibrations during point-to-point scans, the scanner velocity is typically limited to less than 5 cm/s.

The static positioning accuracy for the model is no greater than the trueness of the model, and is estimated at approximately +/- 1mm. Resolution for positioning of the robotic manipulator is 2.5 mils in all directions, determined by the optical encoder/decoder circuitry and the transmission gear ratio.

4.2 Signal Generation

The experiment performed in this work was done using a broadband frequency chirp waveform over the range of 640 Hz to 15 kHz. The equipment lineup is shown by Figure 4.1. The drive signal was created digitally and then converted to analog voltages. After filtering, the signal was sent through separate paths to the F9/F3 piezoelectric/electromagnetic vibration generator. The amplified F3 signal as seen by

the oscilloscope is shown by Figure 4.2. The Fourier transform of this signal is shown by Figure 4.3. Similarly, the amplified F9 signal is shown by Figures 4.4 and 4.5.

Before the amplified signal is passed to the F9, the signal is passed through an impedance matching unit. Matching networks are used to provide the interface between power amplifiers and piezoelectric shakers. The load which the piezoelectric shaker presents to the power amplifier is capacitive (reactive) and decreases almost linearly wit increasing frequency. To provide improved performance form the shaker, impedance matching is needed. The matching network provides a fixed 8:1 voltage step-up to allow the piezoelectric shaker to be driven at its full voltage level. A matching network is not needed with the F3 because electromagnetic shakers present a low, relatively constant, largely resistive input impedance.

The F3/F9 vibration generator combines the low frequency advantage of a electromagnetic shaker (F3) with the high frequency advantage of the piezoelectric shaker (F9). The F3 encircles the F9, and the combined unit is stud-mounted to the model at the centerpoint of the port machinery foundation plate. The F9 is supplied with an impedance head (Z9) mounting base for generator/model interface. The impedance head contains a force transducer to monitor force output from the combined shaker units. This force output (after filtering and digitizing) is shown graphically by Figures 4.6 and 4.7.

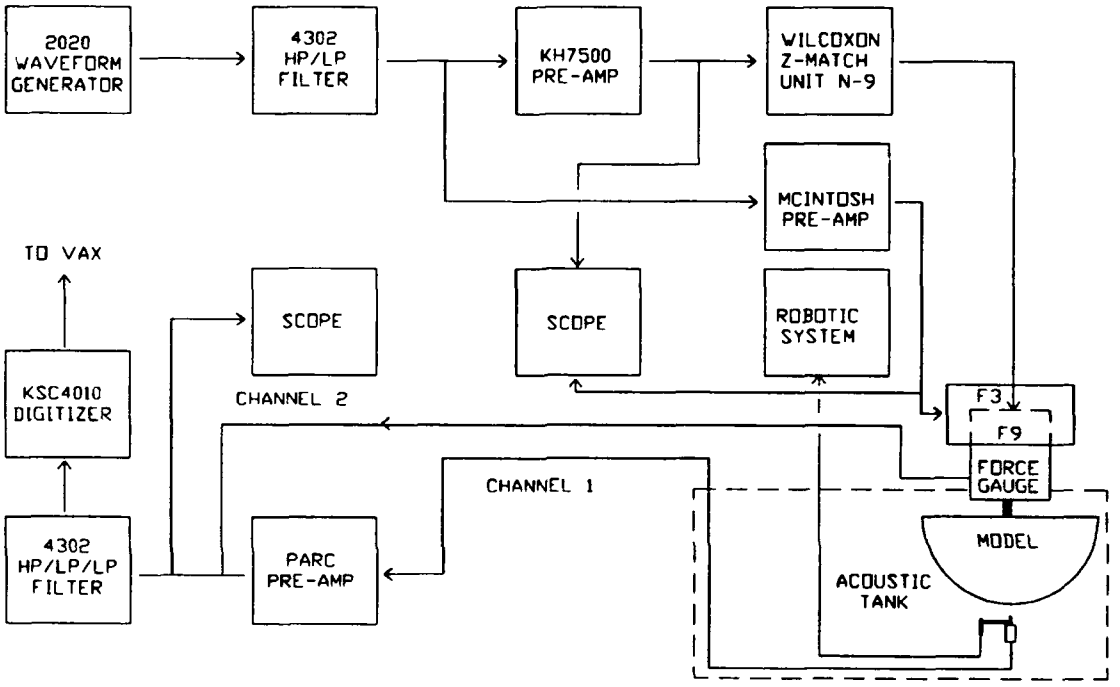

Figure 4.1 Experimental equipment setup for nearfield pressure measurements

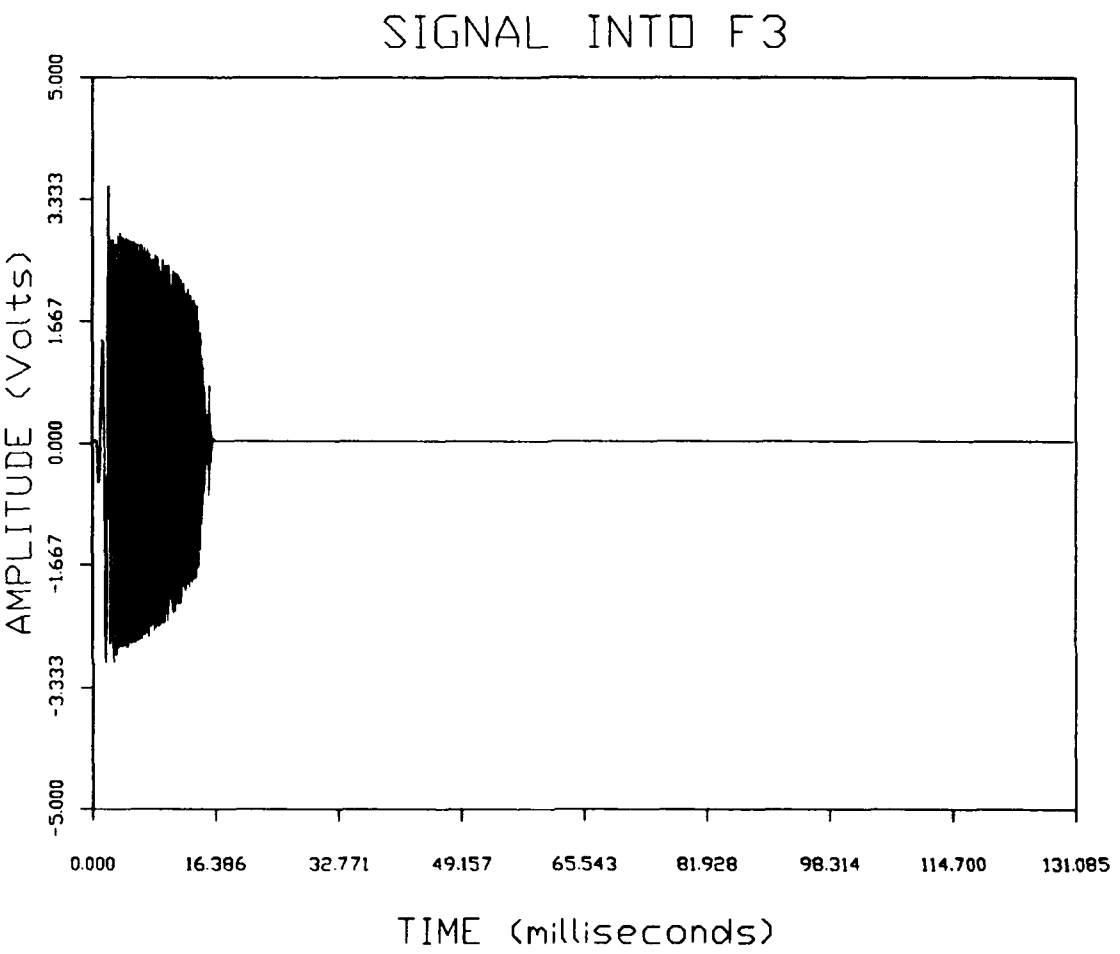

Figure 4.2 Signal into F3

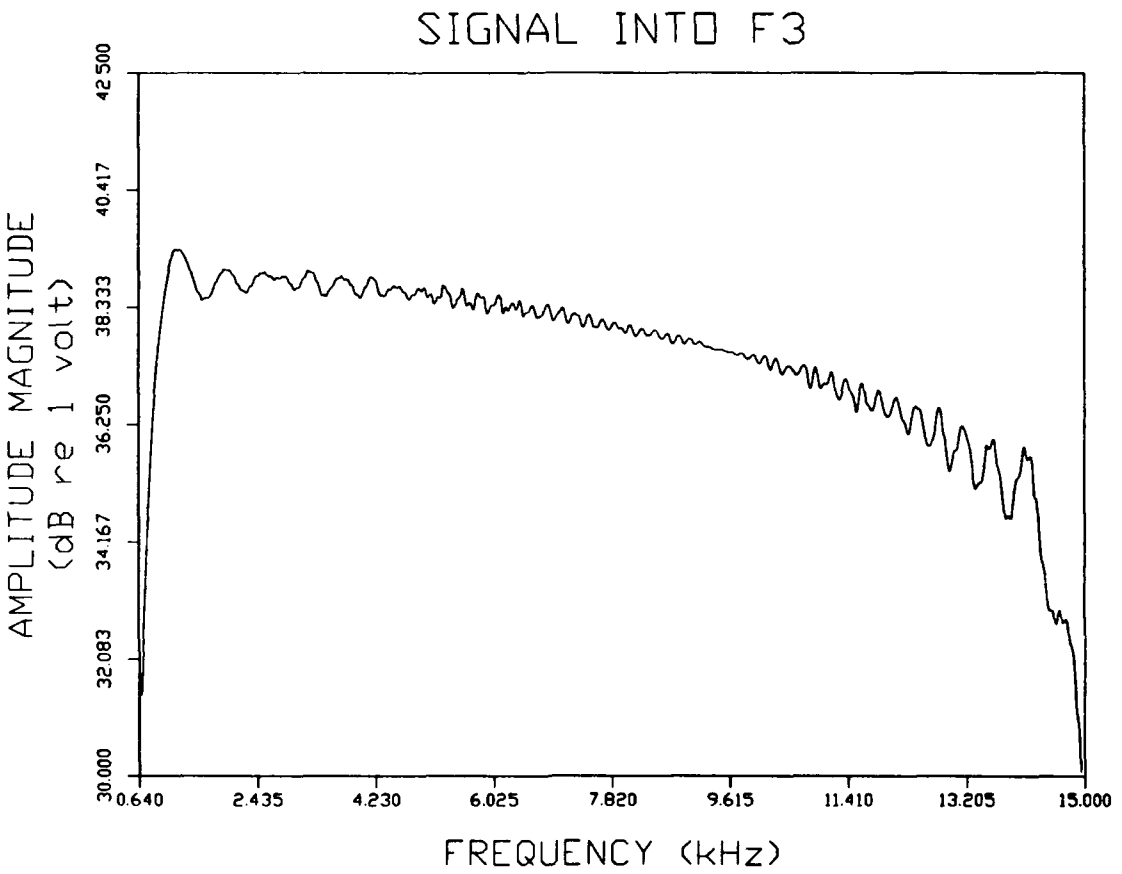

Figure 4.3 Signal into F3

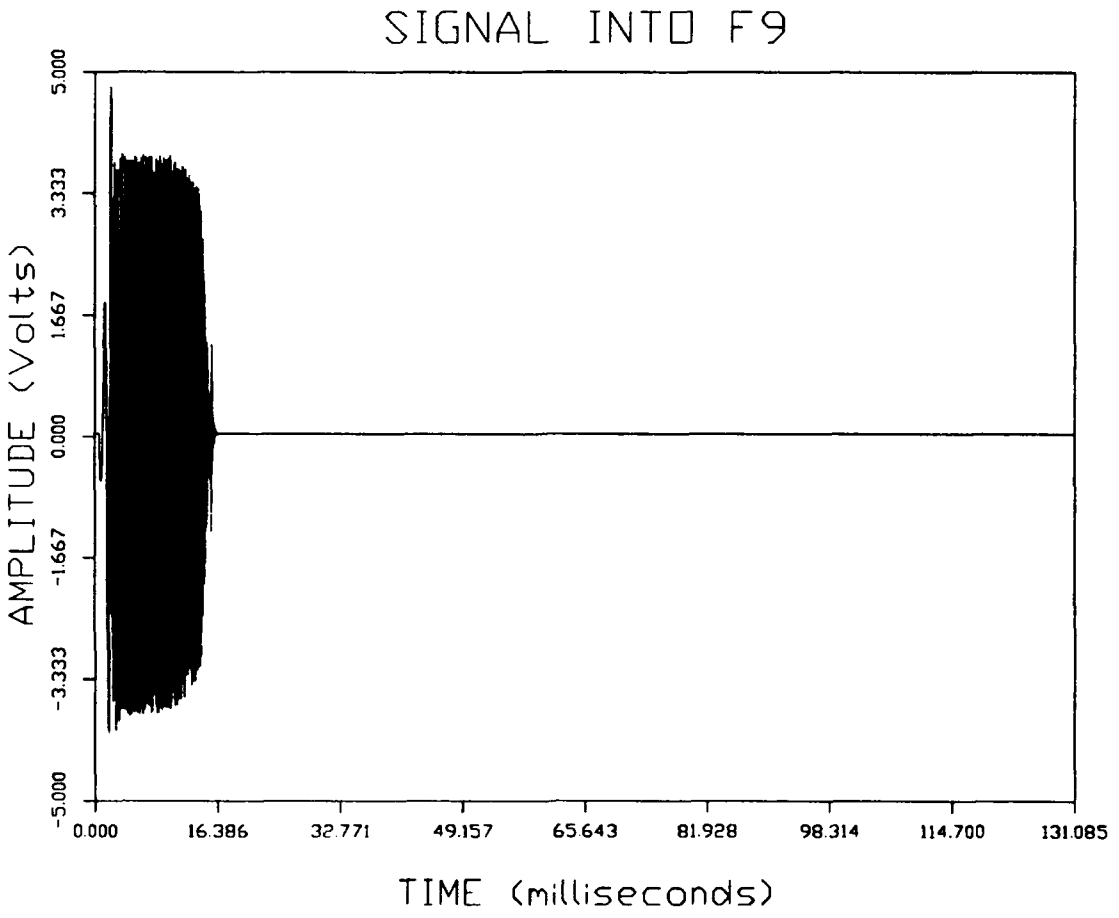

Figure 4.4 Signal into F9

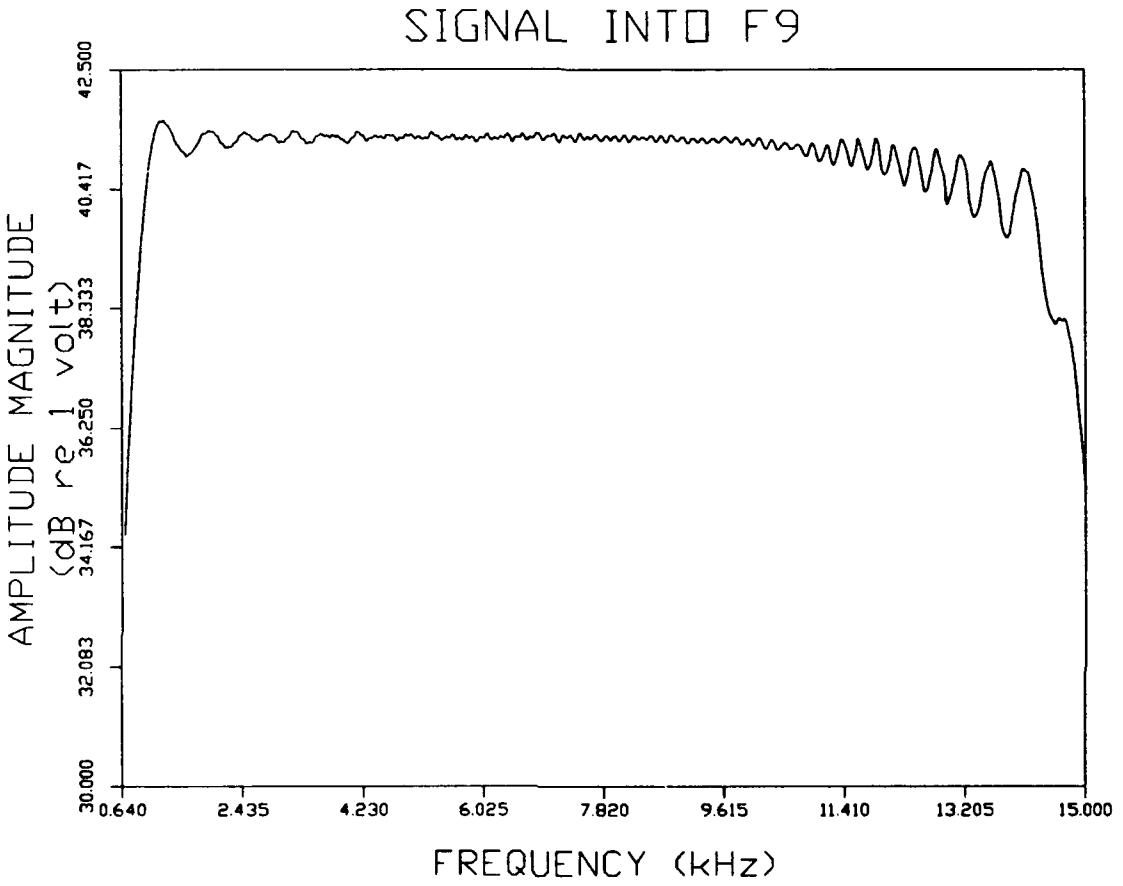

Figure 4.5 Signal into F9

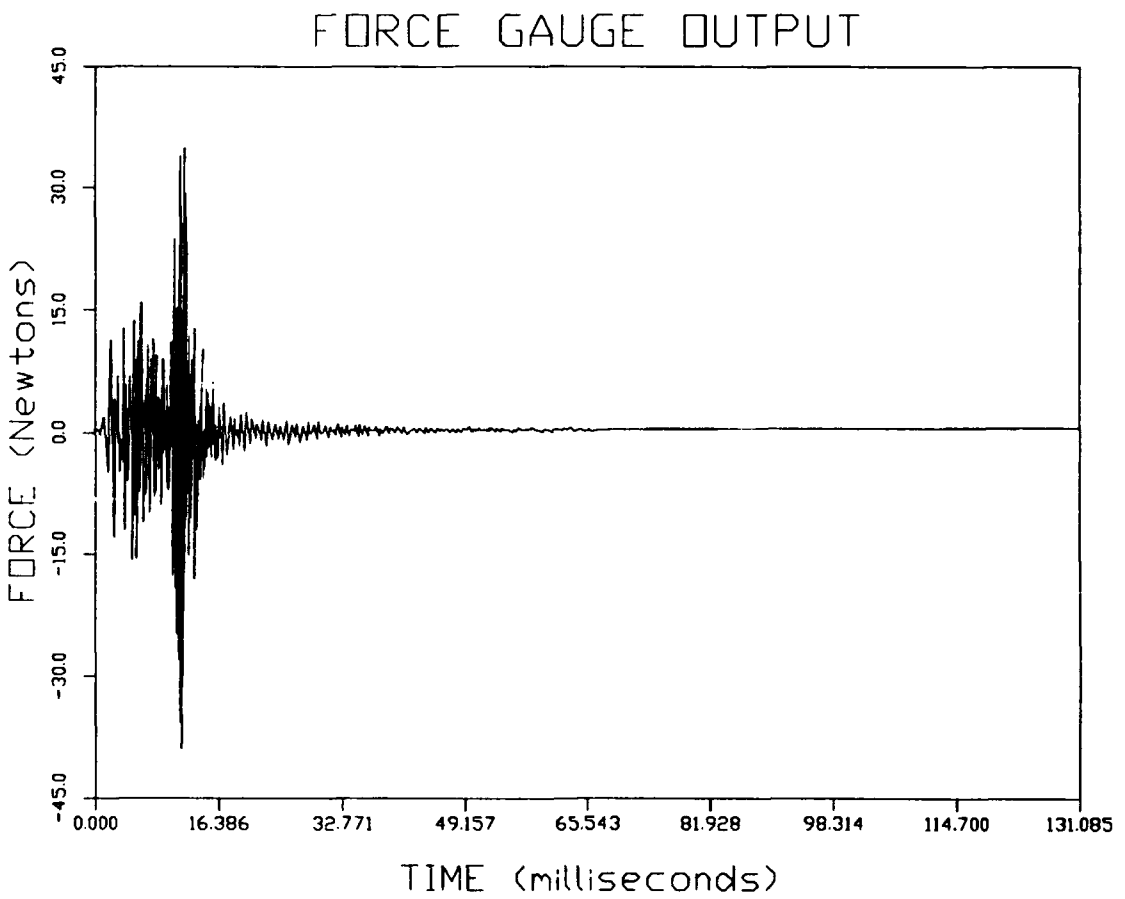

Figure 4.6 Force Gauge Output

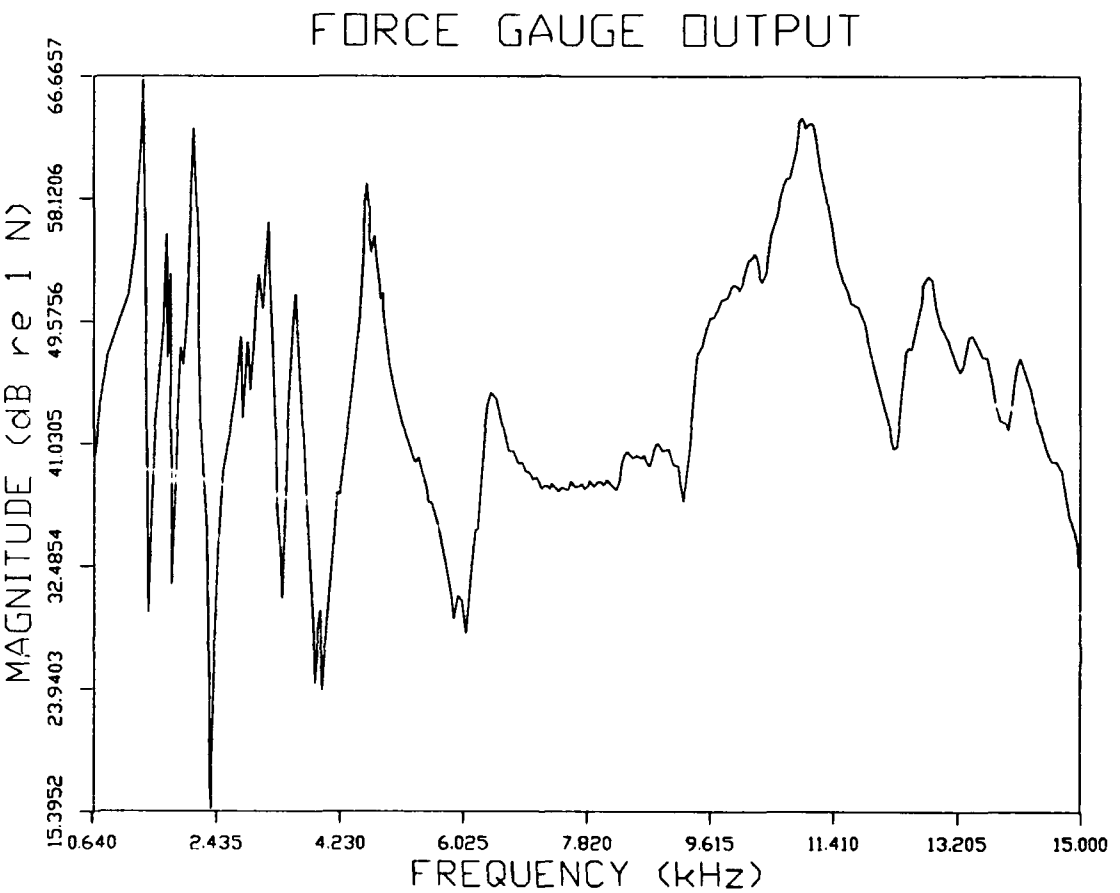

Figure 4.7 Force Gauge Output

4.3 Data Acquisition

A single Brüel and Kjær type 8103 hydrophone was used to collect pressure data following the measurement technique described previously in Section 2.3. The inner plane for data collection was located 1.6 cm radially outward from the model's hull surface. The outer plane was located 2.2 cm radially outward for a plane separation distance of 0.6 cm.

Based on the model's structural wavelength in the frequency band of interest (minimum λ_B=2.2 cm at 15 kHz) and the optimum ranges for $k\Delta r$ and $\Delta r/r$ provided by equations 2.11 and 2.12, a grid mesh with 1 cm spacing between points on the hull surface was chosen. This allowed for 73 grid points axially and 84 grid points circumferentially for a total of 6132 grid points in a single plane. The grid point locations for the inner and outer planes were radial projections of the hull surface grid. A complete listing of parameters for scanning the model are provided by Table 4.1.

Cartesian coordinates were used to establish the hydrophone position. The left-handed axis orientation is depicted in Figure 4.8. The origin is located at the axial and radial centers of the model. The x axis runs port and starboard, with the starboard side being positive values. X-values for positioning the hydrophone range from +36.47 to -36.47 cm. The y axis runs vertically, with the underwater model surfaces having negative y values. Y-values range from -23.9 to -45.0 cm. The z axis runs from bow (+36 cm) to stern (-36 cm). The starting location for data collection was the aft, uppermost, starboard grid point (36.47, -23.9, -36).

Table 4.1 Model Scanning Parameters

Target (model) width	84 cm
Target (model) radius	42 cm
Target (model) length	72 cm
Waterline to bottom of target	24 cm
Minimum distance between water line & tip of hydrophone	5.05 cm
Minimum distance between target surface and hydrophone tip	0.60 cm
Distance between hydrophone tip and acoustical center	0.95 cm
Distance between water line and acoustical center of hydrophone	6.00 cm
Distance between points in lengthwise scan	1.00 cm
Total number of lengthwise scan points	73
Total lengthwise scan length	72 cm
Distance of first scan surface from target surface	1.6 cm
Distance of second scan surface from target surface	2.2 cm
Distance between points on first scan surface along radial arc	1.038 cm
Distance between points on second scan surface along radial arc	1.052 cm
Total number of circumferential scan points	84
Maximum value of $k\Delta r$ (at 15 kHz)	0.39
Maximum value of $\Delta r/r$ (at r=1.55cm)	0.39

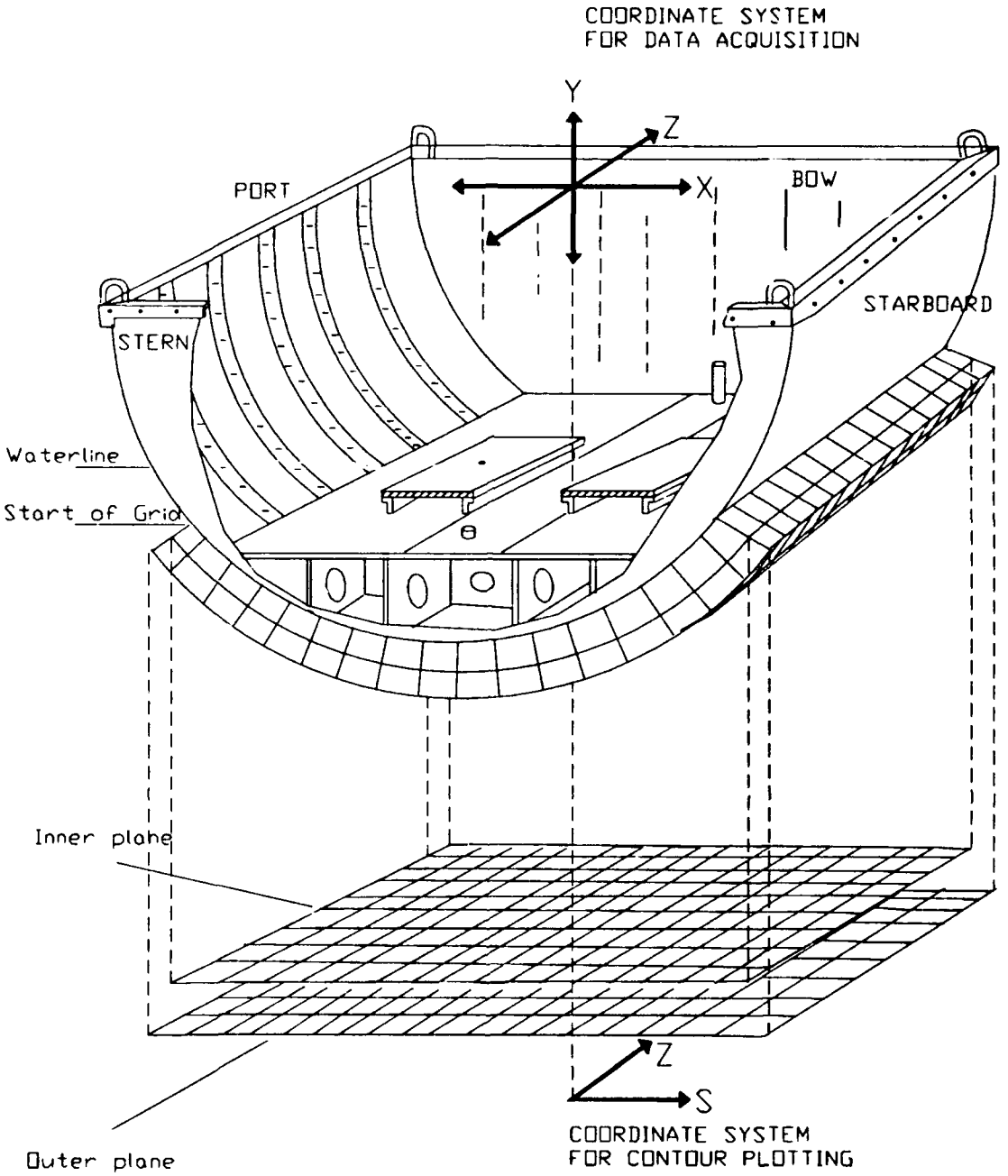

Figure 4.8

Sketch of Grid Overlay and Axis Orientation on Model; Not to Scale

The hydrophone and force gauge sampling frequency was 62,500 Hz, which corresponds to a sampling time interval of 16 μsec. This sampling interval results in a Nyquist frequency of 31,250 Hz (maximum frequency that can be detected), which is well above the desired upper frequency of 15,000 Hz. A record length of 8192 samples was taken for a total digitized time window of 0.131072 seconds. Sixteen averages were taken at each location.

Data acquisition parameters are summarized by Table 4.2.

Table 4.2 Data Acquisition Parameters

Low pass filter setting	16 kHz
High pass filter setting	630 Hz
Sampling frequency (force gauge and hydrophone)	62.5 kHz
Sampling interval	16 μsec
Record length	8192 samples
Number of averages at each location	16
Total digitized time window for sampling	0.131072 sec
FFT frequency bin width	7.629 Hz
Frequency bin corresponding to 640 Hz	84
Frequency bin corresponding to 15 kHz	1966

4.4 Data Post-Processing

Initial data post processing was accomplished at NRL. Hydrophone pressure data was transformed from the time domain to the frequency domain using Fast Fourier Transform (FFT). Similarly, the force gauge data was also transformed.

After FFT, the 8192 time samples yielded 4096 frequency bins ranging from 0 through 31,250 Hz. Each frequency bin had a width of 7.629 Hz. The reduction by half (from 8192 to 4096) is the result of symmetry in the Fourier coefficients; unique terms are given for only half the sample range. This symmetry results when the terms in the time domain series are all real numbers (which is the case for the force and pressure data) [25].

Further post processing was accomplished at MIT. Following the theory presented in Chapter 2, the average acoustic intensity for the 6132 mid-plane grid points was calculated from the frequency content of the pressure cross-spectrum. Only intensity data from the frequency bins covering 640 Hz to 15 kHz was maintained. These frequency bins included 84 through 1966. Intensity data was then collected into third octave bands for contour plotting.

To generate contour plots, the 3-D intensity data was converted to 2-D data. For the 2-D coordinates, the axial coordinate z was maintained. The x and y coordinates were combined to determine a single coordinate s. In this case, s represents the arclength from the "origin" (where s=0). Figure 4.8 shows the coordinate system for contour plotting, and figure 4.9 illustrates the mathematical computation for s.

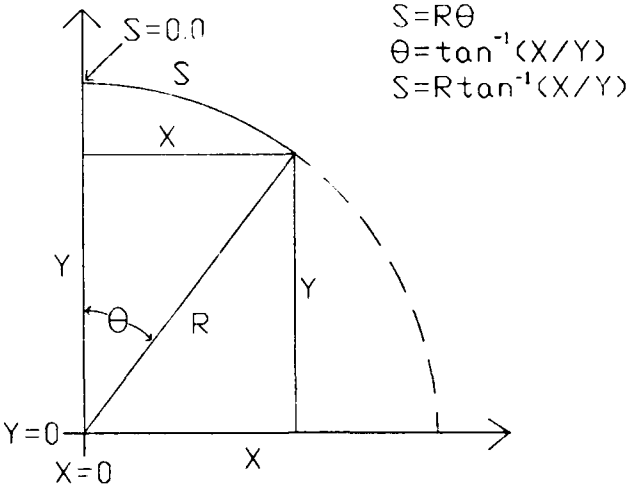

Figure 4.9 Computation of arclength s from x-y coordinates

The Fortran programs used at MIT for data post-processing are documented by Appendix A. Four programs are included:

(1) PROCESS.F: used to compute the acoustic intensity from the pressure cross spectrum,

(2) HEADER.F: used to display the data header contents,

(3) PLOTDAT.F: used to collect the intensity data into third octave bands and to calculate 2-D grid coordinates from the 3-D grid point locations.

(4) POWERRAD.F: used to compute the sound power radiated over the area analyzed.

To verify the computer algorithms for processing the data, a sampling of pressure measurements at 15 kHz and the calculated intensity results were analyzed. This data is included as Appendix B.

CHAPTER 5
EXPERIMENTAL RESULTS

5.1 DESCRIPTION OF DATA PRESENTATION

Experimental results for the two tank conditions, empty and full, are presented by this chapter. Section 5.2 presents the radiated power over the portion of hull surface for which data was analyzed. The radiated power was determined by summing the intensity measurements and multiplying by the appropriate area. The computer program used to generate the radiated power values is documented in Appendix A. Section 5.3 and Section 5.4 present the intensity plots for the two tank conditions, empty and full respectively. Section 5.5 provides a more detailed data analysis comparing the two tank conditions over a limited region of the hull surface.

Data has been collected into thirteen third octave bands for plotting. The lower, center, and upper frequency for each standard third octave band, is provided by Table 5.1. Both contour plots and 3-D plots are included for each third octave band and tank condition. The plots are generated from the acoustic intensity data using the Kriging grid method. A detailed description of the algorithms used in this grid method are provided by Ripley [26].

For the 3-D plots, lines of constant arclength S and constant axial length Z are plotted. The y-axis scale for each 3-D plot was selected to show the maximum range in acoustic intensity values, and subsequently varies considerably from plot to plot within sections 5.3 and 5.4. Care should be taken to note the scale when comparing the relative peak amplitudes between plots.

Table 5.1

Third Octave Band Frequencies for Plotting			
Band #	f_{lower}	f_{center}	f_{upper}
1	713	800	898
2	891	1000	1122
3	1114	1250	1403
4	1425	1600	1796
5	1782	2000	2245
6	2227	2500	2806
7	2806	3150	3536
8	3564	4000	4490
9	4454	5000	5612
10	5613	6300	7072
11	7127	8000	8980
12	8909	10000	11225
13	11136	12500	14031

To correlate the intensity plots with the structural features of the model, figure 5.1 shows the location of the model structural members projected to the plane of intensity measurement in the contour plot format. In the axial direction, the structural ribs are located 12 cm apart. In the circumferential direction, a dashed line represents the origin for the arclength (S) measurements. The inner and outer engine foundation supports are located at S=+/- 8.88 cm and S=+/- 18.33 cm respectively. These supports extend the axial length of the model within the tank section. The tank top intersects the hull at S=+/- 32.47 cm. The outermost grid points are located at S=+/- 43.49 cm, 6 vertical cm below the design waterline.

The plots presented in the remainder of this chapter include only the area on the starboard side of the model from S=0.64 to S=43.49 cm and Z=-36.00 to Z=36.00 cm. This represents half of the underwater area scanned, that being on the side of the model furthest from the shaker.

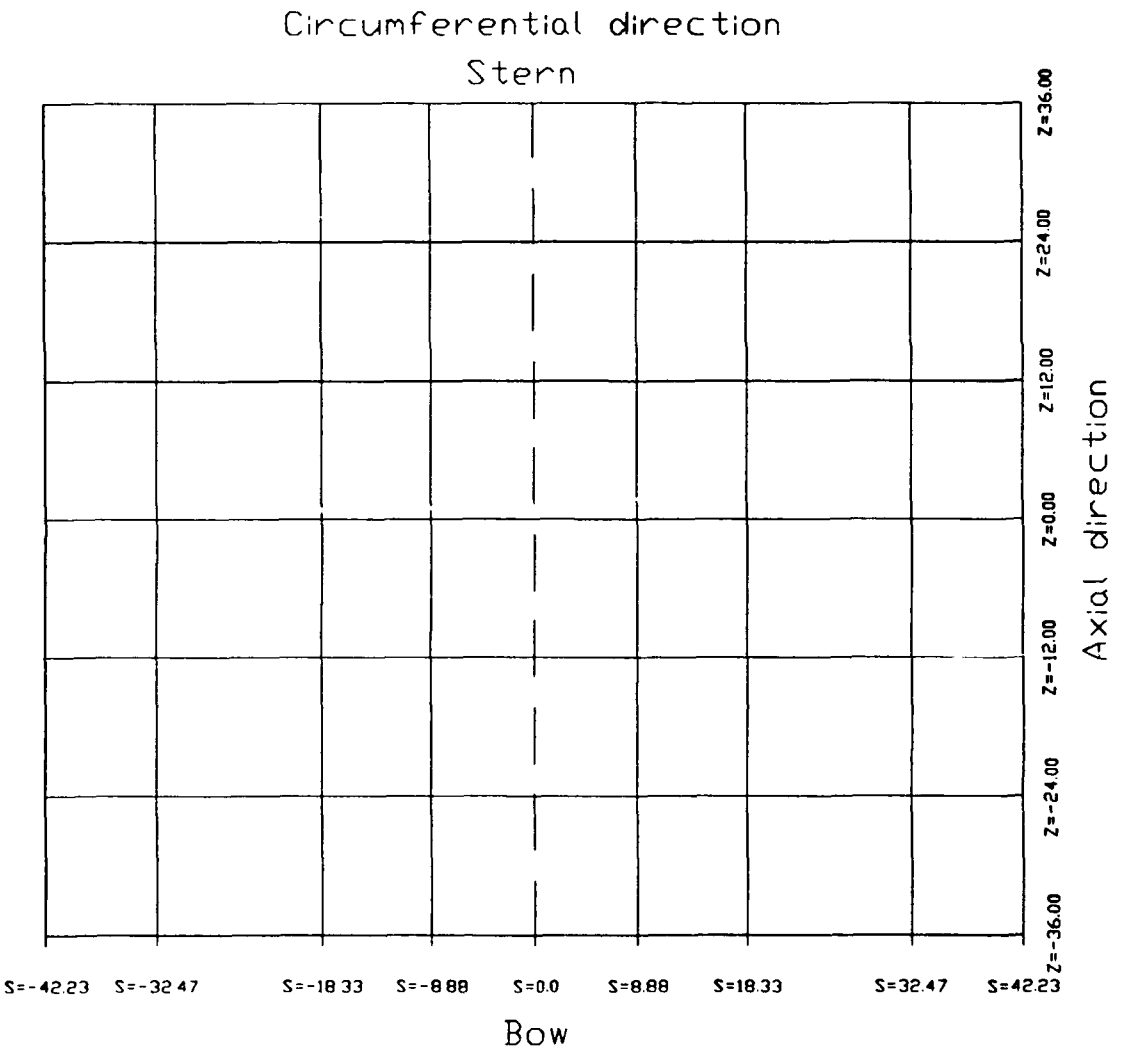

Figure 5.1 Location of Model Structural Members in Intensity Plots

5.2 RADIATED POWER

Figure 5.2 shows the sound power radiated from the model area analyzed for the tank empty and full conditions. As found by Levi [2], the water in the storage tank leads to increased radiated sound power over the entire frequency range of interest (640 Hz to 15 kHz). Also as found by Levi, this increase is greater in the lower and higher third octave bands analyzed than in the intermediate range (5 kHz - 8 kHz). The power radiation values for the tank empty condition in the third octave bands with center frequencies of 6.3 kHz through 12.5 kHz are negative and therefore do not appear in figure 5.2. Negative values for radiated power indicate that a greater amount of nearfield energy is circulating back into the structure relative to that which is going radially outwards. Numerical values for the power radiated are provided by Table 5.2.

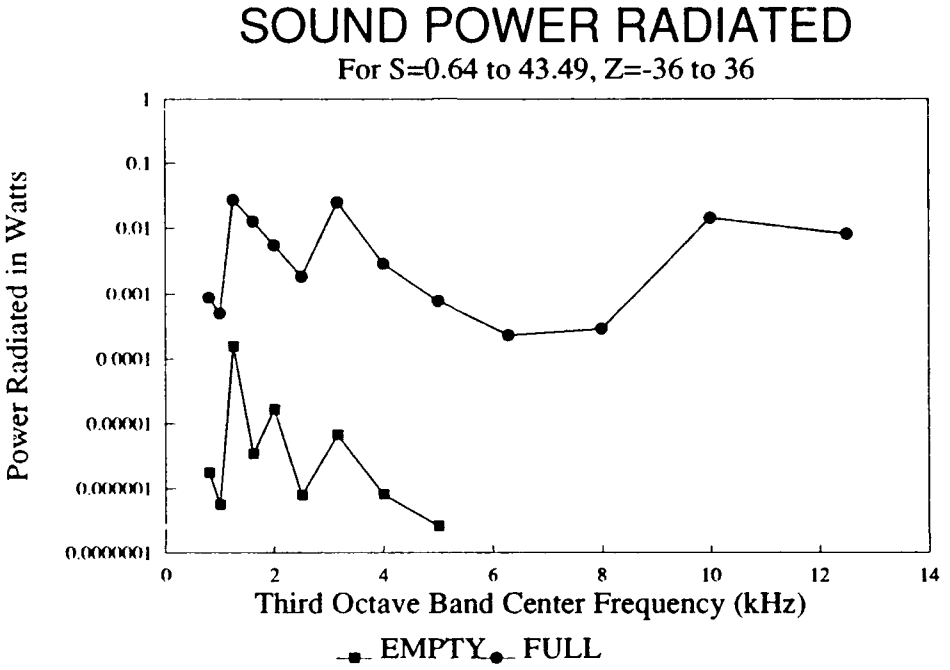

Figure 5.2 Sound Power Radiated

Table 5.2

POWER RADIATED in WATTS over the area S=0.64 to 43.49, Z=-36 to 36			
CENTER FREQUENCY	TANK EMPTY	TANK FULL	DELTA (Full-Empty)
800	1.758E-06	8.705E-04	8.687E-04
1000	5.614E-07	4.961E-04	4.955E-04
1250	1.542E-04	2.667E-02	2.652E-02
1600	3.401E-06	1.263E-02	1.262E-02
2000	1.663E-05	5.508E-03	5.492E-03
2500	7.763E-07	1.801E-03	1.800E-03
3150	6.691E-06	2.495E-02	2.494E-02
4000	7.980E-07	2.842E-03	2.841E-03
5000	2.570E-07	7.485E-04	7.483E-04
6300	-9.478E-08	2.234E-04	2.235E-04
8000	-1.957E-07	2.802E-04	2.804E-04
10000	-5.054E-06	1.425E-02	1.426E-02
12500	-2.010E-06	7.932E-03	7.934E-03

5.3 ACOUSTIC INTENSITY PLOTS FOR TANK EMPTY

Figures 5.3 through 5.15 present the acoustic intensity plots for the tank empty condition. All plots show a line of relatively strong intensity peaks along the arclength S=34.31 cm. As seen from figure 5.1, this arclength is very near and slightly above the structural discontinuity where the tank top intersects the hull surface. There are also two rows of peaks with varying but lesser intensity magnitude along S=22.07 cm and S=6.76 cm for the bands with center frequencies between 0.8 - 1.6 kHz and 8-12.5 kHz. These arclengths correspond with the outer and inner engine foundation supports respectively. For the intermediate third octave bands, these secondary lines of intensity peaks are not as well-defined.

Axially, the major peaks along the tank top structural discontinuity (S=34.31 cm) tend to occur at the locations where the structural ribs connect to the hull. This tendency is most clearly seen in the lower frequency bands and over the ribs closest to the model's stern.

These results are not surprising, in that structural discontinuities are known to be sources of sound radiation.

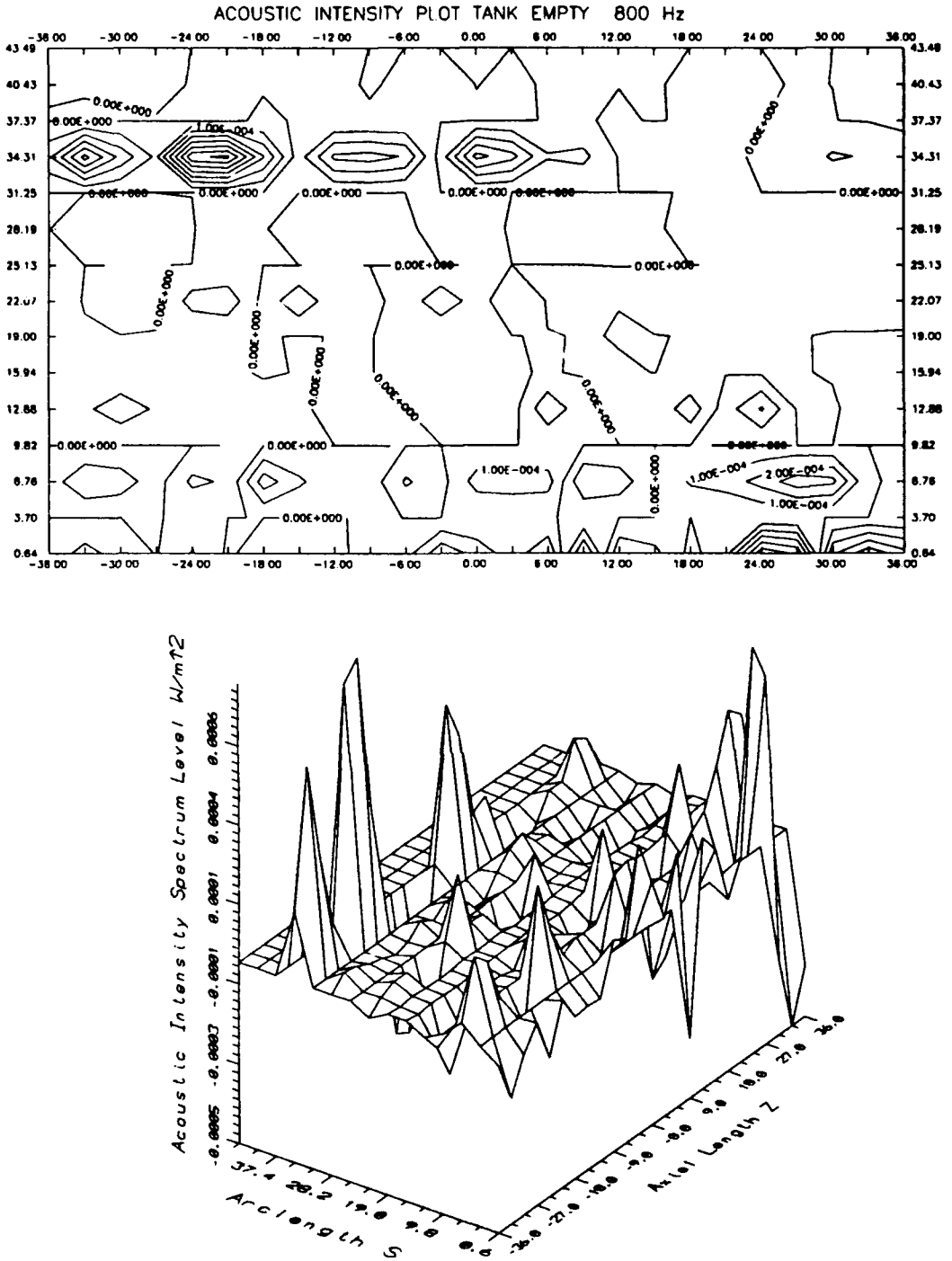

Figure 5.3 Tank Empty 800 Hz

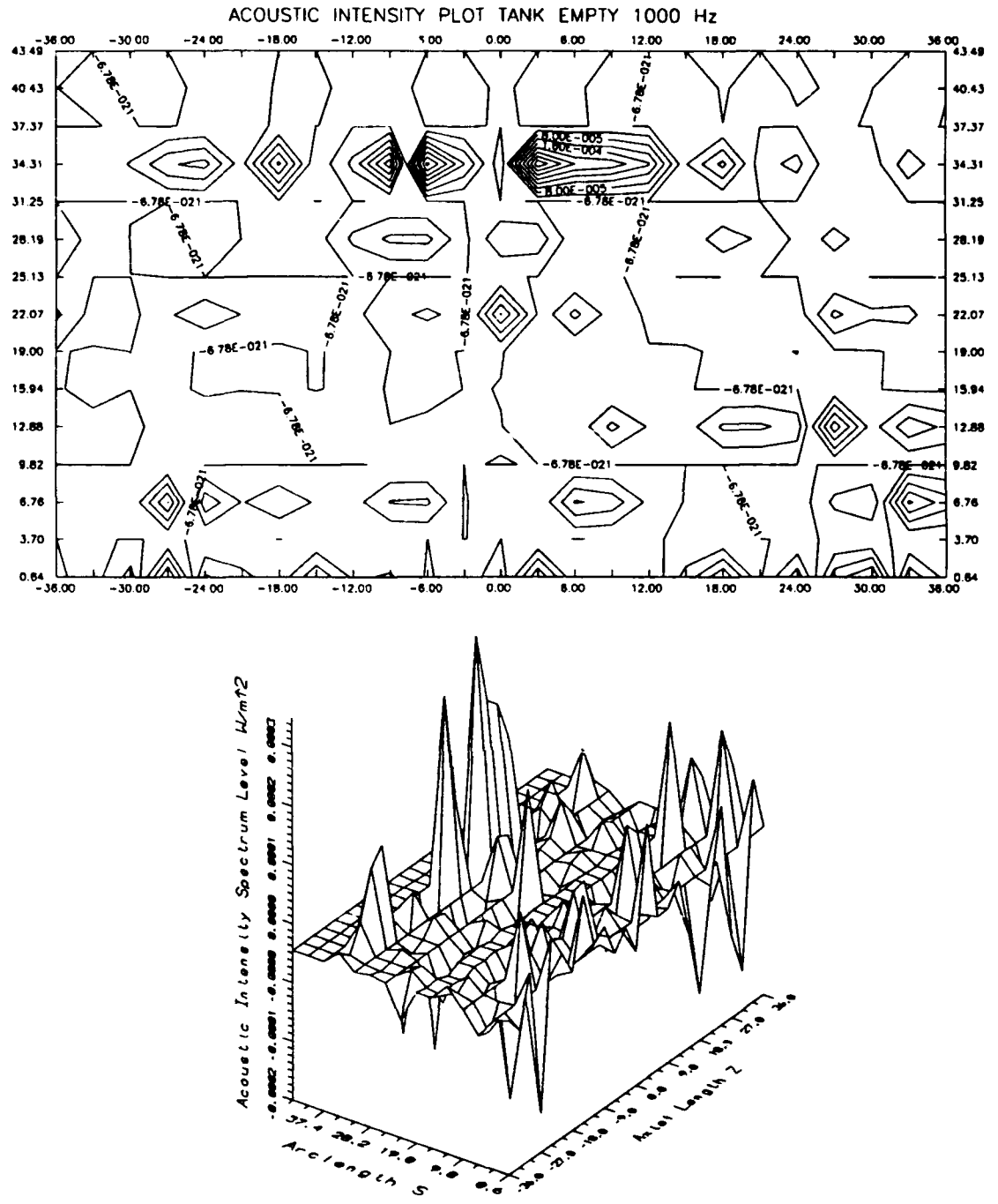

Figure 5.4 Tank Empty 1000 Hz

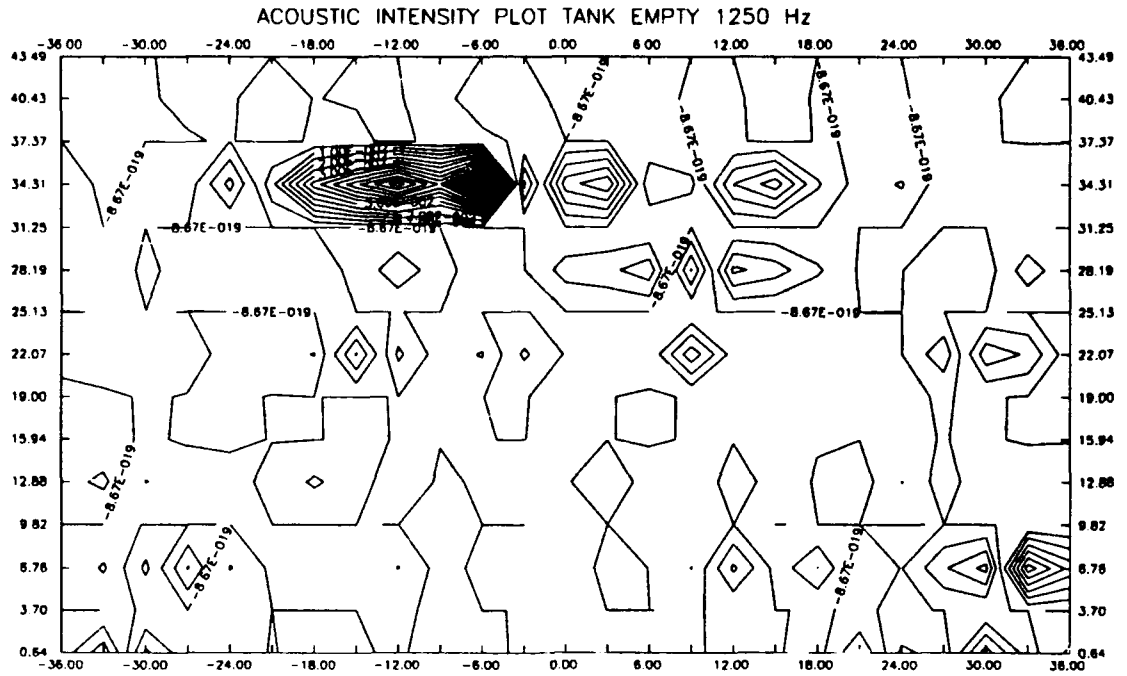

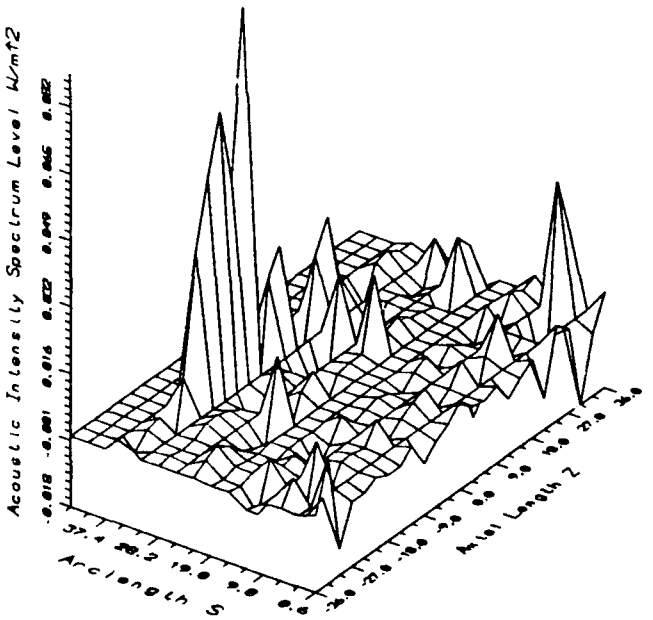

Figure 5.5 Tank Empty 1250 Hz

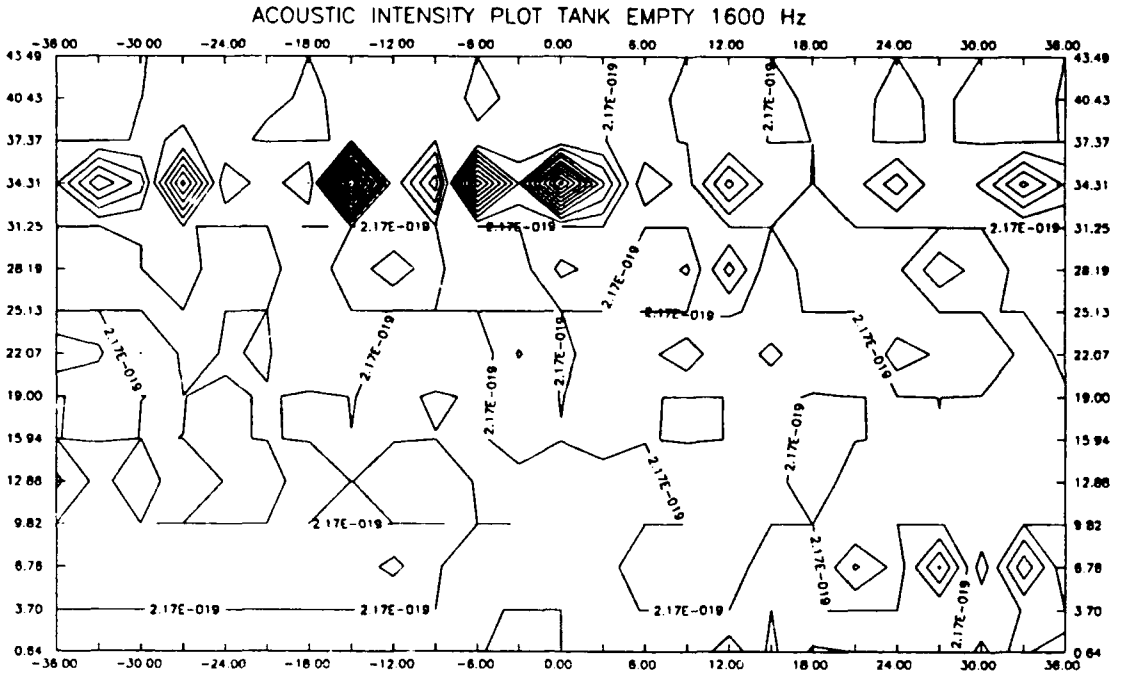

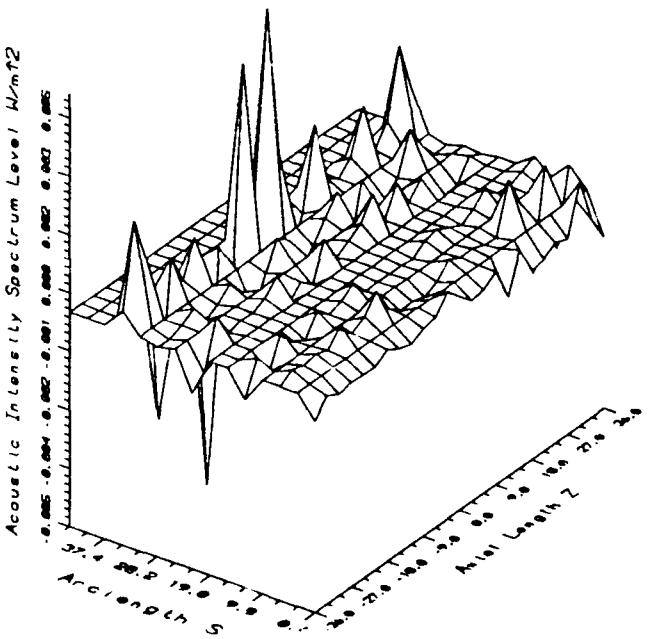

Figure 5.6 Tank Empty 1600 Hz

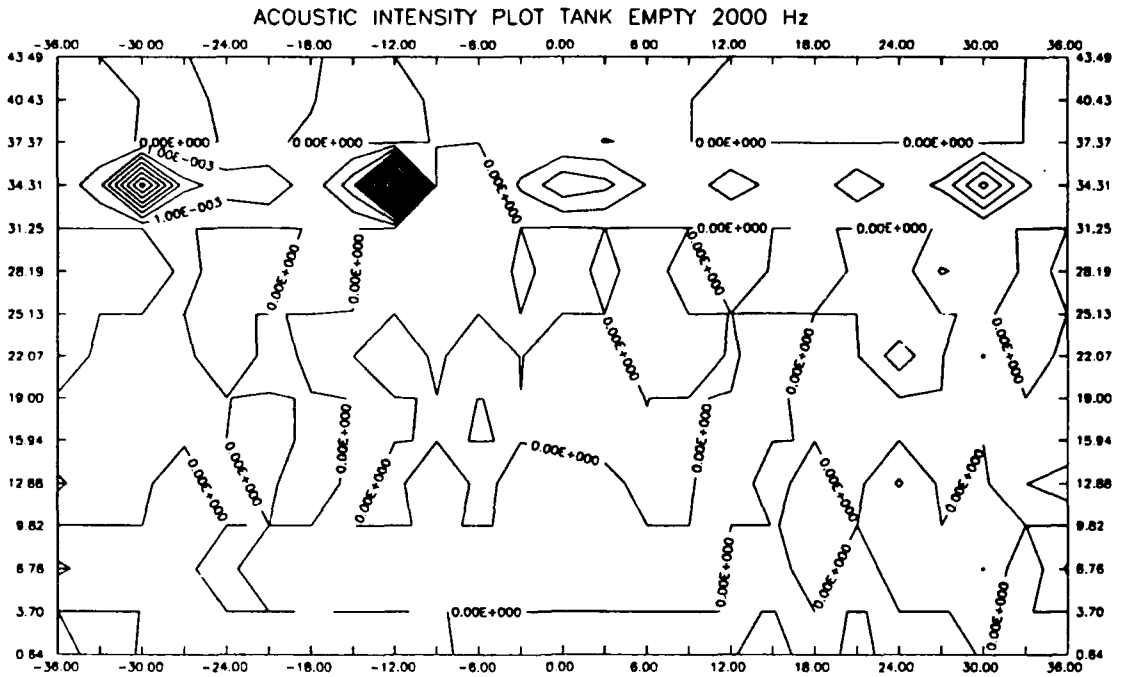

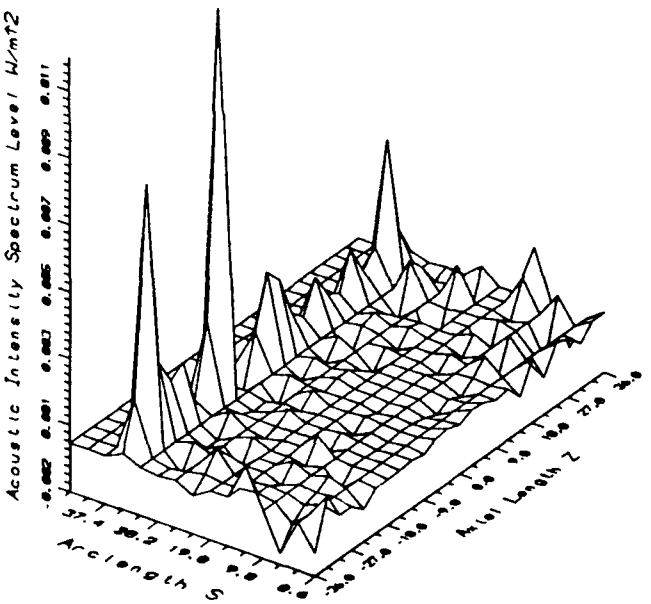

Figure 5.7 Tank Empty 2000 Hz

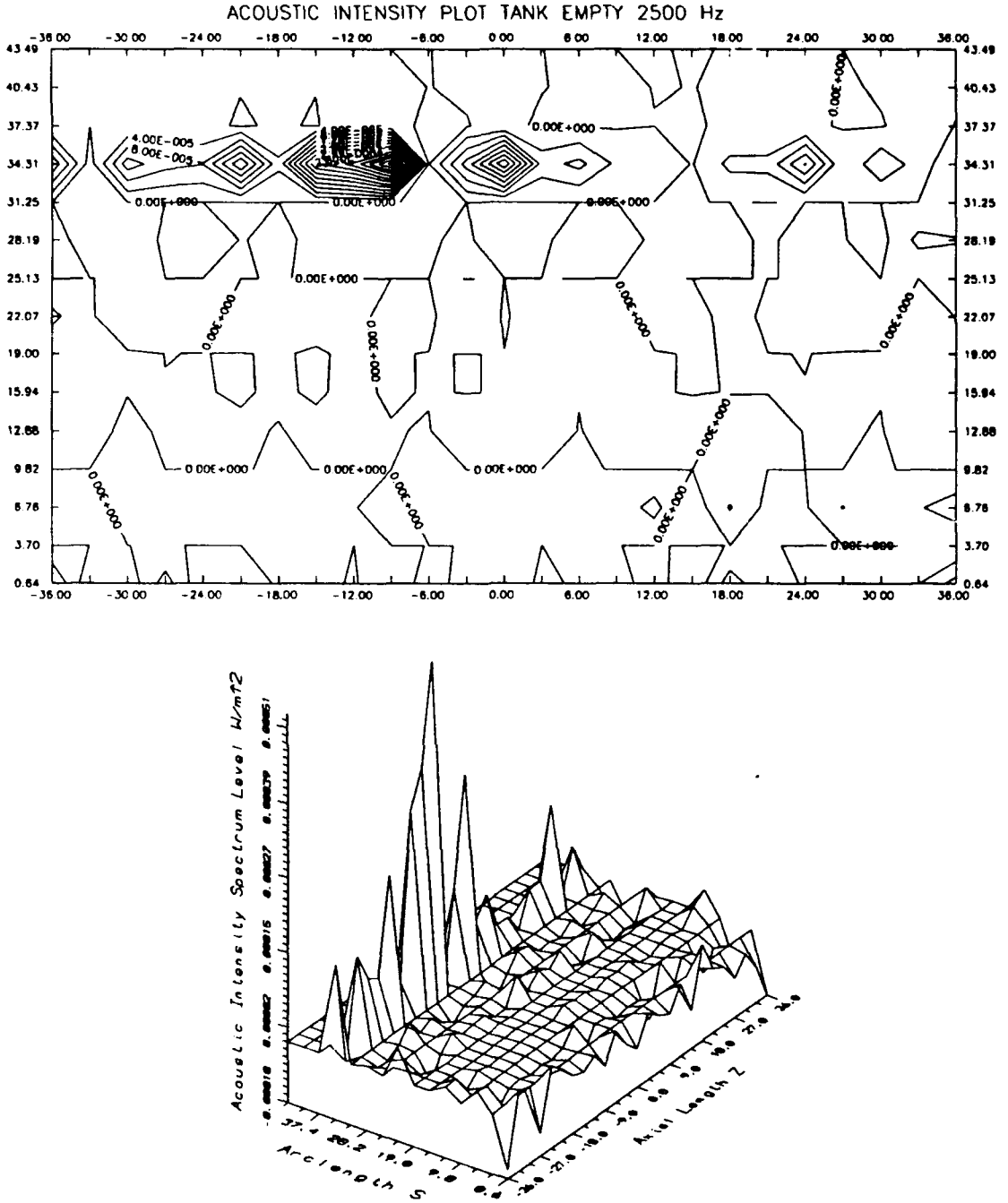

Figure 5.8 Tank Empty 2500 Hz

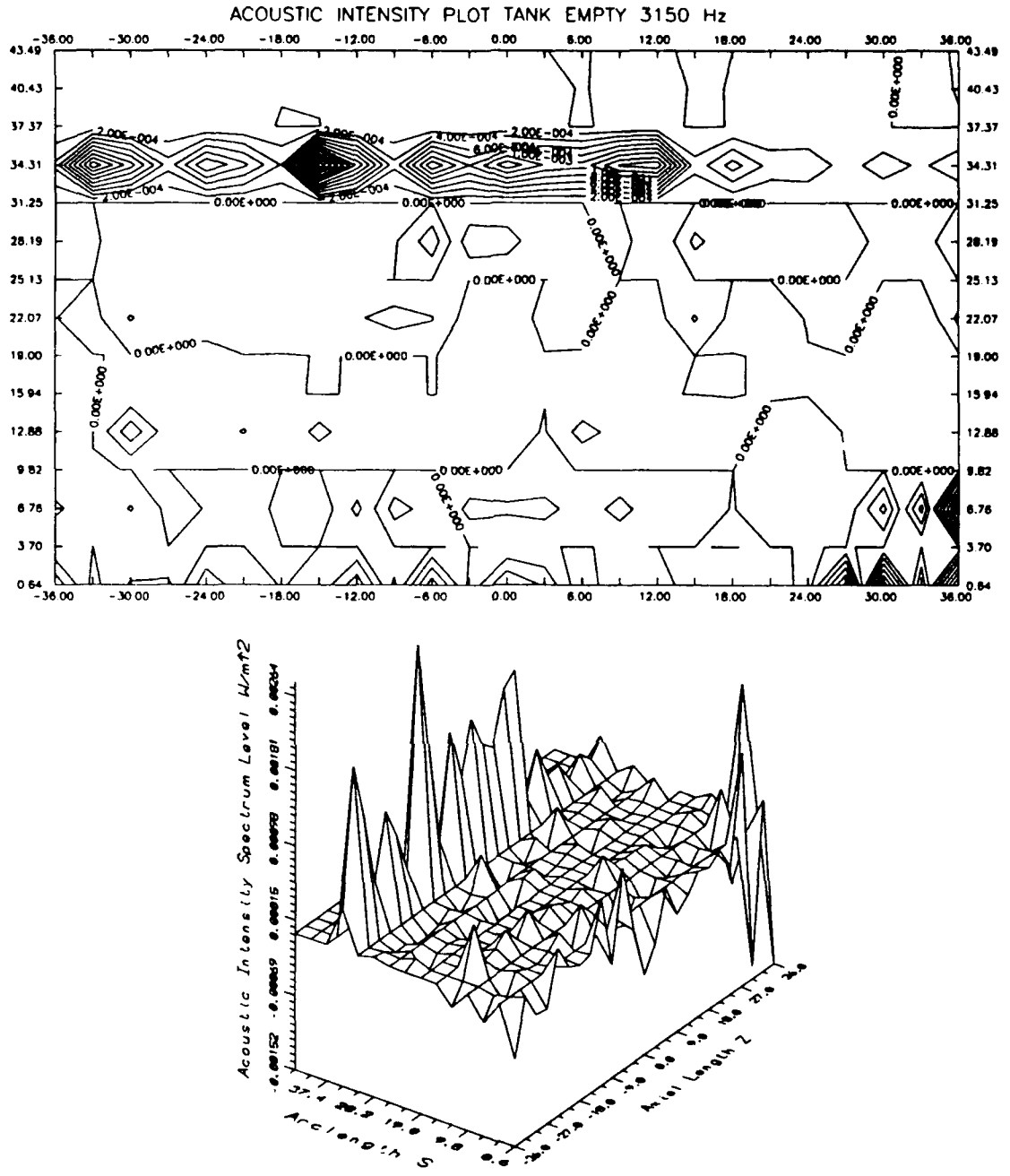

Figure 5.9 Tank Empty 3150 Hz

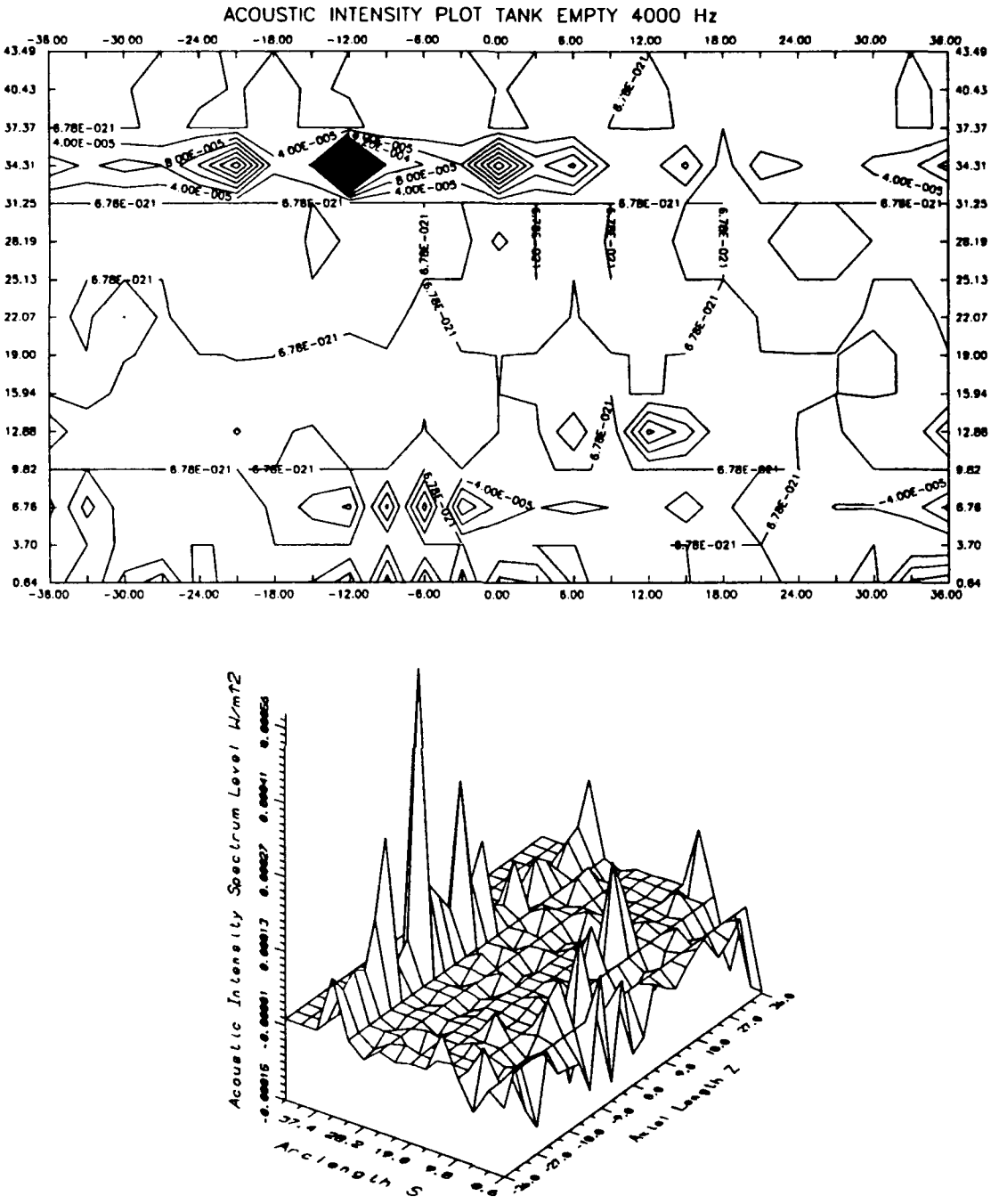

Figure 5.10 Tank Empty 4000 Hz

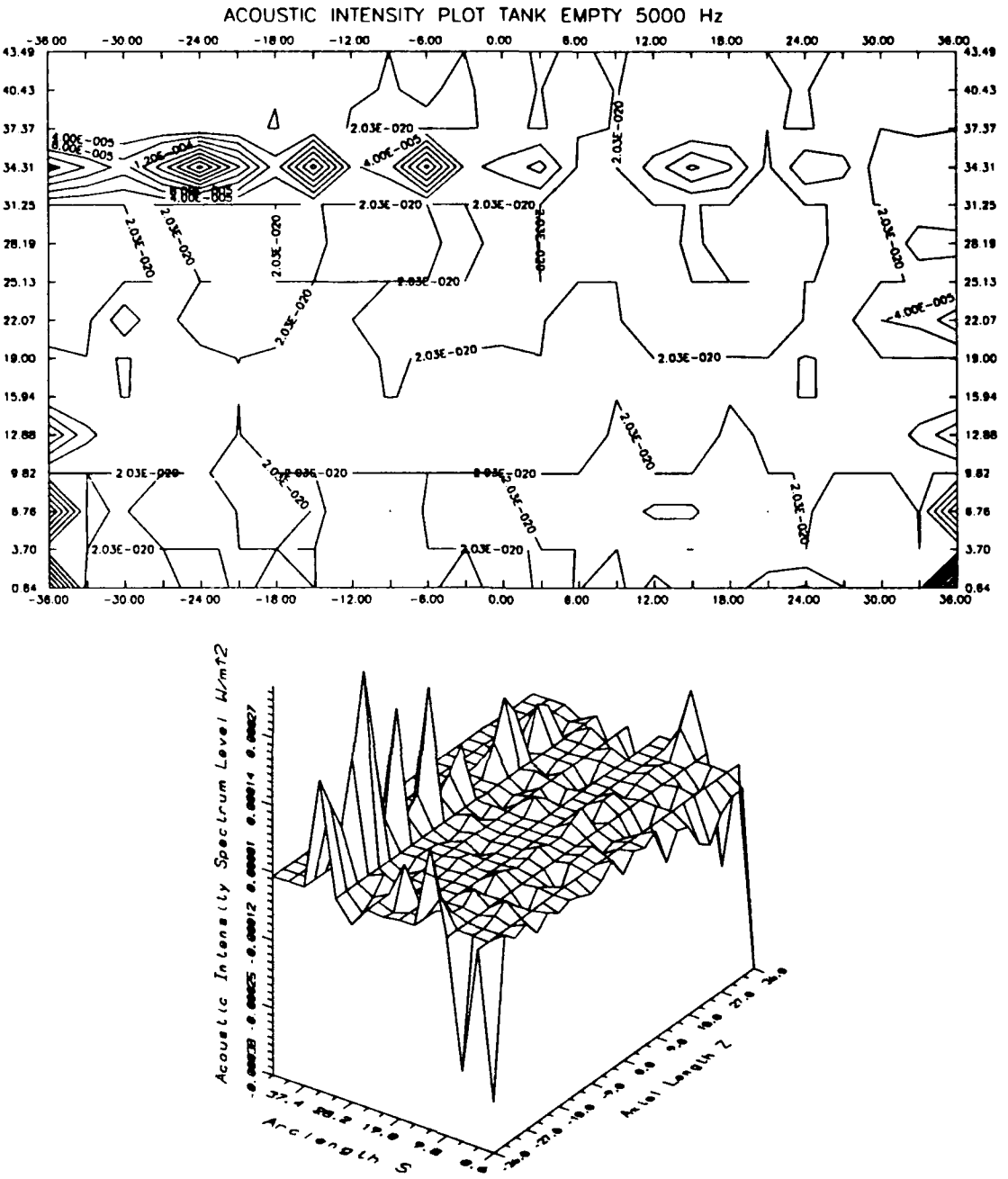

Figure 5.11 Tank Empty 5000 Hz

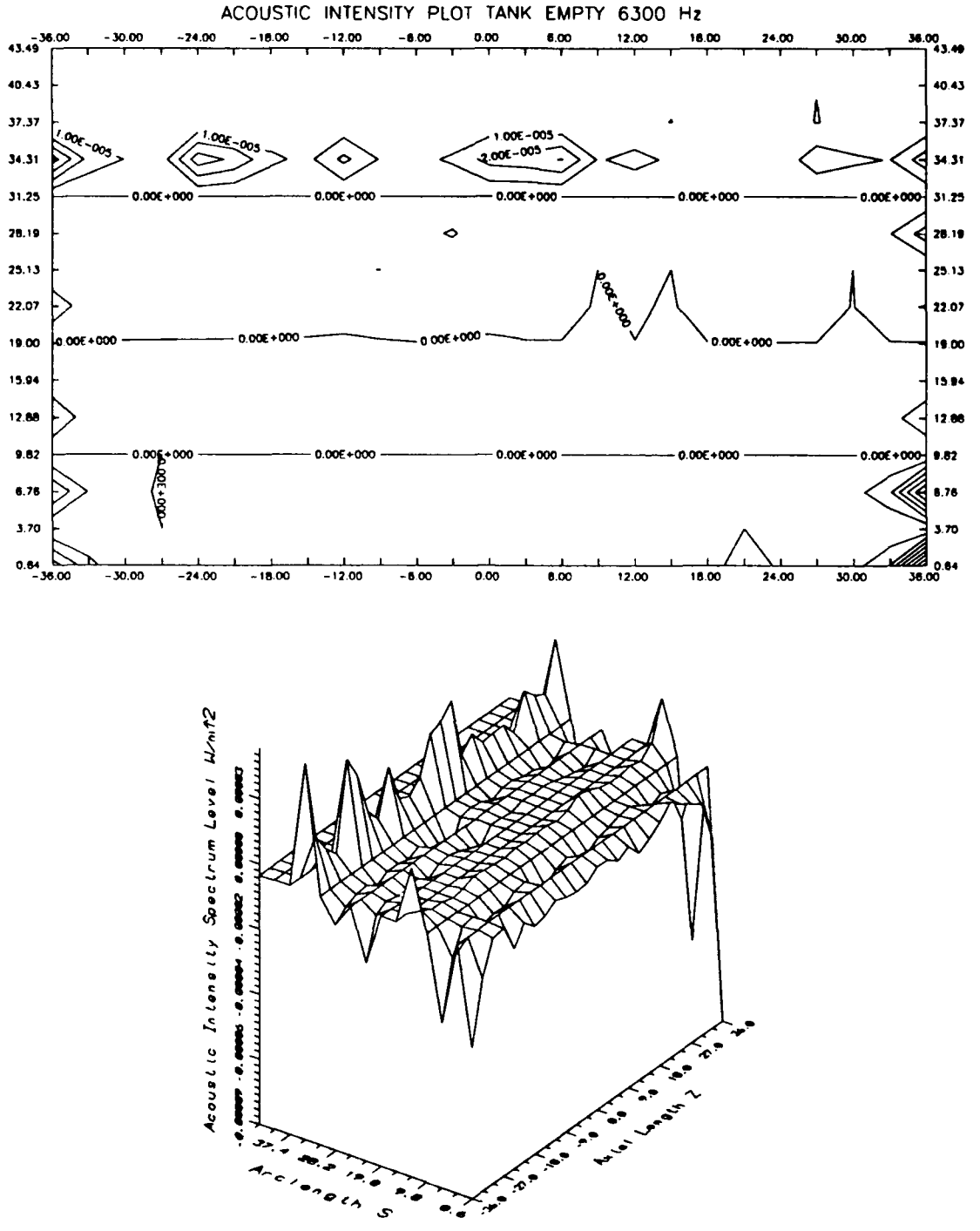

Figure 5.12 Tank Empty 6300 Hz

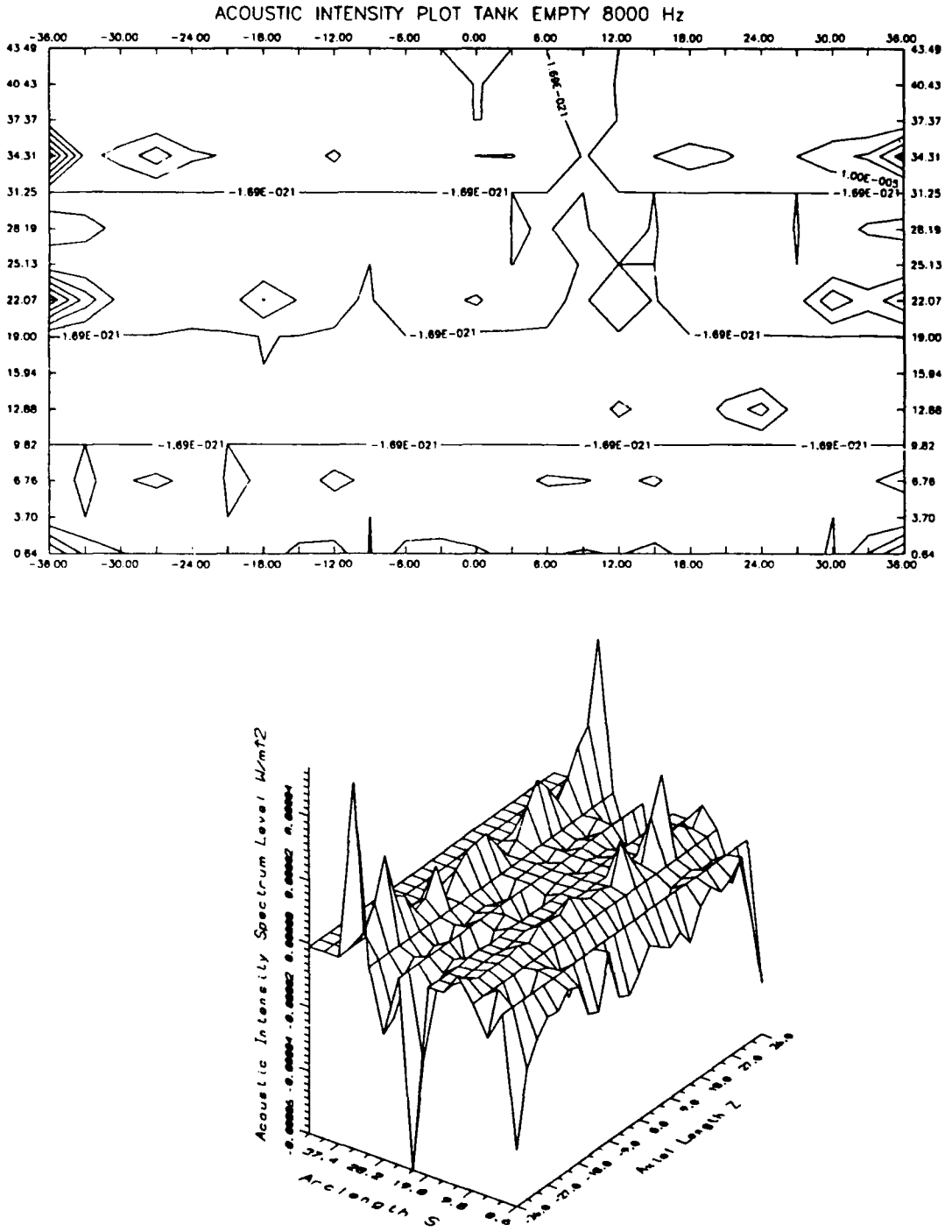

Figure 5.13 Tank Empty 8000 Hz

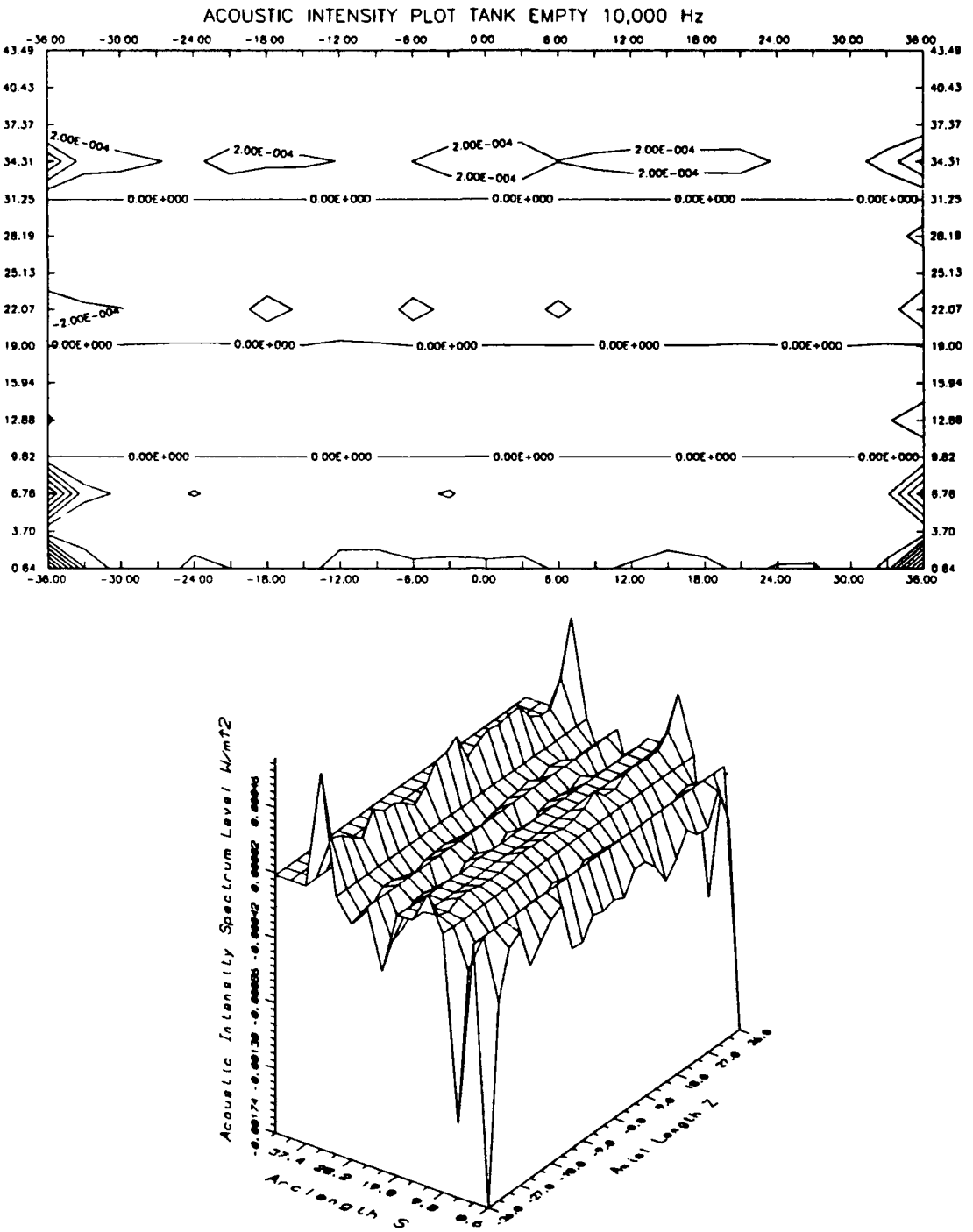

Figure 5.14 Tank Empty 10,000 Hz

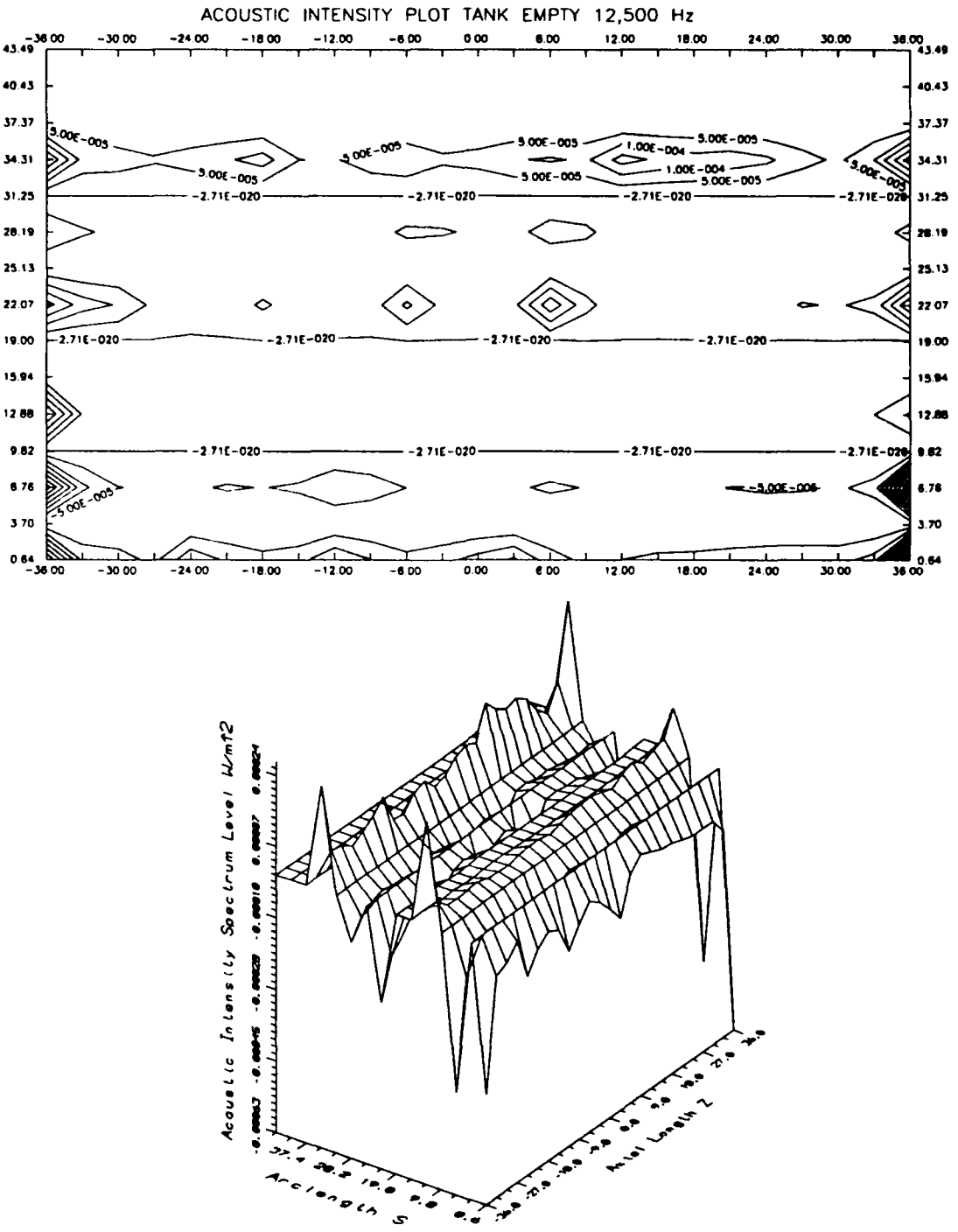

Figure 5.15 Tank Empty 12,500 Hz

5.4 ACOUSTIC INTENSITY PLOTS FOR TANK FULL

Figures 5.16 through 5.28 present the acoustic intensity plots for the tank full condition. These plots are characterized by a single broad line of intensity peaks with bases ranging between the arclengths S=22.07 cm and S=32.47 cm. The maximum intensity values tend to occur along S=28.19 cm. Note that these maximum intensity values are significantly greater compared to those for the tank empty condition. This region of intensity peaks encompasses the tank top structural discontinuity and the top 5.8 vertical cm of the tank hull plating. (From figure 3.3, the maximum depth of the tank is 11 cm.) This region is illustrated by figure 5.29.

Between the arclengths S=0.64 cm to S=22.07 cm, all plots exhibit acoustic intensity values that are essentially zero relative to the maximum intensity peaks. The plots show no significant peaks corresponding to the engine support structural discontinuities. There is also no conclusive correlation between the location of the structural ribs and the acoustic intensity peaks in the primary region of sound radiation.

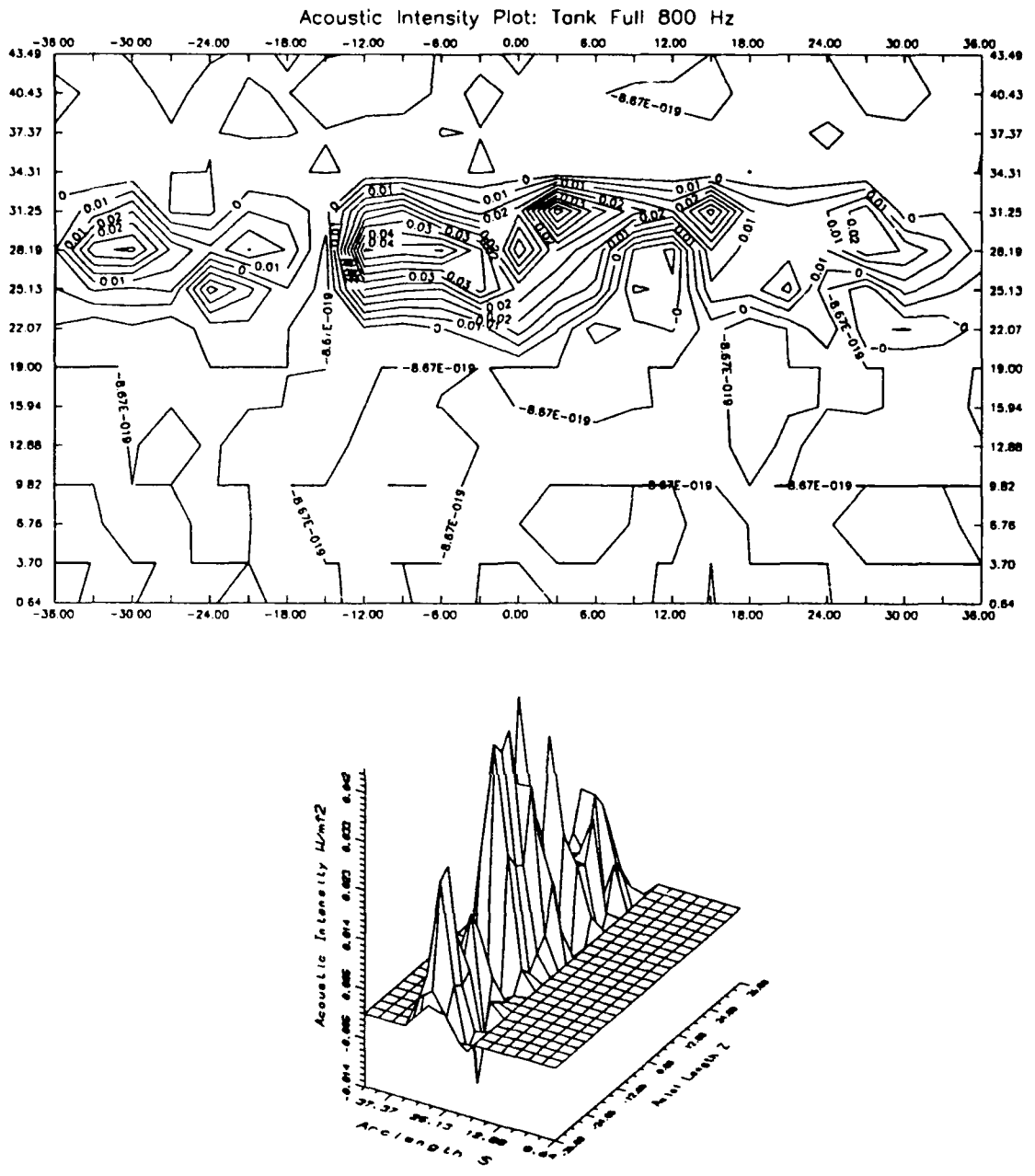

Figure 5.16 Tank Full 800 Hz

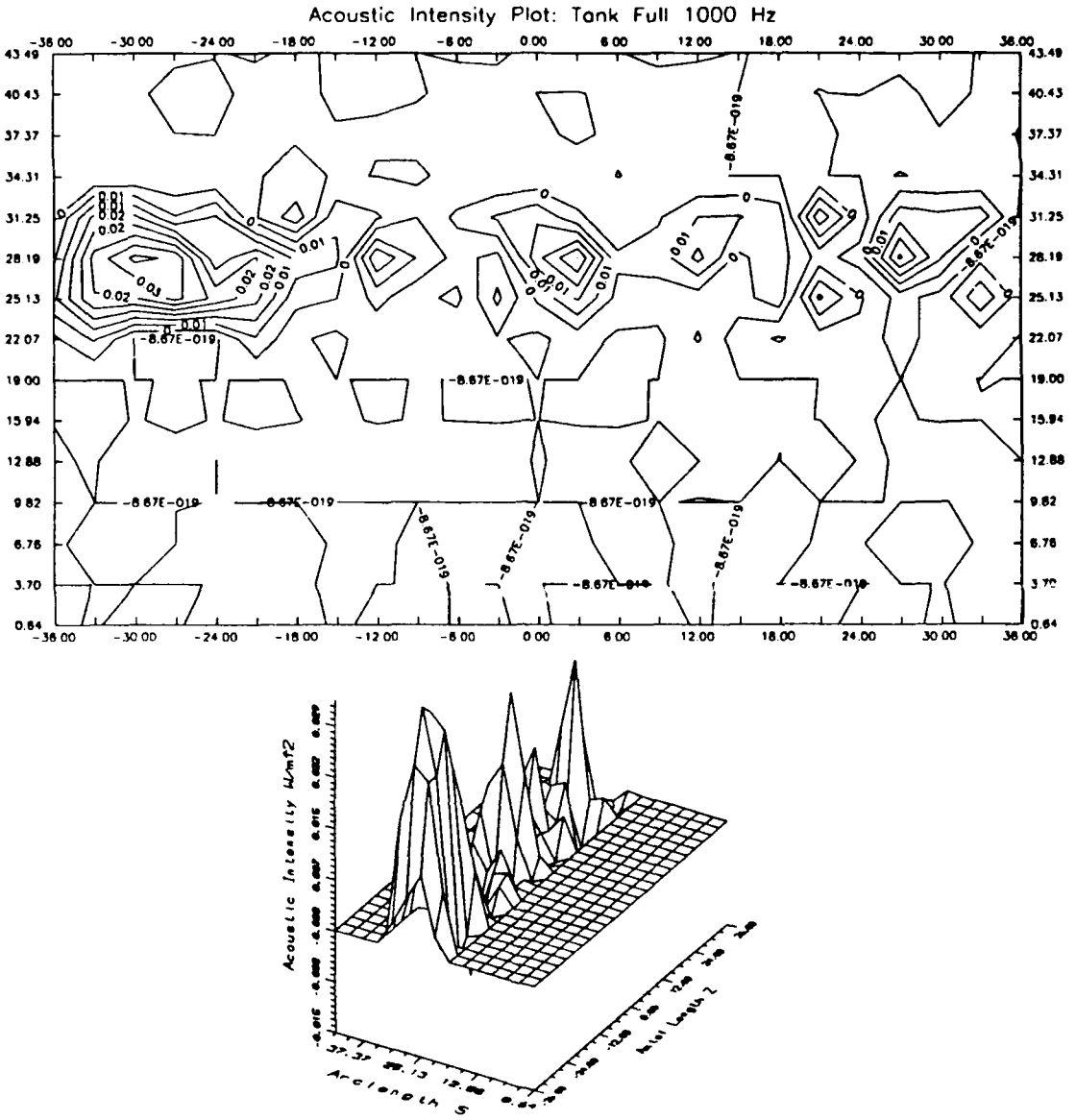

Figure 5.17 Tank Full 1000 Hz

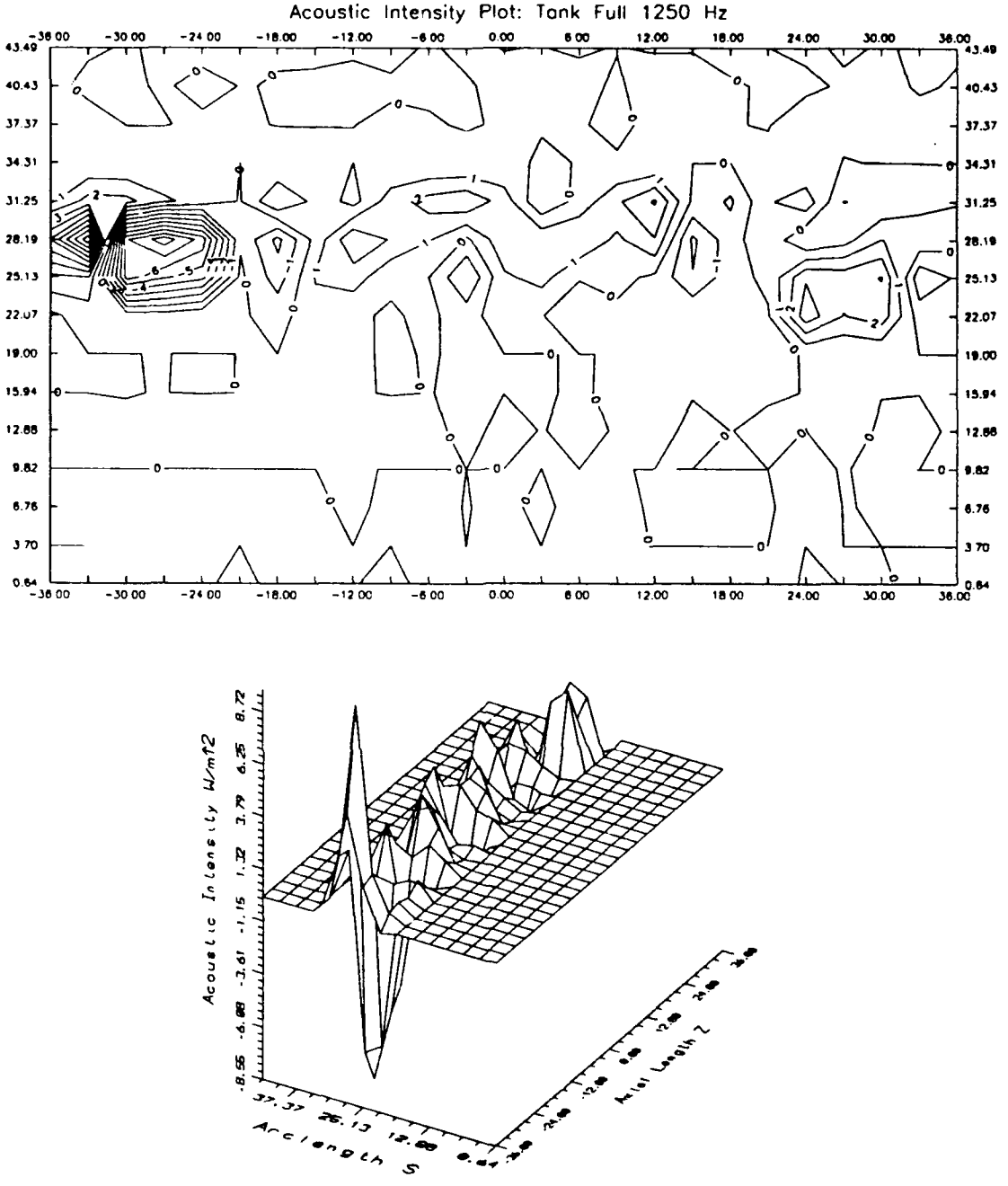

Figure 5.18 Tank Full 1250 Hz

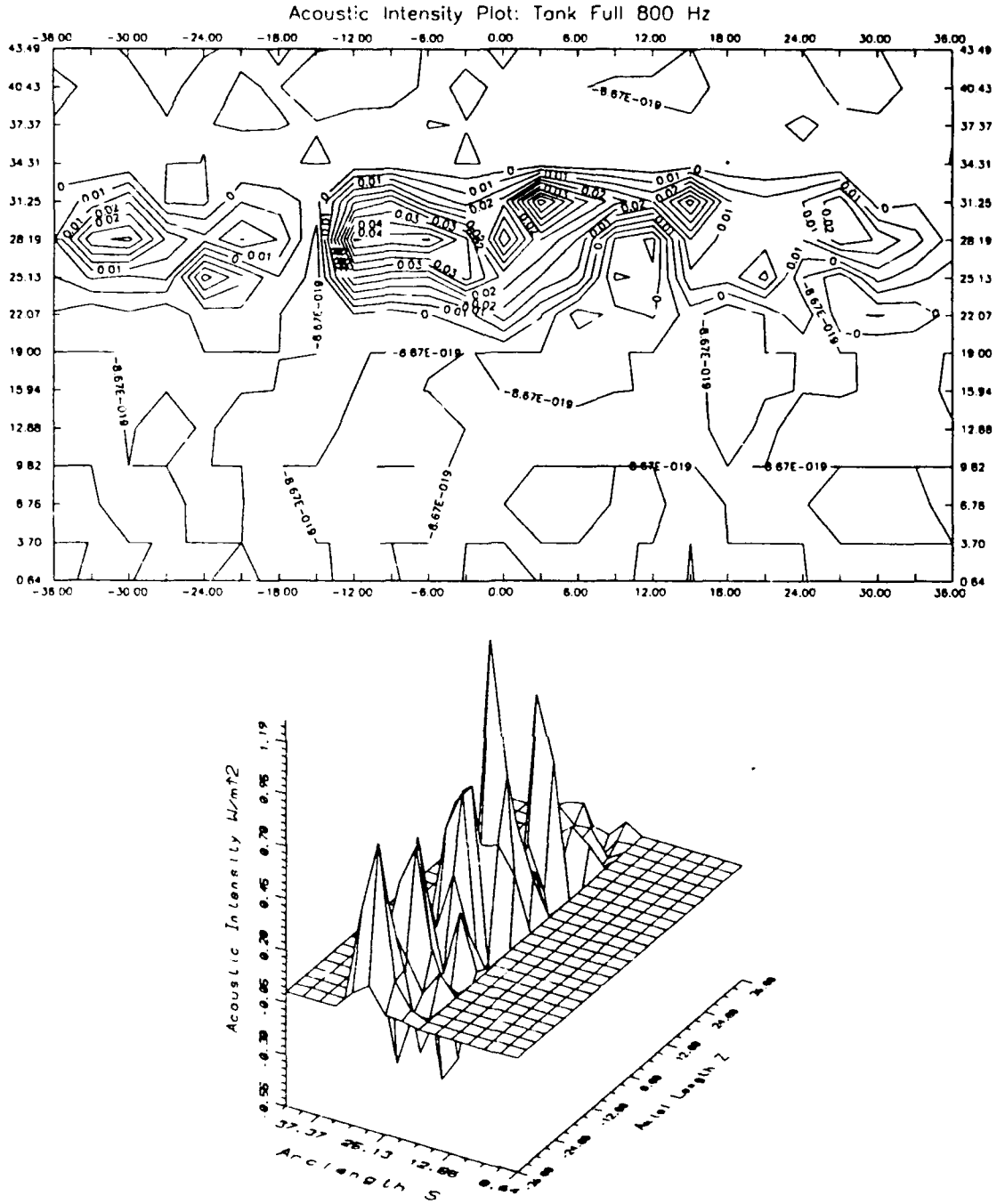

Figure 5.19 Tank Full 1600 Hz

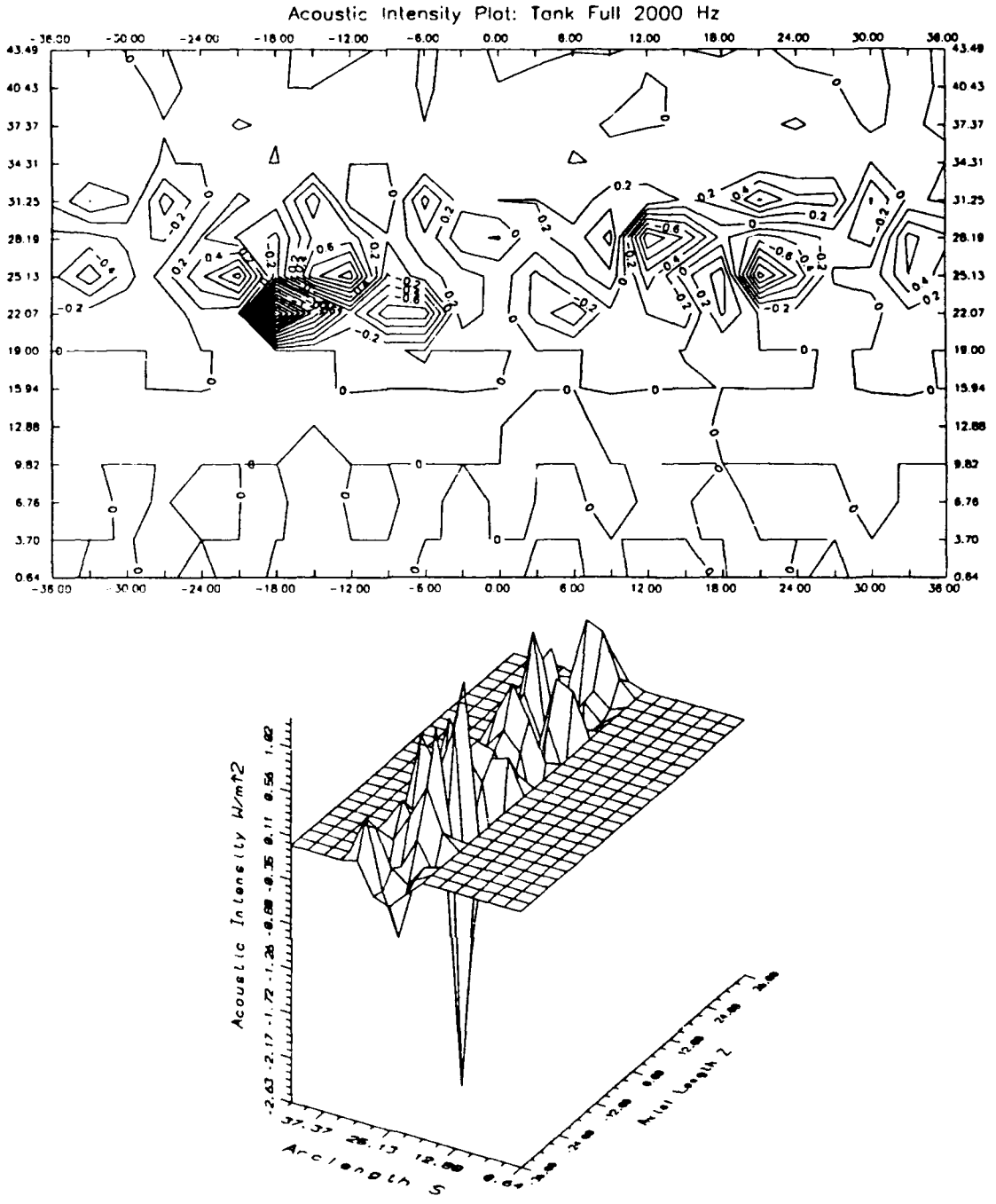

Figure 5.20 Tank Full 2000 Hz

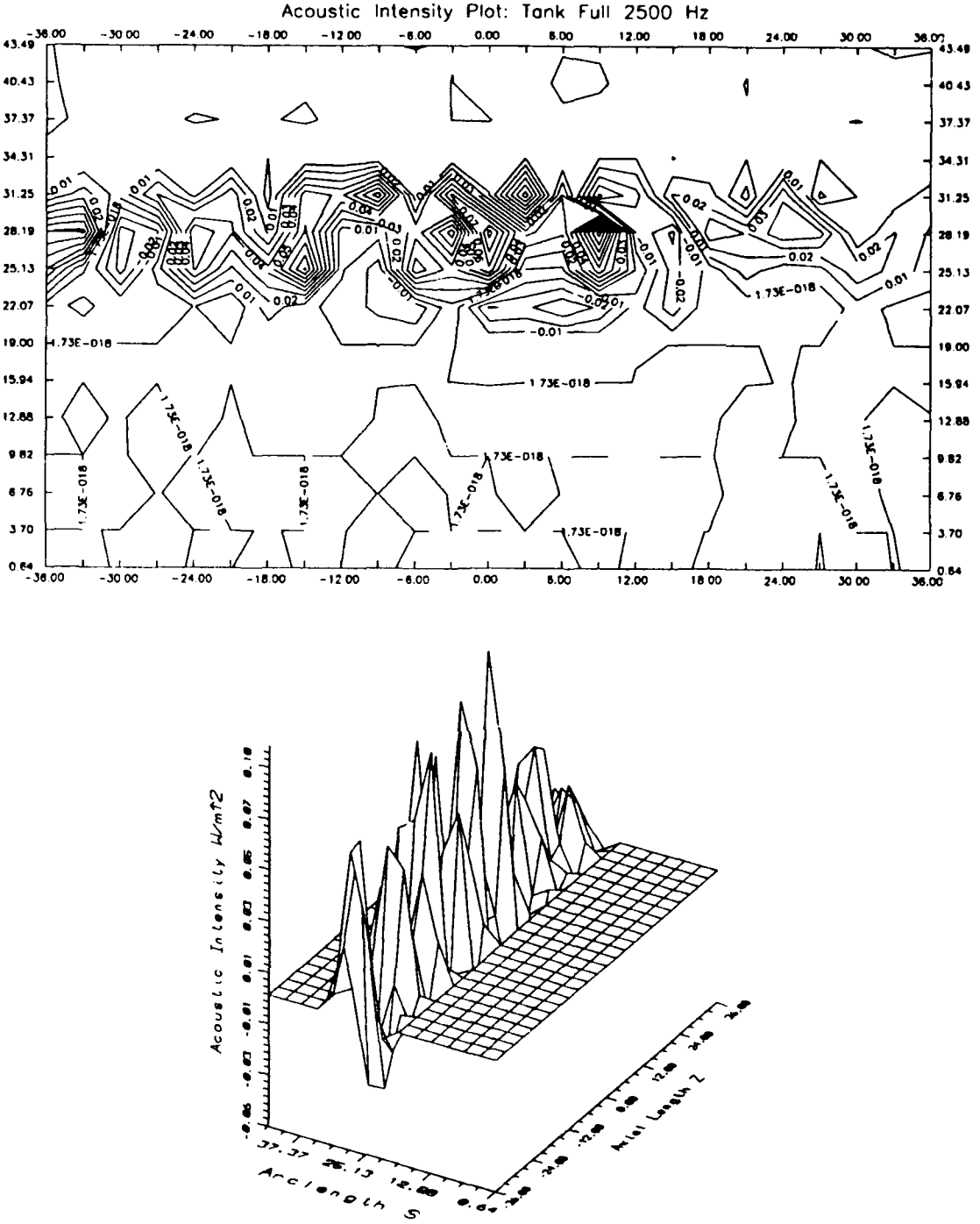

Figure 5.21 Tank Full 2500 Hz

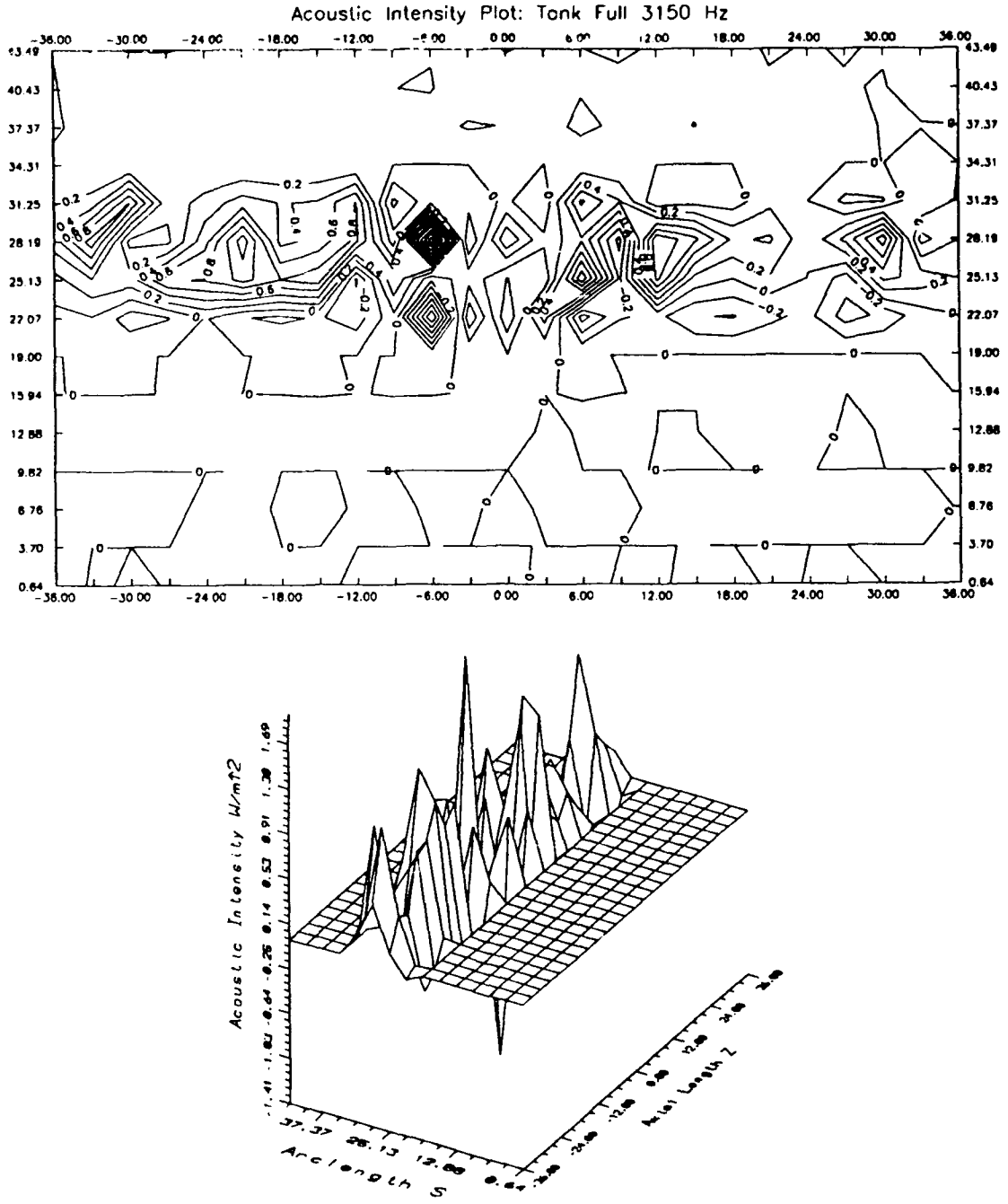

Figure 5.22 Tank Full 3150 Hz

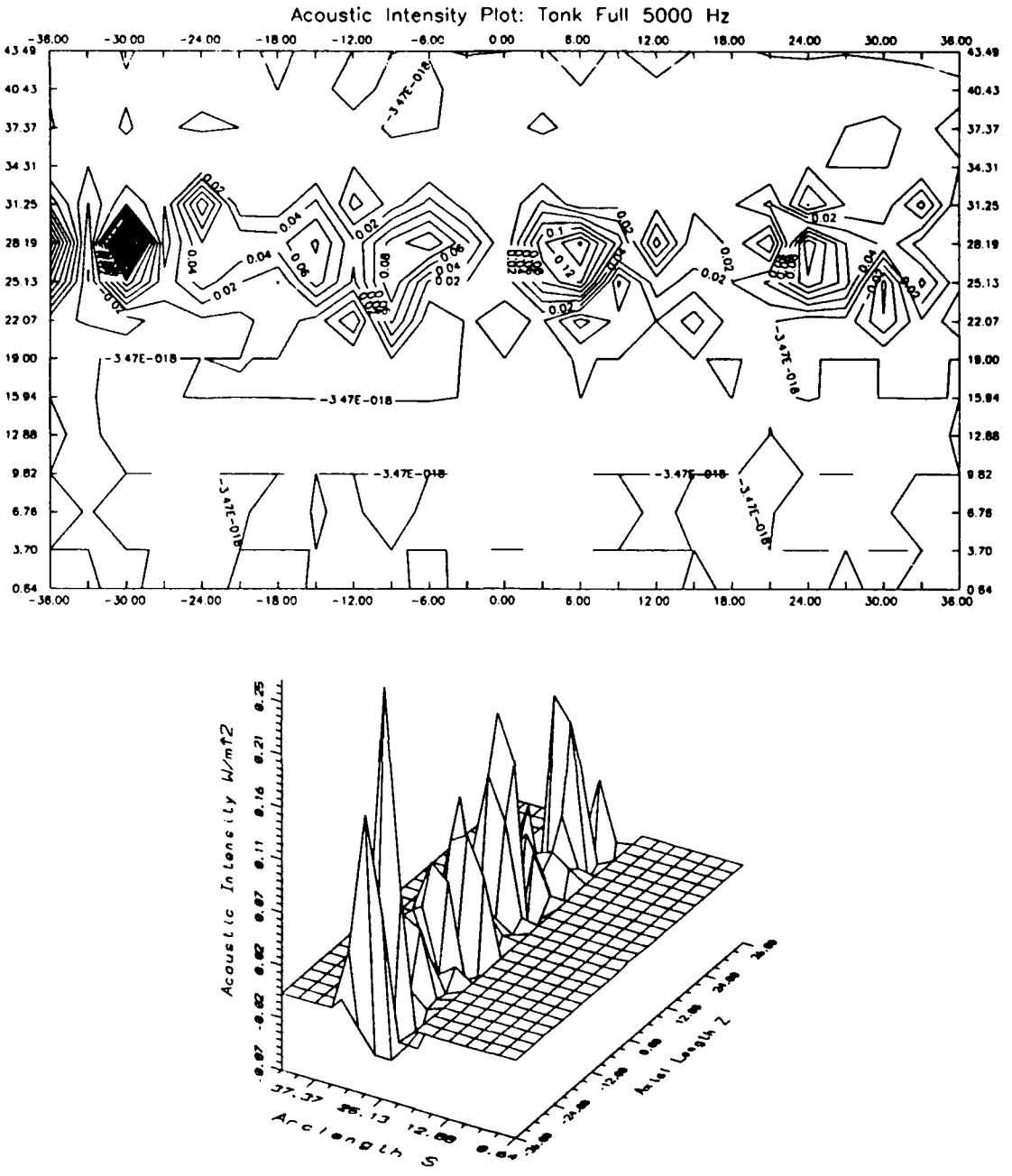

Figure 5.23 Tank Full 4000 Hz

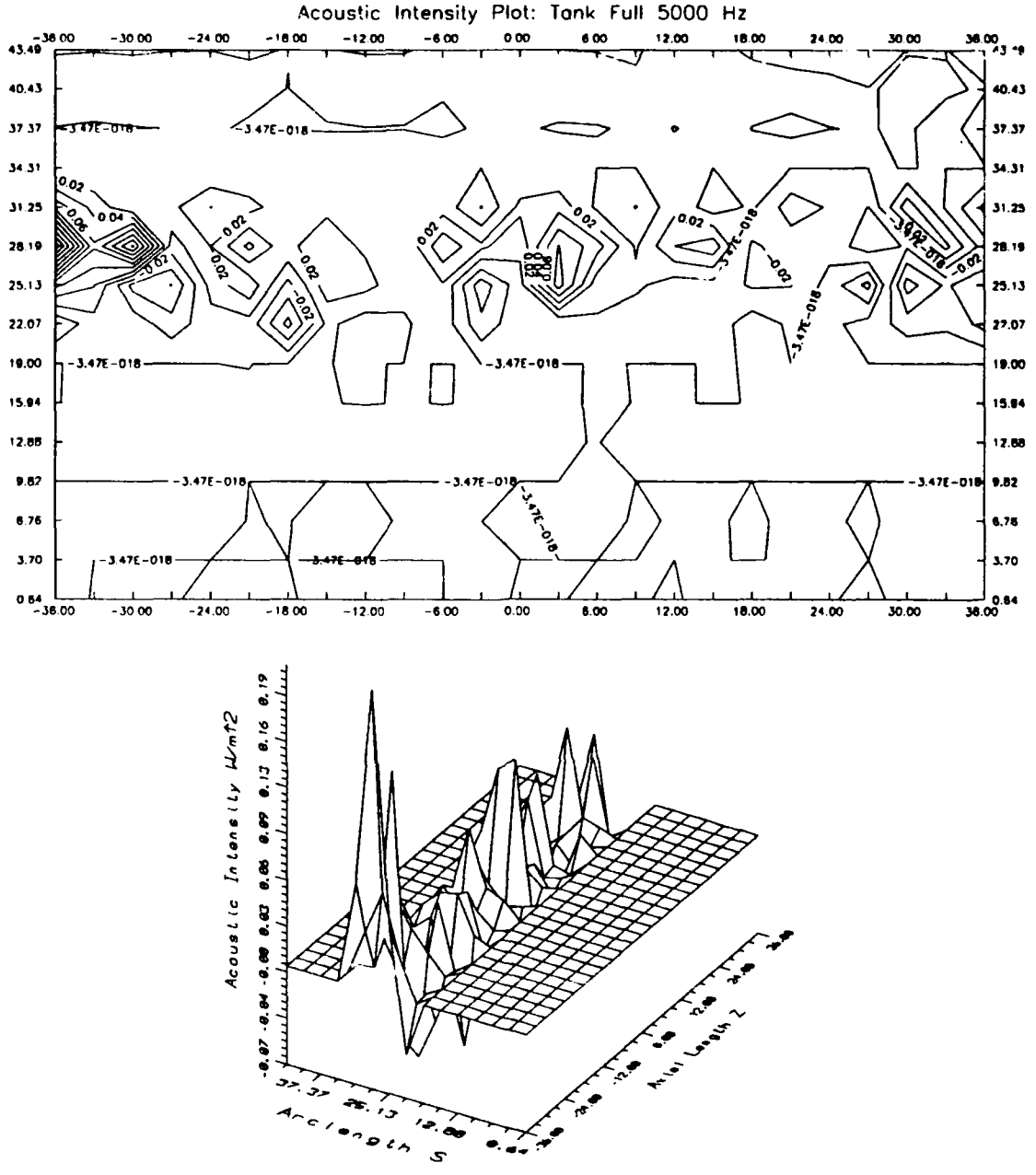

Figure 5.24 Tank Full 5000 Hz

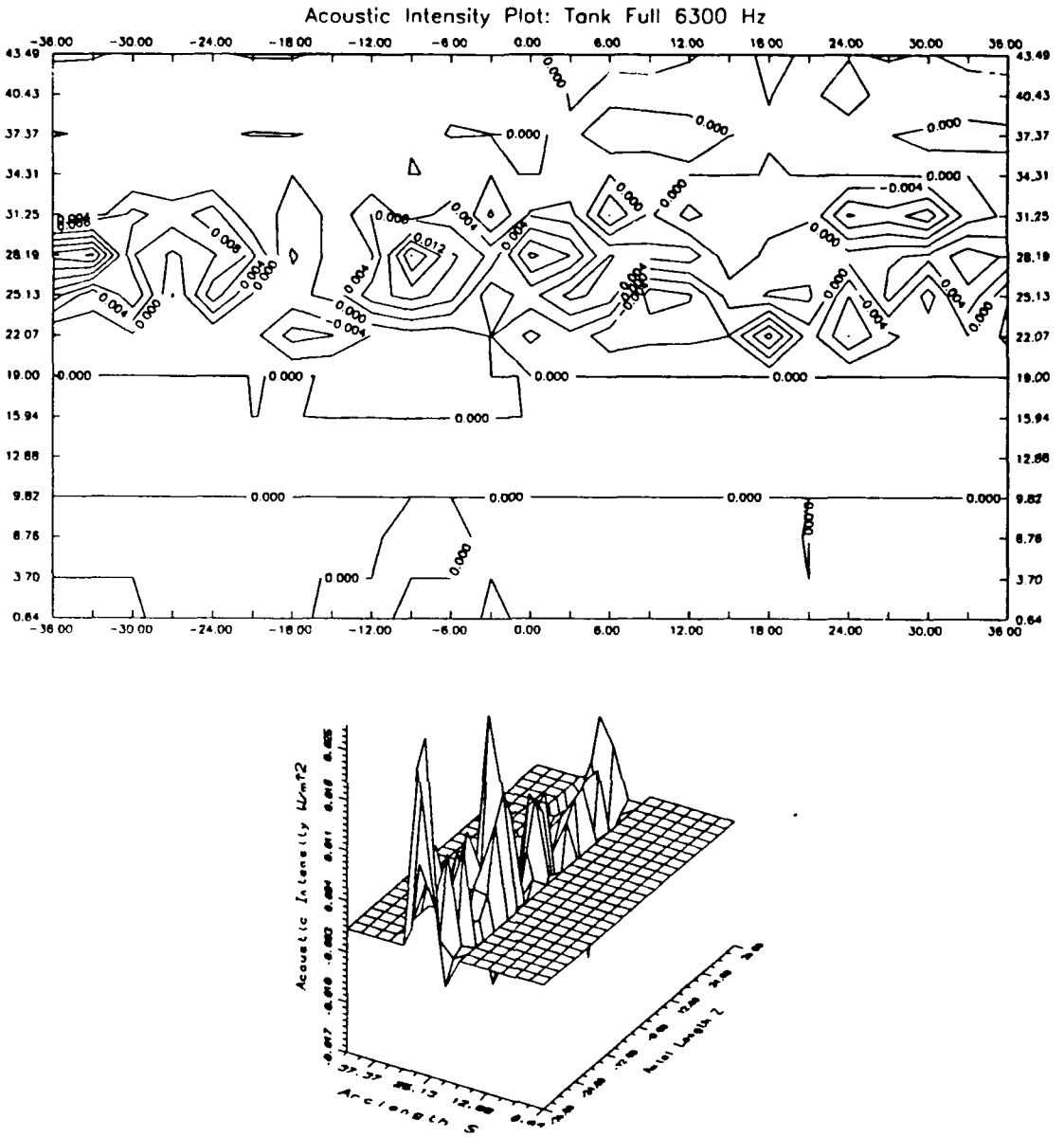

Figure 5.25 Tank Full 6300 Hz

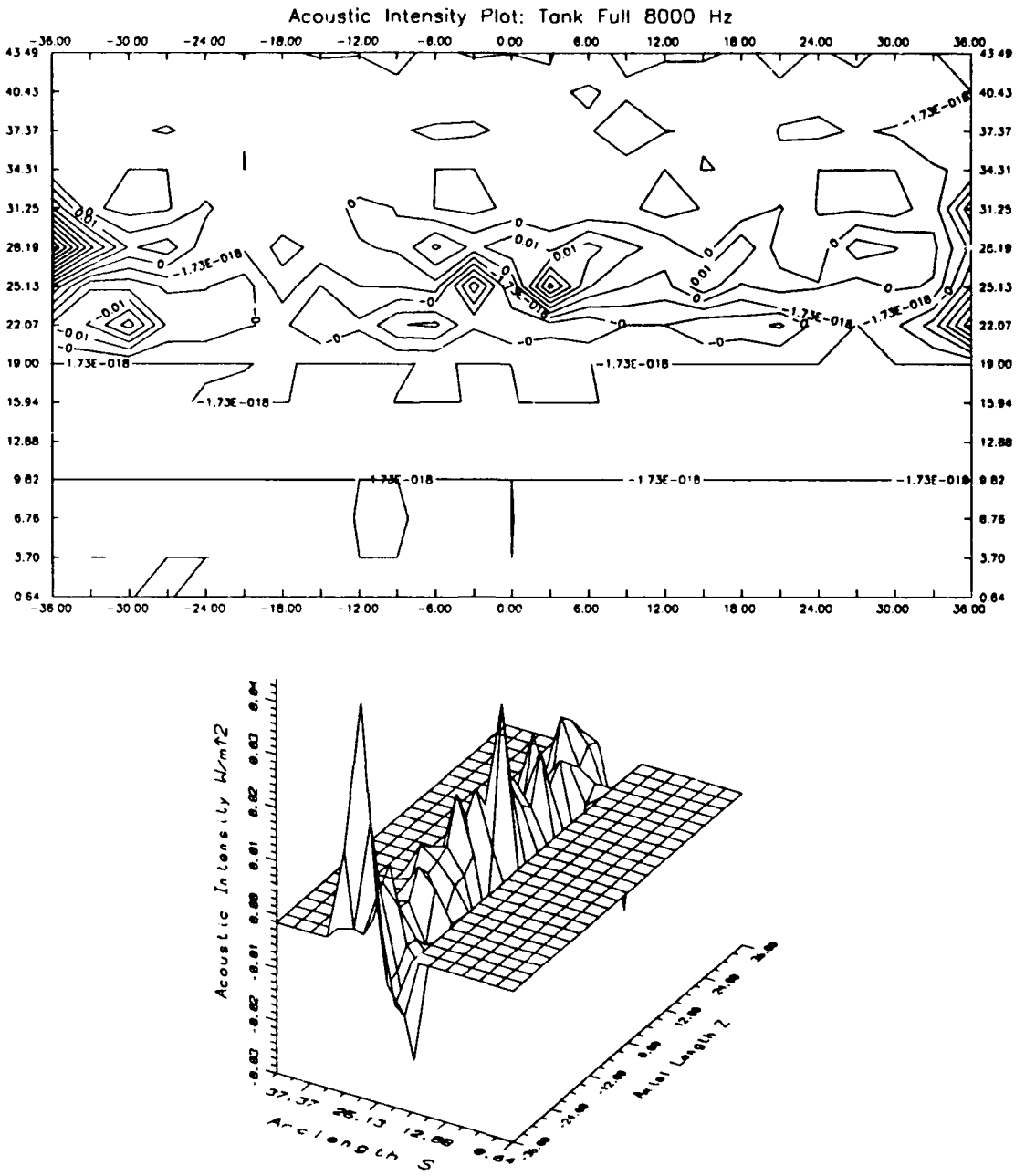

Figure 5.26 Tank Full 8000 Hz

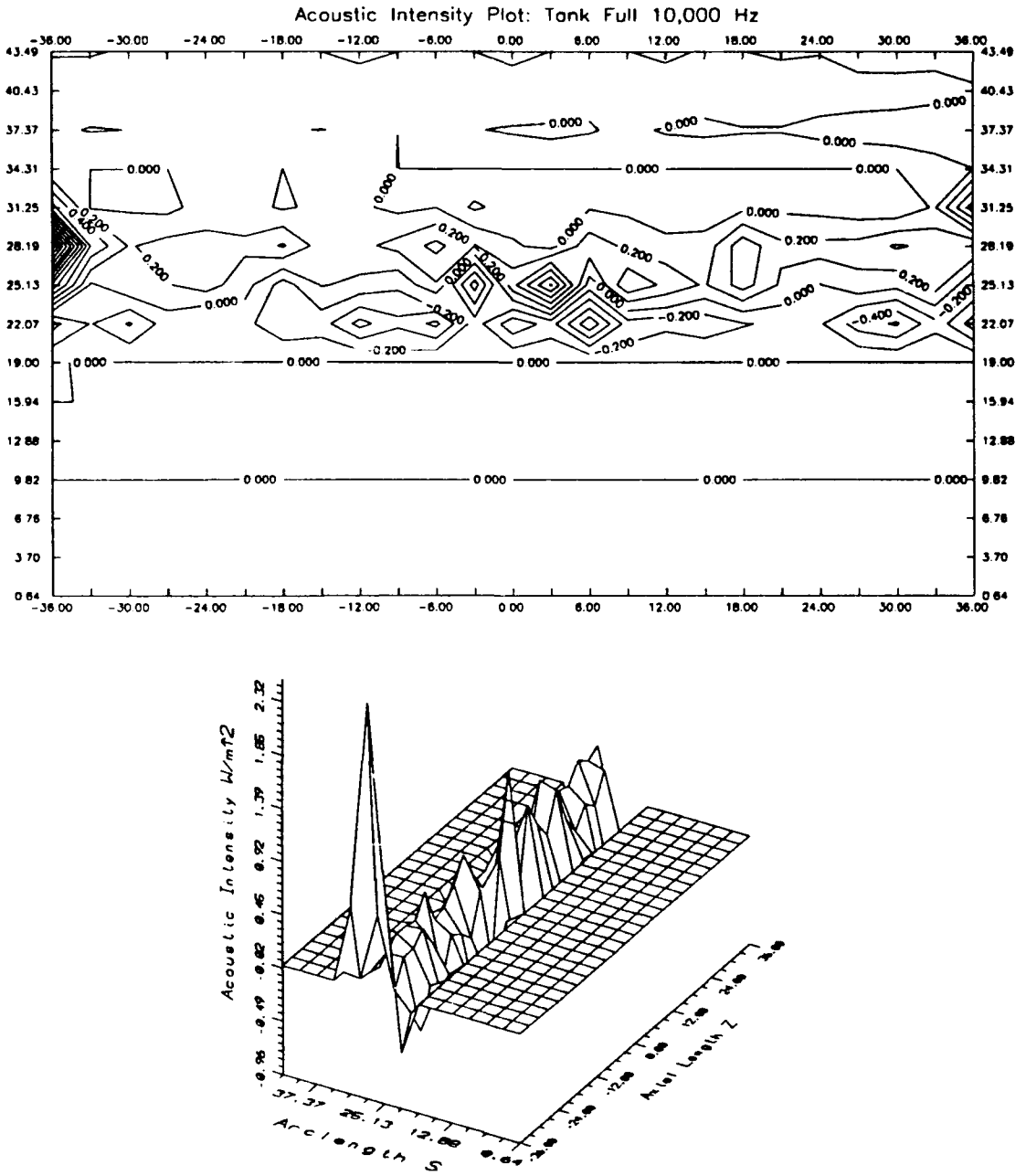

Figure 5.27 Tank Full 10000 Hz

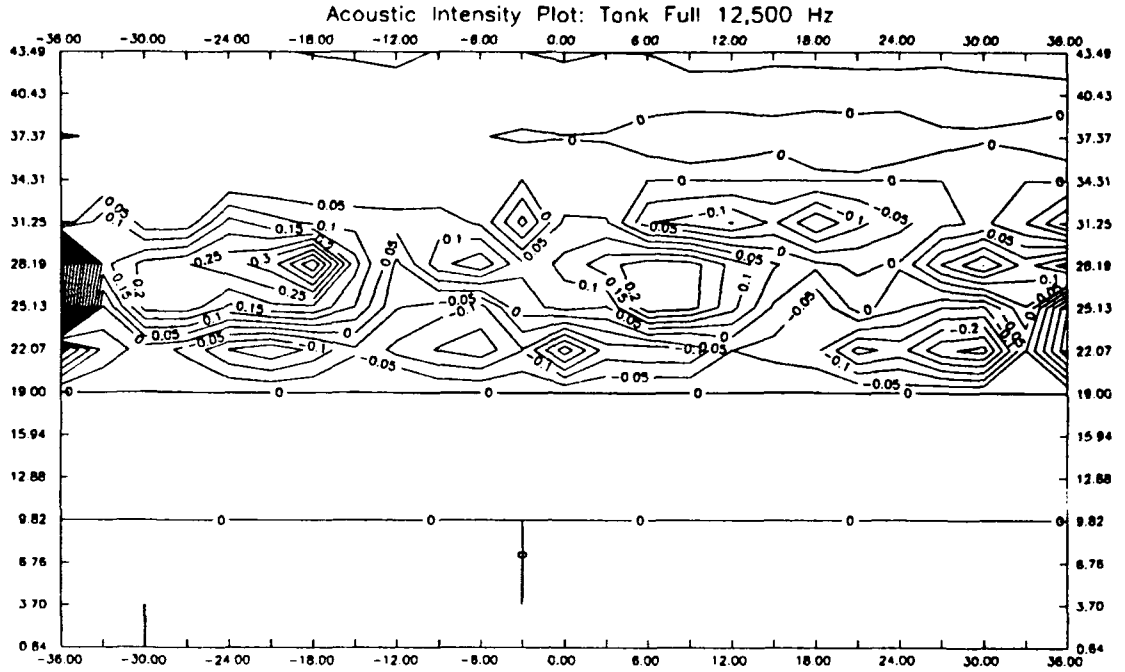

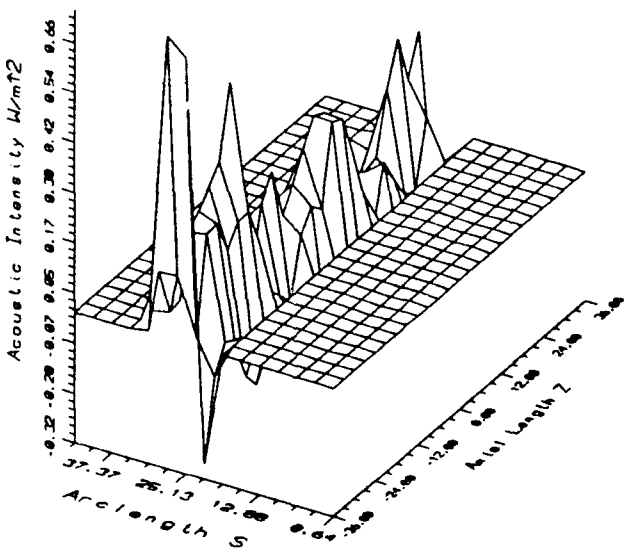

Figure 5.28 Tank Full 12500 Hz

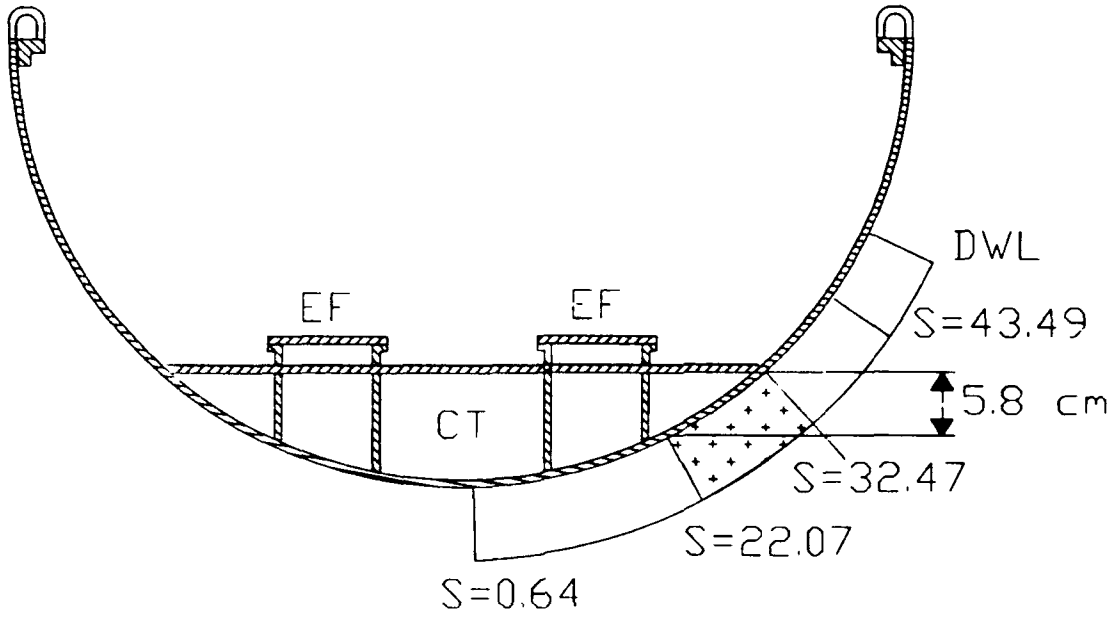

DWL Design Waterline projected radially

S=43.49 cm Measurement Grid Start Point

S=0.64 cm Data Analysis End Point

Area designated by + is primary sound radiation area.

Figure 5.29 Area of Primary Sound Radiation when Tank Full

5.5 ACOUSTIC INTENSITY PLOTS COMPARING TANK CONDITIONS

The varying scales on the intensity plots presented in sections 5.3 and 5.4 do not allow easy comparison between the magnitudes of the intensity peaks for the thirteen third octave bands and two tank conditions presented. To facilitate this comparison, Table 5.3 is provided. This table lists the minimum and maximum acoustic intensity values plotted, as well as the range in intensity values (maximum - minimum). Table 5.3 clearly shows the significant difference in the maximum and minimum intensity values between the tank full and tank empty conditions for the plots presented in the previous sections.

To compare the two conditions in the region where the tank full condition appeared essentially flat, Table 5.4 along with Figures 5.30 and 5.31 are provided. Table 5.4 shows that the difference in maximum and minimum acoustic intensity values between the two tank conditions is not significant when contrasted to the entire starboard region. Intensity plots showing representative trends for this lower tank region are provided by Figures 5.30 and 5.31. These 3-D plots illustrate that there is no significant difference between the two tank conditions in the same third octave band with regard to the number or shape of acoustic intensity peaks.

Table 5.3

Comparison of Minimum and Maximum Acoustic Intensity Values Plotted

Full Starboard Region S=0.64 to S=43.49 cm, Z=-36.00 to Z=36.00 cm

	Tank Empty			Tank Full			
Center Frequency	Min Value	Max Value	Range	Min Value	Max Value	Range	Scale Factor
800 Hz	-0.00050	0.00070	0.00120	-0.01380	0.04640	0.06020	50.2
1000 Hz	-0.00020	0.00030	0.00050	-0.01490	0.03300	0.04790	95.8
1250 Hz	-0.01750	0.09000	0.10750	-8.54820	9.76570	18.31390	170.4
1600 Hz	-0.00510	0.00520	0.01030	-0.54660	1.29910	1.84570	179.2
2000 Hz	-0.00160	0.01250	0.01410	-2.62670	1.31990	3.94660	279.9
2500 Hz	-0.00010	0.00050	0.00060	-0.05580	0.10570	0.16150	270.5
3150 Hz	-0.00150	0.00280	0.00430	-1.41400	1.94690	3.36090	781.6
4000 Hz	-0.00020	0.00060	0.00080	-0.06640	0.26940	0.33580	419.8
5000 Hz	-0.00040	0.00040	0.00080	-0.06930	0.21300	0.28230	352.9
6300 Hz	-0.00009	0.00004	0.00013	-0.01740	0.02870	0.04610	347.0
8000 Hz	-0.00006	0.00006	0.00011	-0.02750	0.04430	0.07180	634.4
10000 Hz	-0.00170	0.00080	0.00250	-0.95640	2.52150	3.47790	1391.2
12500 Hz	-0.00060	0.00030	0.00090	-0.31830	0.74520	1.06350	1181.7

Table 5.4

Comparison of Minimum and Maximum Acoustic Intensity Values Plotted

Starboard Lower Tank Region S=0.64 to S=20.50 cm, Z=-36.00 to Z=36.00 cm

	Tank Empty			Tank Full			
Center Frequency	Min Value	Max Value	Range	Min Value	Max Value	Range	Scale Factor
800 Hz	-0.00517	0.00465	0.00982	-0.00068	0.00053	0.00121	0.12
1000 Hz	-0.00246	0.00428	0.00674	-0.00040	0.00024	0.00064	0.10
1250 Hz	-0.17274	0.28989	0.46262	-0.04858	0.07565	0.12423	0.27
1600 Hz	-0.01783	0.01264	0.03047	-0.01071	0.01093	0.02165	0.71
2000 Hz	-0.02565	0.04022	0.06587	-0.01200	0.01076	0.02276	0.35
2500 Hz	-0.00083	0.00082	0.00165	-0.00089	0.00121	0.00210	1.27
3150 Hz	-0.01167	0.01621	0.02788	-0.01615	0.03168	0.04782	1.72
4000 Hz	-0.00160	0.00384	0.00544	-0.00192	0.00923	0.01115	2.05
5000 Hz	-0.00242	0.00350	0.00592	-0.00478	0.01088	0.01566	2.65
6300 Hz	-0.00055	0.00046	0.00101	-0.00057	0.00070	0.00127	1.26
8000 Hz	-0.00027	0.00057	0.00083	-0.00134	0.00151	0.00285	3.43
10000 Hz	-0.01092	0.00832	0.01925	-0.05483	0.06874	0.12357	6.42
12500 Hz	-0.00394	0.00579	0.00973	-0.02741	0.03034	0.05775	5.94

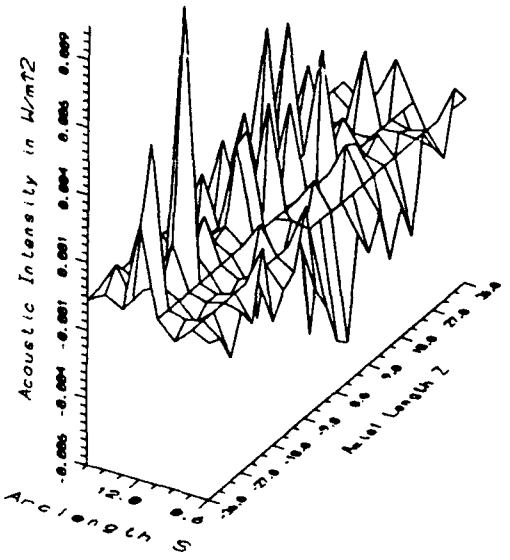

TANK FULL-1250 Hz

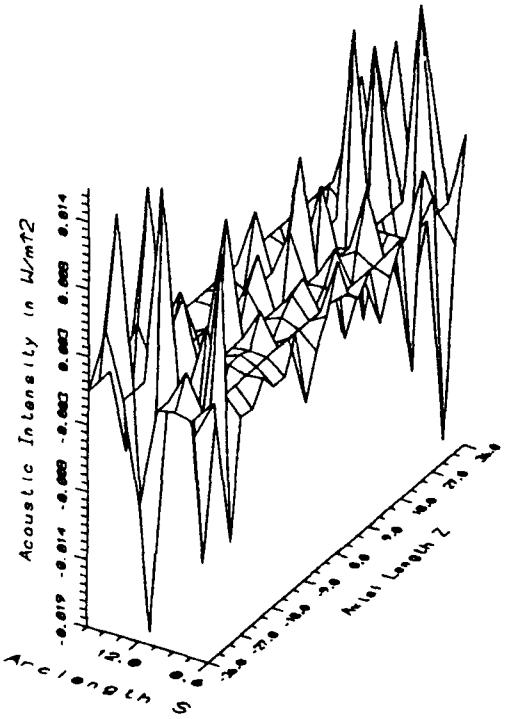

TANK EMPTY-1250 Hz

Figure 5.30 1250 Hz Comparison

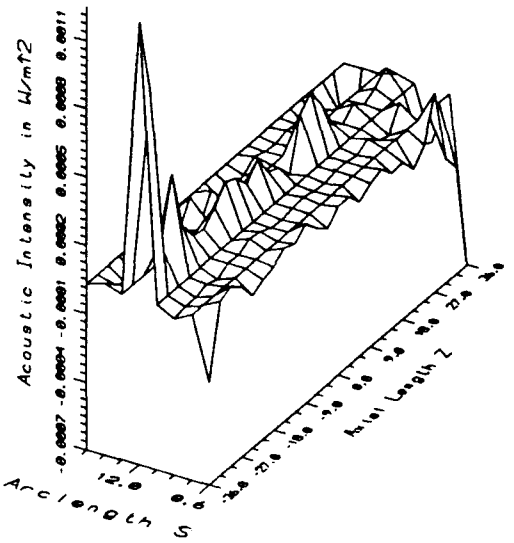

TANK FULL-5000 Hz

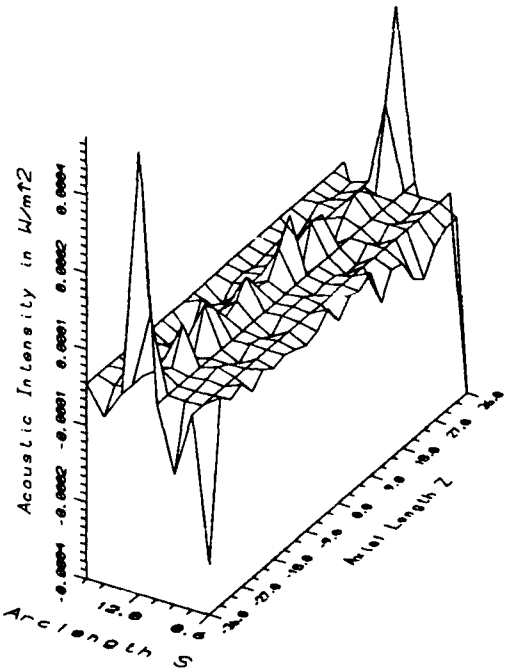

TANK EMPTY-5000 Hz

Figure 5.31 5000 Hz Comparison

To further compare the range of acoustic intensity values under the two tank-loading conditions, a "scale factor" was determined. This scale factor was determined from:

(Intensity range tank empty)*(Scale factor)=(Intensity range tank full)

The scale factors for each third octave band are included in Tables 5.3 and 5.4. They are also plotted in Figure 5.32. In this figure, region 1 includes the entire starboard region as described by Table 5.3, while region 2 is for the lower tank region as described by Table 5.4. Figure 5.32 indicates that for both regions, the scale factor between the two tank condition intensity ranges shows a linear dependence on frequency when plotted on a log scale.

This linear dependence on frequency might possibly be explained by the conclusions drawn by Shimomura [3]. As described in section 1.3, Shimomura concluded that at low frequencies sound radiation from the structural plates to the water spaces was negligibly small, and that water was not importanat as a sound transmission path. However, as frequency increased, the water did serve as an important transmission path. Extending Shimomura's conclusions to these experimental results, as the water in the storage tank becomes more important as a transmission path, there is a corresponding increase in the resulting acoustic intensity peaks external to the tank hull plating.

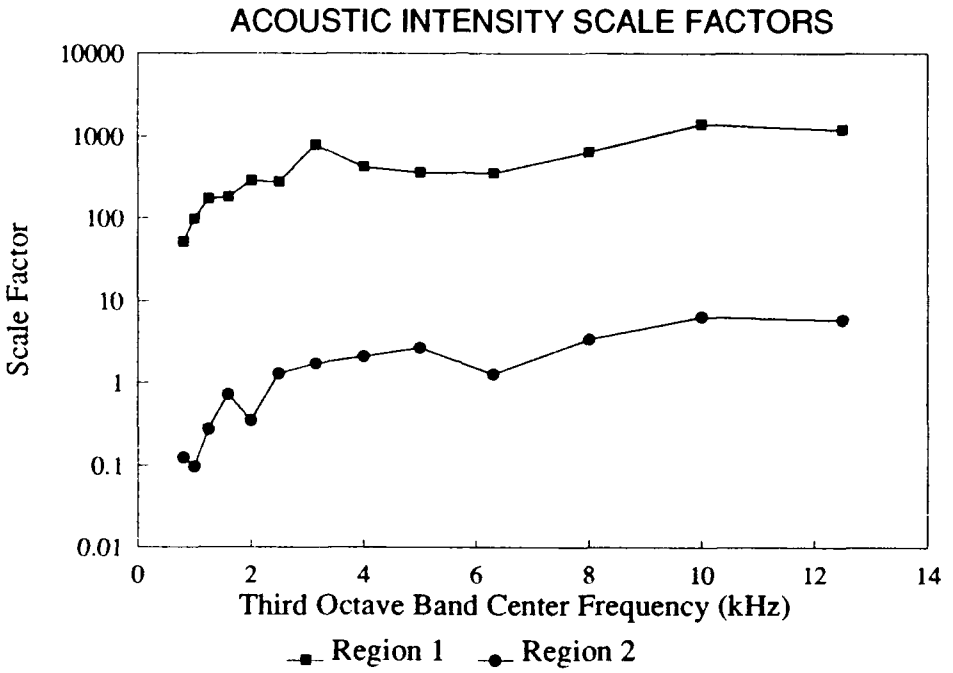

Region 1: S=0.64 to 43.49 cm, Z=-36.00 to 36.00 cm
Region 2: S=0.64 to 20.50 cm, Z=-36.00 to 36.00 cm

Figure 5.32 Comparison of Acoustic Intensity Ranges

CHAPTER 6
CONCLUSIONS AND RECOMMENDATIONS

6.1 DISCUSSION OF RESULTS

The motivation for this thesis was to attempt verification of conclusions drawn by Levi [2] with respect to the effect of internal fluid containers on the sound radiated externally from a surface ship. To reiterate Levi's conclusions, he found:

1) Liquid-filled storage tanks in surface ships have the effect of increasing sound power radiated externally in the frequency range of 63 Hz to 3.15 kHz for the prototype ship.

2) Dominant contributions to the total radiated power when the storage tanks are filled resulted from hull subsystems and the acoustical water spaces.

Based on these conclusions, Levi hypothesized that the liquid in the storage tank added a highly conductive and shorter sound path which transmits the power directly to the external acoustic meduium through the hull plates.

The experimental results in this thesis clearly substantiate Levi's first conclusion over the experimental frequency range corresponding to 64 Hz to 1.5 kHz for the prototype ship. The results presented in section 5.2 clearly show radiated sound power is increased by full surface ship liquid storage tanks in each of the frequency bands analyzed. Like Levi's results, this increase was shown to be greater in the lower and upper frequency bands analyzed relative to the intermediate frequency bands.

Levi's second conclusion is also supported by the experimental results, as the dominant contribution to radiated power for the tank full condition included both the structural discontinuity at the tank top junction with the hull and the adjacent lower hull plating. However Levi's hypothesis that the tank liquid serves as the transmission path is not clearly verified. The surprising aspect of the experimental results presented by section 5.4 is that the acoustic intensity peaks are limited to only the upper portion of tank hull plating. If the tank liquid was indeed the vibration transmission path, one would not expect the nearfield intensity pattern to show such a rapid decrease in intensity peak amplitude within the tank region. Also, this hypothesis does not explain why the lower tank region shows relatively no intensity peaks when compared with the upper region.

Questions might arise as to whether air pockets within the tank could be a possible cause for the localization in the acoustic intensity peaks. This is not likely, particularly since the peaks extended over a tank depth of approximately 6 cm. The model is arranged such that the tank fill connection is on the opposite end from the tank overflow vent pipe. Cutouts within the tank allow the liquid free access to all portions of the tank. When filling the tank, water was added until the water came out through the overflow pipe. This pipe extends approximately 4-5 cm above the tank top plate. Additionally, the model was rocked to allow entrapped air to escape. These procedures were undertaken to insure that the tank top plate would be contact with water.

6.2 CONCLUSIONS

Summarizing, the principal conclusions reached in this thesis are provided below.

- Full internal fluid containers have the effect of increasing the external sound radiation from surface ships in the frequency range of 64 Hz to 1.5 kHz for the prototype ship.
- The increase in measured sound radiated power due to filling the storage tank with water was more significant for the low frequency range (1.25-4 kHz for the model) and for the high frequency range (10-12.5 kHz).
- The dominant contributions to the total radiated power when the storage tank is empty are from structual discontinuites. The primary contributor is the tank top junction with the model hull.
- The dominant contributions to the total radiated power when the storage tank is full are from the tank top-hull junction structural discontinuity and the hull plating immediately below this discontinuity. The structural discontinuites at the engine support-hull junctions provided little contribution to the total radiated power.
- Filling the storage tank with water greatly increased the range of acoustic intensity peak amplitudes in the dominant region of sound radiation. This increase in range showed a linear dependence on frequency when plotted on a log scale, and is attributed to the greater importance of water as a sound transmission path with increased frequency.

6.3 SUGGESTIONS FOR FURTHER WORK

Possible further work suggested by the results of this thesis include:

- Complete data post-processing for the port side of the model to determine if the intensity patterns for the tank full condition show the same localization effects around the tank top - hull junction discontinuity. Since the shaker was mounted off centerline, on the model's port side, the intensity patterns are not expected to be symmetrical.
- Conduct additional experiments to determine if the intensity patterns for the tank full condition are repeatable. This is considered appropriate due to the unexpected rapid decrease in acoustic intensity values midway down the tank hull plating.
- If the intensity patterns prove to be repeatable for the tank full condition, develop a hypothesis to explain this behavior.
- To further investigate the dependence of range in acoustic intensity peak values on frequency.

REFERENCES

1. Blake, W.K., D. Feit, W. Reader, M. Sevik, and J. Lee, "Unclassified Notes for 'Elements of Ships Acoustics'", unpublished, 1989.

2. Levi, A. "Effect of Internal Fluid Containers on Sound Radiated Externally from a Surface Ship", M.I.T., Department of Ocean Engineering, M.S. Thesis, January 1989.

3. Shimomura, Y. "The Effect of a Liquid Storage Tank on Sound Transmission through Ship Structures", M.I.T., Department of Ocean Engineering, Ocean Engineer Thesis, October 1985.

4. Horton, C.W. and G.S. Innis, Jr. "The Computation of Far-Field Radiation Patterns from Measurements made near the Source", Journal of the Acoustical Society of America, 33 (7), July 1961, pgs 877-880.

5. Baker, D.D., "Determination of Far-Field Characteristics of Large Underwater Sound Transducers from Near-Field Measurements", Journal of the Acoustical Society of America, 34 (11), November 1962, pgs 1737-1744.

6. Stephanishen, P.R. and H.W. Chen, "Nearfield Pressures and Surface Intensity for Cylindrical Vibrators", Journal of the Acoustical Society of America, 76 (3), September 1984, pgs 942-948.

7. Williams, E.G., H.D. Dardy, and R.G. Fink, "Nearfield Acoustical Holography using an Underwater Automated Scanner", Journal of the Acoustical Society of America, 78 (2), August 1985, pgs 789-798.

8. Maynard, J.D., E.G. Williams, and Y. Lee, "Nearfield Acoustic Holography: I. Theory of Generalized Holography and the Development of NAH", Journal of the Acoustical Society of America, 78 (4), October 1985, pgs 1395-1413.

9. Williams, E.G., H.D. Dardy, and K.B. Washburn, "Generalized nearfield acoustical holography for cylindrical geometry: Theory and experiment", Journal of the Acoustical Society of America, 81 (2), February 1987, pgs 389-407.

10. Williams, E.G., B.H. Houston, and J.A. Bucaro, "Broadband Nearfield Acoustical Holography for Vibrating Cylinders", Journal of the Acoustical Society of America, 86 (2), August 1989, pgs 674-679.

11. Clark, A.R., and P.S. Watkinson, "Measurements of Underwater Acoustic Intensity in the Nearfield of a Point Excited Periodically Ribbed Cylinder", 2nd International Symposium on Shipboard Acoustics, The Hague, The Netherlands, October 1986.

12. Rayleigh, J.W.S., Theory of Sound, First American Edition, Dover Publications, New York, 1945.

13. Olson, H.F., 1932 U.S. Patent No. 1,892,644. A system responsive to the energy flow of sound waves.

14. Fahy, F.J., "Measurement of acoustic intensity using the cross-spectral density of two microphone signals", Journal of the Acoustical Society of America, 62, 1977, pgs 1057-1059.

15. Bendat, J.S. and A.G. Piersol, Random Data: Analysis and Measurement Procedures, John Wiley and Sons, Inc., New York, 1971, pgs 4-34.

16. Chung, J.Y., "Cross-spectral method of measuring acoustic intensity without phase mismatch", Journal of the Acoustical Society of America, 64 (16), December 1978, pgs 1613-1616.

17. Elliot, S.J., "Errors in Acoustic Intensity Measurements", Journal of Sound and Vibration 78 (3), 1981, pgs 439-445.

18. Pavic, G., "Measurement of Sound Intensity", Journal of Sound and Vibration, 51 (4), 1977, pgs 533-545.

19. Thompson, J.K. and D.R. Tree, "Finite Difference Approximation Errors in Acoustic Intensity Measurements", Journal of Sound and Vibration 75 (2), 1981, pgs 229-238.

20. Seybert, A.F., Statistical Errors in Acoustic Intensity Measurements", Journal of Sound and Vibration 75 (4), 1981, pgs 519-526.

21. Lyon, R.H., Machinery Noise and Diagnostics, Butterworths, 1987.

22. Rasmussen, G., "Intensity - Its Measurement and Uses", Sound and Vibration Instrumentation Reference Issue, March 1989, pgs 12-21.

23. Brito, J.D., "Sound Intensity Patterns for Vibrating Surfaces", M.I.T. Department of Mechanical Engineering, PhD Thesis, October 1976.

24. Abramson, H.N. and G.E. Neville, Jr., "Some Modern Developments in the Application of Scale-Models in Dynamic Testing", Colloqium on "Use of Models and Scaling in Shock and Vibration", ASME, New York, 1963.

25. Newland, D.E., An Introduction to Random Vibrations and Spectral Analysis, Second edition, Bath Press, 1984.

26. Ripley, B.D., Spatial Statistics, Wiley-Interscience, 1981.

27. Fahy, F., Sound and Structural Vibration, Academic Press, 1985.

28. Smith, P.W., Jr. and R.H. Lyon, "Sound and Structural Vibration", NASA Contractor Report CR-160, 1962.

29. Chervenak, "A new NRL acoustic research tank facility," Naval Research Laboratory Report 6822, Washington, D.C., 1969.

30. Tratch, J.J., "Vibration Transmission through Machinery Foundation and Ship Bottom Structure", M.I.T., Department of Mechanical Engineering, M.S. and Mechanical Engineer Thesis, 1985.

31. Junger, M.C. and Feit, D., Sound, Structures and their Interaction, M.I.T. Press, 1986.

APPENDIX A
PROGRAM DOCUMENTATION

This appendix provides documentation for the programs used in processing the data. Program descriptions are provided within the text of each program.

A.1 PROCESS.F

```
C*************************************************************************      C
C                                                                              C
C AUTHOR:  AMY R. SMITH                                                        C
C DATE: 20 FEBRUARY 1990                                                       C
C PURPOSE:  THESIS WORK AT MIT                                                 C
C                                                                              C
C PROGRAM DESCRIPTION                                                          C
C   THIS PROGRAM CALCULATES THE AVERAGE ACOUSTIC INTENSITY FROM THE            C
C   IMAGINARY PART OF THE PRESSURE CROSS-SPECTRUM.  THREE OUTPUT FILES         C
C   ARE PRODUCED.  THE FIRST FILE, HEADER.CON, STORES THE                      C
C   INFORMATION CONTAINED IN THE FILE HEADER.  THE SECOND FILE,                C
C   FULINTEN.DAT, PROVIDES THE X,Y,AND Z COORDINATES OF THE MIDPLANE           C
C   GRID POINT AND THE AVERAGE ACOUSTIC INTENSITY FOR THE FREQUENCY            C
C   RANGE 640 HZ TO 15 KHZ WHICH INCLUDES FREQUENCY BINS 84 TO 1966.           C
C   THE THIRD FILE,CHECK.DAT,IS INTENDED FOR USE IN VERIFYING CORRECT          C
C   DATA PROCESSING.  IT CONTAINS THE X,Y, AND Z COORDINATES FOR THE           C
C   INNER, OUTER, AND CALCULATED MID-PLANE.  IT ALSO CONTAINS THE              C
C   COMPLEX PRESSURE DATA FOR THE INNER AND OUTER PLANES, AND THE              C
C   CALCULATED AVERAGE INTENSITY AT THE MID-PLANE.                             C
C                                                                              C
C VARIABLE DEFINITIONS                                                         C
C   DELR = SEPARATION BETWEEN INNER AND OUTER PLANES = 0.0060 METERS           C
C   DENOM(I) = FREQ * RHO * DELR FOR FREQUENCY BIN I;                          C
C          USED IN INTENSITY CALCULATION                                       C
C   FREQ(I) = RADIAN FREQUENCY ASSOCIATED WITH BIN I = 47.93689*I              C
C          (7.629 Hz PER BIN)                                                  C
C   INTENS(I,J)= AVERAGE ACOUSTIC INTENSITY FOR GRID POINT I                   C
C          (MID-PLANE) AND FREQUENCY BIN J                                     C
C   M = # OF CIRCUMFERENTIAL ROWS OF GRID POINTS = 84                          C
C   N = # OF GRID POINTS IN A GIVEN AXIAL ROW = 73                             C
C   R(1)= RADIUS OF INNER PLANE = 0.4355 METERS                                C
C   R(2)= RADIUS OF OUTER PLANE = 0.4415 METERS                                C
C   R(3)= RADIUS OF MID-PLANE = 0.4385 METERS                                  C
C   RHO = DENSITY OF TANK WATER AT 17.9C = 983.75 KG/METER^3                   C
C   P(I,1)= COMPLEX PRESSURE DATA FOR INNER PLANE FOR FREQUENCY BIN            C
C         1966 (15 kHz); USED TO CHECK COMPUTER ALGORITHMS                     C
C   P(I,2)= COMPLEX PRESSURE DATA FOR OUTER PLANE FOR FREQUENCY BIN            C
C         1966 (15 kHz); USED TO CHECK COMPUTER AL GORITHMS                    C
C   PDATA(I,J) = COMPLEX PRESSURE DATA FOR GRIL POINT I AND FREQUENCY          C
C          BIN J                                                               C
C   PCONJ(I,J)= COMPLEX CONJUGATE OF COMPLEX PRESSURE IN OUTER PLANE           C
C          FOR GRID POINT I AND FREQUENCY BIN J                                C
C   T = TOTAL # OF GRID POINTS IN SINGLE PLANE = N*M = 6132                    C
C   XSPEC(I,J)= IMAGINARY PART OF PRESSURE CROSS-SPECTRUM FOR GRID             C
C          POINT I (MID-PLANE) AND FREQUENCY BIN J                             C
C   X IS HORIZONTAL COORDINATE (POSITIVE STARBOARD)                            C
```

```
C   X(I,1)= INNER PLANE X-AXIS COORDINATE OF GRID POINT I                    C
C   X(I,2)= OUTER PLANE X-AXIS COORDINATE OF GRID POINT I                    C
C   X(I,3)= MID-PLANE X-AXIS COORDINATE                                      C
C   Y IS VERTICAL COORDINATE (POSITIVE DOWNWARDS)                            C
C   Y(I,1)= INNER PLANE Y-AXIS COORDINATE OF GRID POINT I                    C
C   Y(I,2)= OUTER PLANE Y-AXIS COORDINATE OF GRID POINT I                    C
C   Y(I,3)= MID-PLANE Y-AXIS COORDINATE                                      C
C   Z IS AXIAL COORDINATE (POSITIVE BOW)                                     C
C   Z(I,1)= INNER PLANE Z-AXIS COORDINATE OF GRID POINT I                    C
C   Z(I,2)= OUTER PLANE Z-AXIS COORDINATE OF GRID POINT I                    C
C   Z(I,3)= MID-PLANE Z-AXIS COORDINATE                                      C
C                                                                            C
C*****************************************************************************
      INTEGER A,B
      INTEGER*4 HEADER(8192)
      REAL X(73,3),Y(73,3),Z(73,3),DENOM(84:1966)
      REAL INTENS(73,84:1966), XSPEC(73,84:1966)
          COMPLEX*8 P(73,2), PDATA(146,4095), PCONJ(73,84:1966)
      PARAMETER (N=73, M=84, T=6132)
      PARAMETER (RHO=983.75, DELR=0.006)
C
C READ IN HEADER DATA TO HEADER ARRAY AND OUTPUT IT TO FILE
C
      OPEN (UNIT=1, FILE ='SAMPLE_PRESSURE.RFT', ACCESS = 'SEQUENTIAL',
     +     FORM = 'UNFORMATTED', STATUS = 'OLD')
      OPEN (UNIT=4, FILE = 'HEADER.CON', FORM = 'UNFORMATTED')
C
      READ (UNIT=1) (HEADER(I), I=1,8191)
          WRITE (UNIT=4) (HEADER(I), I=1,8191)
C
C  READ IN COMPLEX PRESSURE DATA FOR PROCESSING: 146 RECORDS AT A TIME
C  (EQUIVALENT TO ONE AXIAL ROW, INNER AND OUTER PLANES); REPEAT
C  FOR ALL 84 CIRCUMFERENTIAL ROWS.
C
      OPEN (UNIT=2, FILE = 'CHECK.DAT', FORM = 'FORMATTED')
      OPEN (UNIT=3, FILE = 'FULINTEN.DAT', FORM = 'UNFORMATTED')
      DO 10 B = 1, 84
        DO 100 I = 1,146
          READ (UNIT=1) (PDATA(I,J), J=1,4095)
 100    CONTINUE
C
C  EXTRACT INNER PLANE AXIS COORDINATES AND ASSOCIATED 15 kHz PRESSURE
C  DATA
C
        DO 200 I = 1,73
          X(I,1) = REAL (PDATA (I,4094))
          Y(I,1) = AIMAG (PDATA (I,4095))
          Z(I,1) = REAL (PDATA (I,4095))
          P(I,1) = PDATA (I,1966)
 200    CONTINUE
C
C  EXTRACT OUTER PLANE AXIS COORDINATES TO CORRESPOND WITH INNER
PLANE
C  COORDINATES AND ASSOCIATED 15 kHz DATA
C
        A = 73
        DO 300 I = 74,146
          X(A,2) = REAL (PDATA(I,4094))
          Y(A,2) = AIMAG (PDATA(I,4095))
          Z(A,2) = REAL (PDATA(I,4095))
          P(A,2) = PDATA(I,1966)
          A = A-1
 300    CONTINUE
C
```

```
C  CALCULATE MID-PLANE COORDINATES
C
      DO 400 I = 1,73
        X(I,3) = (X(I,1)+X(I,2))/2
        Y(I,3) = (Y(I,1)+Y(I,2))/2
        Z(I,3) = (Z(I,1)+Z(I,2))/2
 400  CONTINUE
C
C  CALCULATE AVERAGE ACOUSTIC INTENSITY FOR FREQUENCY BINS OF INTEREST
C
      DO 500 I = 84,1966
        DENOM(I) = 47.93689*I*RHO*DELR*2
 500  CONTINUE
      A = 146
      DO 600 I = 1,73
        DO 700 J = 84,1966
          PCONJ(I,J) = CONJG(PDATA(A,J))
          XSPEC(I,J) = AIMAG(PDATA(I,J)*PCONJ(I,J))
          INTENS(I,J) = (XSPEC(I,J)/DENOM(J))
 700      CONTINUE
        A = A-1
 600  CONTINUE
C
C  WRITE DATA TO OUTPUT FILES
C
      DO 800 I = 1,73
        WRITE (2,1000) X(I,1),X(I,2),X(I,3),Y(I,1),Y(I,2),Y(I,3),
     +              Z(I,1),Z(I,2),Z(I,3)
        WRITE (2,1100) P(I,1), P(I,2), INTENS(I,1966)
        WRITE (UNIT=3) X(I,3), Y(I,3), Z(I,3)
        WRITE (UNIT=3) (INTENS(I,J), J = 84,1966)
 800  CONTINUE
 10  CONTINUE
C
 1000  FORMAT (1X,9G12.6)
 1100  FORMAT (1X,5G12.6)
C
      CLOSE (UNIT=1, STATUS = 'KEEP')
      CLOSE (UNIT=2, STATUS = 'KEEP')
      CLOSE (UNIT=3, STATUS = 'KEEP')
    END
```

A.2 HEADER.F

```
C*************************************************************************      C
C                                                                              C
C AUTHOR:  AMY R. SMITH                                                        C
C DATE: 26 FEBRUARY 1990                                                       C
C PURPOSE:  THESIS WORK AT MIT                                                 C
C                                                                              C
C PROGRAM DESCRIPTION                                                          C
C   THIS PROGRAM DISPLAYS THE HEADER CONTENTS USING AS INPUT THE FILE          C
C   HEADER.CON CREATED BY PROCESS.F                                            C
C C*************************************************************************   C
                                                                               C
      INTEGER*4 IHDR(1024), HEADER(8192)
      REAL*4 RHDR(1024)
      CHARACTER*1024  CHDR
      EQUIVALENCE (HEADER(1), CHDR(1:1))
      EQUIVALENCE (HEADER(257), IHDR(1))
      EQUIVALENCE (HEADER(1281), RHDR(1))
C
C READ IN HEADER DATA TO HEADER ARRAY AND OUTPUT IT TO FILE
C
      OPEN (UNIT=1, FILE ='HEADER.CON', ACCESS = 'SEQUENTIAL',
     +     FORM = 'UNFORMATTED', STATUS = 'OLD')
      OPEN (UNIT=4, FILE = 'HEADER.DAT', FORM = 'FORMATTED')
C
      READ (UNIT=1) (HEADER(I), I=1,8191)
C
C     WRITE HEADER CONTENTS TO OUTPUT FILE
C
      WRITE (4,1) CHDR(251:280)
    1 FORMAT(/,2X,A30)
      WRITE (4,2) CHDR(121:180)
    2 FORMAT(/,2X,A60)
      WRITE (4,3) CHDR(181:210)
    3 FORMAT (/2X'TARGET IS 'A30)
      WRITE (4,4) CHDR(211:240)
    4 FORMAT (/2X'SOURCE WAVEFORM IS 'A30)
      WRITE (4,5) IHDR(33)
    5 FORMAT (/2X,'RUN IS 'I2)
      WRITE (4,6) (IHDR(I), I=1,6)
    6 FORMAT (/2X,'FILE CREATED ON 'I2'/'I2'/'I2,1X,I2':'I2':'I2)
      WRITE (4,7) CHDR(91:120)
    7 FORMAT (5X,'USING 'A30)
      WRITE (4,8) IHDR(7),IHDR(10)
    8 FORMAT (5X,'COLLECTING 'I5' RECORDS OF COMPLEX('I5') DATA')
      WRITE (4,9) IHDR(8),IHDR(9)
    9 FORMAT (5X,'EACH 'I4' SAMPLES LONG WITH 'I2' BYTES PER SAMPLE.')
      WRITE (4,11) CHDR(241:250)
   11 FORMAT (/2X,'TYPE OF DIGITIZER THAT ACQUIRED DATA IS 'A10)
      WRITE (4,12) IHDR(28)
   12 FORMAT (5X,'FOR A TOTAL OF 'I4' DIGITIZER CHANNELS'/,
     +       10X'OF DATA ACQUIRED.')
      WRITE (4,13) IHDR(29)
   13 FORMAT (5X,'NUMBER OF AVERAGES USED IN DATA ACQUISTION IS 'I3'.')
      WRITE (4,14) IHDR(30)
   14 FORMAT(2X,'NUMBER OF BITS DIGITIZED IN DATA ACQUISITION IS
     +        'I3'.')
      WRITE (4,15) RHDR(70)
   15 FORMAT (/2X,'TRIGGER DELAY IS 'F9.3' MICROSECONDS.')
      WRITE (4,16) RHDR(71)
   16 FORMAT (2X,'DIGITIZATION SAMPLE INTERVAL IS 'F9.3'MICROSECONDS.')
      WRITE (4,17) RHDR(72)
```

```
17  FORMAT (2X,'REPETITION RATE OF SOURCE FIRING IS 'F9.3' HERTZ.')
    WRITE (4,18) RHDR(73)
18  FORMAT (/2X,'DIGITIZER"S PEAK RANGE IS 'F9.3' VOLTS.')
    WRITE (4,19) RHDR(74)
19  FORMAT (/2X,'FREQUENCY INTERVAL (BIN WIDTH) IS 'F9.3' HERTZ.'/)
    WRITE (4,21) RHDR(80)
21  FORMAT (/2X,'SOURCE TRANSDUCER IS 'F9.3' VOLTS PEAK-TO-PEAK.')
    WRITE (4,22) RHDR(81)
22  FORMAT (2X, 'SOURCE WAVEFORM GENERATOR PEAK VOLTAGE IS 'F7.3'.')
    WRITE (4,23) RHDR(82),RHDR(83)
23  FORMAT (2X,'BANDWIDTH IS FROM 'F10.4' KHZ TO 'F10.4' KHZ.'/)
    WRITE (4,24) RHDR(13)
24  FORMAT (2X,'RECEIVER STARTING X POSITION IS 'F7.2 'INCHES.')
    WRITE (4,25) RHDR(14)
25  FORMAT (2X,'RECEIVER ENDING X POSITION IS 'F7.2' INCHES.')
    WRITE (4,26) RHDR(15)
26  FORMAT (2X,'RECEIVER INCREMENTAL ALONG X-AXIS IS 'F7.2' INCHES.')
    WRITE (4,27) RHDR(16)
27  FORMAT (2X,'X SETTLING TIME FOR RECEIVER IS 'F7.1' SECONDS.')
    WRITE (4,28) RHDR(17)
28  FORMAT (2X,'RECEIVER STARTING Y POSITION IS 'F7.2 'INCHES.')
    WRITE (4,29) RHDR(18)
29  FORMAT (2X,'RECEIVER ENDING Y POSITION IS 'F7.2' INCHES.')
    WRITE (4,31) RHDR(19)
31  FORMAT (2X,'RECEIVER INCREMENTAL ALONG Y-AXIS IS 'F7.2' INCHES.')
    WRITE (4,32) RHDR(20)
32  FORMAT (2X,'Y SETTLING TIME FOR RECEIVER IS 'F7.1' SECONDS.')
    WRITE (4,33) RHDR(21)
33  FORMAT (2X,'RECEIVER STARTING Z POSITION IS 'F7.2 'INCHES.')
    WRITE (4,34) RHDR(22)
34  FORMAT (2X,'RECEIVER ENDING Z POSITION IS 'F7.2' INCHES.')
    WRITE (4,35) RHDR(23)
35  FORMAT (2X,'RECEIVER INCREMENTAL ALONG Z-AXIS IS 'F7.2' INCHES.')
    WRITE (4,36) RHDR(24)
36  FORMAT (2X,'Z SETTLING TIME FOR RECEIVER IS 'F7.1' SECONDS.')
    WRITE (4,37) IHDR(31)
37  FORMAT (2X,'NUMBER OF SENSORS/ACCELEROMETERS USED WAS 'I3'.')
    WRITE (4,38) IHDR(32)
38  FORMAT (2X,'NUMBER OF DRIVERS/SHAKERS USED WAS 'I3'.')
    CLOSE (UNIT=1, STATUS = 'KEEP')
    CLOSE (UNIT=4, STATUS = 'KEEP')
    END
```

A.3 PLOTDAT.F

```
C*************************************************************************      C
C                                                                              C
C AUTHOR:  AMY R. SMITH                                                        C
C DATE: 20 FEBRUARY 1990                                                       C
C PURPOSE:  THESIS WORK AT MIT                                                 C
C                                                                              C
C PROGRAM DESCRIPTION                                                          C
C   THIS PROGRAM USES AS INPUT THE FILE 'FULINTEN.DAT' (WHICH PROVIDES         C
C   THE  AVERAGE ACOUSTIC INTENSITY OVER A 3-D MODEL SURFACE FOR 1882          C
C   FREQUENCY BINS).  THE PROGRAM COLLECTS THE INTENSITY DATA INTO             C
C   PRE-ESTABLISHED 1/3 OCTAVE BANDS AND PROCESSES THE DATA INTO A             C
C   FORM SUITABLE FOR 2-D CONTOUR PLOTTING.                                    C
C                                                                              C
C VARIABLE DEFINITIONS                                                         C
C  CFREQ3OB(I) = CENTER FREQUENCY IN HERTZ FOR Ith 1/3 OCTAVE BAND             C
C  FREQ(I) = CIRCULAR FREQUENCY ASSOCIATED WITH BIN I = 47.93689*I             C
C          (7.629 Hz PER BIN)                                                  C
C  INTENS(I,J)=AVERAGE ACOUSTIC INTENSITY FOR GRID POINT I (MID-PLANE)         C
C           AND FREQUENCY BIN J                                                C
C  INTEN3OB(I,J)=AVERAGE 1/3 OCTAVE BAND ACOUSTIC INTENSITY FOR GRID           C
C             POINT I (MID-PLANE) AND Jth 1/3 OCTAVE BAND                      C
C  M = # OF CIRCUMFERENTIAL ROWS OF GRID POINTS = 84                           C
C  N = # OF GRID POINTS IN A GIVEN AXIAL ROW = 73                              C
C  S(I)=ARCLENGTH DETERMINED FROM COORDINATES X(I,3) AND Y(I,3) FOR            C
C     2-D CONTOUR PLOT                                                         C
C  T = TOTAL # OF GRID POINTS IN SINGLE PLANE = N*M = 6132                     C
C  X IS HORIZONTAL COORDINATE (POSITIVE STARBOARD)                             C
C  X(I)= MID-PLANE X-AXIS COORDINATE; SIMILAR FOR Y AND Z COORDINATES          C
C  Y IS VERTICAL COORDINATE (POSITIVE DOWNWARDS)                               C
C  Z IS AXIAL COORDINATE (POSITIVE BOW)                                        C
C                                                                              C
C*************************************************************************      C
    REAL X(6132),Y(6132),Z(6132), CFREQ3OB(14), S(6132)
    REAL INTENS(6132,84:1966), INTEN3OB(6132,13)
    DATA CFREQ3OB/800.,1000.,1250.,1600.,2000.,2500.,3150.,4000.,
   +          5000.,6300.,8000.,10000.,12500./
C
C   INITIALIZE ARRAY INTEN3OB
C
    DO 50 J=1,13
      DO 60 I=1,6132
        INTEN3OB(I,J)=0.0
 60     CONTINUE
 50   CONTINUE
C
C  READ IN COORDINATE AND INTENSITY DATA FOR PROCESSING
C
    OPEN (UNIT=3,FILE='FULINTEN.DAT',FORM='UNFORMATTED',STATUS='OLD',
   +     ACCESS='SEQUENTIAL')
    DO 100 I = 1,6132
      READ (UNIT=3) X(I), Y(I), Z(I)
      READ (UNIT=3) (INTENS(I,J), J = 84,1966)
 100  CONTINUE
    CLOSE (UNIT=3,STATUS='KEEP')
C
C  CALCULATE ARCLENGTH AND COLLECT INTENSITY DATA INTO
PRE-ESTABLISHED
C  1/3 OCTAVE BANDS
C
    DO 200 I = 1,6132
      S(I) = 0.4385*ATAN2(X(I),Y(I))
```

```
      DO 210 J=92,116
        INTEN3OB(I,1)=INTEN3OB(I,1)+INTENS(I,J)
210   CONTINUE
      DO 220 J=117,146
        INTEN3OB(I,2)=INTEN3OB(I,2)+INTENS(I,J)
220   CONTINUE
      DO 230 J=147,184
        INTEN3OB(I,3)=INTEN3OB(I,3)+INTENS(I,J)
230   CONTINUE
      DO 240 J=185,232
        INTEN3OB(I,4)=INTEN3OB(I,4)+INTENS(I,J)
240   CONTINUE
      DO 250 J=233,292
        INTEN3OB(I,5)=INTEN3OB(I,5)+INTENS(I,J)
250   CONTINUE
      DO 260 J=293,368
        INTEN3OB(I,6)=INTEN3OB(I,6)+INTENS(I,J)
260   CONTINUE
      DO 270 J=369,463
        INTEN3OB(I,7)=INTEN3OB(I,7)+INTENS(I,J)
270   CONTINUE
      DO 280 J=464,584
        INTEN3OB(I,8)=INTEN3OB(I,8)+INTENS(I,J)
280   CONTINUE
      DO 290 J=585,736
        INTEN3OB(I,9)=INTEN3OB(I,9)+INTENS(I,J)
290   CONTINUE
      DO 300 J=737,927
        INTEN3OB(I,10)=INTEN3OB(I,10)+INTENS(I,J)
300   CONTINUE
      DO 310 J=928,1168
        INTEN3OB(I,11)=INTEN3OB(I,11)+INTENS(I,J)
310   CONTINUE
      DO 320 J=1169,1471
        INTEN3OB(I,12)=INTEN3OB(I,12)+INTENS(I,J)
320   CONTINUE
      DO 330 J=1472,1854
        INTEN3OB(I,13)=INTEN3OB(I,13)+INTENS(I,J)
330   CONTINUE
200 CONTINUE
C
C
C CONVERT BAND LEVELS TO SPECTRUM LEVELS
C
    DO 300 I=1,6132
          INTEN3OB(I,1)=INTEN3OB(I,1)/(182*6.2831853)
          INTEN3OB(I,2)=INTEN3OB(I,2)/(230*6.2831853)
          INTEN3OB(I,3)=INTEN3OB(I,3)/(289*6.2831853)
          INTEN3OB(I,4)=INTEN3OB(I,4)/(365*6.2831853)
          INTEN3OB(I,5)=INTEN3OB(I,5)/(459*6.2831853)
          INTEN3OB(I,6)=INTEN3OB(I,6)/(579*6.2831853)
          INTEN3OB(I,7)=INTEN3OB(I,7)/(730*6.2831853)
          INTEN3OB(I,8)=INTEN3OB(I,8)/(918*6.2831853)
          INTEN3OB(I,9)=INTEN3OB(I,9)/(1156*6.2831853)
          INTEN3OB(I,10)=INTEN3OB(I,10)/(1459*6.2831853)
          INTEN3OB(I,11)=INTEN3OB(I,11)/(1838*6.2831853)
          INTEN3OB(I,12)=INTEN3OB(I,12)/(2316*6.2831853)
          INTEN3OB(I,13)=INTEN3OB(I,13)/(2917*6.2831853)
300 CONTINUE
C
C  OUTPUT DATA TO 13 THIRD-OCTAVE BAND FILES IN A FORM SUITABLE FOR
C  2-D PLOTTING
C
    OPEN (UNIT=6, FILE='PLT3OB1.DAT',FORM ='FORMATTED',STATUS='NEW')
```

```
      DO 400 I=1,6132
        WRITE (6,2100) S(I), Z(I), INTEN3OB(I,1)
400   CONTINUE
      CLOSE (UNIT=6, STATUS='KEEP')
      OPEN (UNIT=7, FILE='PLT3OB2.DAT',FORM ='FORMATTED',STATUS='NEW')
      DO 410 I=1,6132
        WRITE (7,2100) S(I), Z(I), INTEN3OB(I,2)
410   CONTINUE
      CLOSE (UNIT=7, STATUS='KEEP')
      OPEN (UNIT=8, FILE='PLT3OB3.DAT',FORM ='FORMATTED',STATUS='NEW')
      DO 420 I=1,6132
        WRITE (8,2100) S(I), Z(I), INTEN3OB(I,3)
420   CONTINUE
      CLOSE (UNIT=8, STATUS='KEEP')
      OPEN (UNIT=9, FILE='PLT3OB4.DAT',FORM ='FORMATTED',STATUS='NEW')
      DO 430 I=1,6132
        WRITE (9,2100) S(I), Z(I), INTEN3OB(I,4)
430   CONTINUE
      CLOSE (UNIT=9, STATUS='KEEP')
      OPEN (UNIT=10,FILE='PLT3OB5.DAT',FORM ='FORMATTED',STATUS='NEW')
      DO 440 I=1,6132
        WRITE (10,2100) S(I), Z(I), INTEN3OB(I,5)
440   CONTINUE
      CLOSE (UNIT=10, STATUS='KEEP')
      OPEN (UNIT=11,FILE='PLT3OB6.DAT',FORM ='FORMATTED',STATUS='NEW')
      DO 450 I=1,6132
        WRITE (11,2100) S(I), Z(I), INTEN3OB(I,6)
450   CONTINUE
      CLOSE (UNIT=11, STATUS='KEEP')
      OPEN (UNIT=12,FILE='PLT3OB7.DAT',FORM ='FORMATTED',STATUS='NEW')
      DO 460 I=1,6132
        WRITE (12,2100) S(I), Z(I), INTEN3OB(I,7)
460   CONTINUE
      CLOSE (UNIT=12, STATUS='KEEP')
      OPEN (UNIT=13,FILE='PLT3OB8.DAT',FORM ='FORMATTED',STATUS='NEW')
      DO 470 I=1,6132
        WRITE (13,2100) S(I), Z(I), INTEN3OB(I,8)
470   CONTINUE
      CLOSE (UNIT=13, STATUS='KEEP')
      OPEN (UNIT=14,FILE='PLT3OB9.DAT',FORM ='FORMATTED',STATUS='NEW')
      DO 480 I=1,6132
        WRITE (14,2100) S(I), Z(I), INTEN3OB(I,9)
480   CONTINUE
      CLOSE (UNIT=14, STATUS='KEEP')
      OPEN (UNIT=15,FILE='PLT3OB10.DAT',FORM ='FORMATTED',STATUS='NEW')
      DO 490 I=1,6132
        WRITE (15,2100) S(I), Z(I), INTEN3OB(I,10)
490   CONTINUE
      CLOSE (UNIT=15, STATUS='KEEP')
      OPEN (UNIT=16,FILE='PLT3OB11.DAT',FORM ='FORMATTED',STATUS='NEW')
      DO 500 I=1,6132
        WRITE (16,2100) S(I), Z(I), INTEN3OB(I,11)
500   CONTINUE
      CLOSE (UNIT=16, STATUS='KEEP')
      OPEN (UNIT=17,FILE='PLT3OB12.DAT',FORM ='FORMATTED',STATUS='NEW')
      DO 510 I=1,6132
        WRITE (17,2100) S(I), Z(I), INTEN3OB(I,12)
510   CONTINUE
      CLOSE (UNIT=17, STATUS='KEEP')
      OPEN (UNIT=18,FILE='PLT3OB13.DAT',FORM ='FORMATTED',STATUS='NEW')
      DO 520 I=1,6132
        WRITE (18,2100) S(I), Z(I), INTEN3OB(I,13)
520   CONTINUE
```

```
      CLOSE (UNIT=18, STATUS='KEEP')
2100  FORMAT (1X,3G12.6)
      END
```

A.4 POWERRAD.F

```
C*************************************************************************
C
C AUTHOR:  AMY R. SMITH
C DATE: 1 MAY 1990
C PURPOSE:  THESIS WORK AT MIT
C
C PROGRAM DESCRIPTION
C  This program finds the total sound power radiated over rows 1-42
C  from the acoustic intensity spectrum included in the files
C  wt#b?.dat (where # refers to the data tape number and ? refers to the
C  appropriate third octave band number). WT#B?.DAT files consist of
C  intensity data for 21 rows.  Results are outputted to the file
C  totalpwr.dat
C
C VARIABLE DESCRIPTION
C   Z(I) IS THE MODEL AXIAL COORDINATE
C   S(I) IS THE PLOTTING ARCLENGTH
C   INTEN3OB(I) IS THE ACOUSTIC INTENSITY IN A THE Ith THIRD OCTAVE BAND
C     FOR THE DATA RECORD BEING READ.
C   SUM(I) IS THE SUM OF ACOUSTIC INTENSITIES IN WATTS PER METER SQUARED.
C   TOTAL(I) IS THE TOTAL POWER RADIATED IN WATTS.
C
C*************************************************************************
C
    REAL Z(3066), S(3066), INTEN3OB(3066), SUM(13), TOTAL(13)
C
C   SUM THE ACOUSTIC INTENSITIES IN EACH BAND, AND MULTIPLY BY THE AVERAGE
C   CELL AREA (1.0063*E-4 meters squared) TO DETERMINE POWER RADIATED.
C
C   BAND 1
C
    OPEN (UNIT =1, FILE = 'wt5b1.dat', STATUS = 'OLD',
   +     ACCESS='SEQUENTIAL', FORM='FORMATTED')
    OPEN (UNIT =2, FILE = 'wt6b1.dat', STATUS = 'OLD',
   +     ACCESS='SEQUENTIAL', FORM='FORMATTED')
    SUM(1)=0.0
    DO 10 I=1,1533
      READ (1,1000) Z(I), S(I), INTEN3OB(I)
 10  CONTINUE
    DO 20 I=1534,3066
      READ (2,1000) Z(I), S(I), INTEN3OB(I)
 20  CONTINUE
    DO 30 I=1,3066
      SUM(1)=SUM(1)+INTEN3OB(I)
 30  CONTINUE
    TOTAL(1)=SUM(1)*0.0001006260
    CLOSE (UNIT=1, STATUS='KEEP')
    CLOSE (UNIT=2, STATUS='KEEP')
C
C   BAND 2
C
    OPEN (UNIT =1, FILE = 'wt5b2.dat', STATUS = 'OLD',
   +     ACCESS='SEQUENTIAL', FORM='FORMATTED')
    OPEN (UNIT =2, FILE = 'wt6b2.dat', STATUS = 'OLD',
   +     ACCESS='SEQUENTIAL', FORM='FORMATTED')
    SUM(2)=0.0
    DO 40 I=1,1533
      READ (1,1000) Z(I), S(I), INTEN3OB(I)
 40  CONTINUE
    DO 50 I=1534,3066
      READ (2,1000) Z(I), S(I), INTEN3OB(I)
```

```
 50   CONTINUE
      DO 60 I=1,3066
        SUM(2)=SUM(2)+INTEN3OB(I)
 60   CONTINUE
      TOTAL(2)=SUM(2)*0.0001006260
      CLOSE (UNIT=1, STATUS='KEEP')
      CLOSE (UNIT=2, STATUS='KEEP')
C
C     BAND 3
C
      OPEN (UNIT =1, FILE = 'wt5b3.dat', STATUS = 'OLD',
     +      ACCESS='SEQUENTIAL', FORM='FORMATTED')
      OPEN (UNIT =2, FILE = 'wt6b3.dat', STATUS = 'OLD',
     +      ACCESS='SEQUENTIAL', FORM='FORMATTED')
      SUM(3)=0.0
      DO 70 I=1,1533
        READ (1,1000) Z(I), S(I), INTEN3OB(I)
 70   CONTINUE
      DO 80 I=1534,3066
        READ (2,1000) Z(I), S(I), INTEN3OB(I)
 80   CONTINUE
      DO 90 I=1,3066
        SUM(3)=SUM(3)+INTEN3OB(I)
 90   CONTINUE
      TOTAL(3)=SUM(3)*0.0001006260
      CLOSE (UNIT=1, STATUS='KEEP')
      CLOSE (UNIT=2, STATUS='KEEP')
C
C     BAND 4
C
      OPEN (UNIT =1, FILE = 'wt5b4.dat', STATUS = 'OLD',
     +      ACCESS='SEQUENTIAL', FORM='FORMATTED')
      OPEN (UNIT =2, FILE = 'wt6b4.dat', STATUS = 'OLD',
     +      ACCESS='SEQUENTIAL', FORM='FORMATTED')
      SUM(4)=0.0
      DO 100 I=1,1533
        READ (1,1000) Z(I), S(I), INTEN3OB(I)
 100  CONTINUE
      DO 110 I=1534,3066
        READ (2,1000) Z(I), S(I), INTEN3OB(I)
 110  CONTINUE
      DO 120 I=1,3066
        SUM(4)=SUM(4)+INTEN3OB(I)
 120  CONTINUE
      TOTAL(4)=SUM(4)*0.0001006260
      CLOSE (UNIT=1, STATUS='KEEP')
      CLOSE (UNIT=2, STATUS='KEEP')
C
C     BAND 5
C
      OPEN (UNIT =1, FILE = 'wt5b5.dat', STATUS = 'OLD',
     +      ACCESS='SEQUENTIAL', FORM='FORMATTED')
      OPEN (UNIT =2, FILE = 'wt6b5.dat', STATUS = 'OLD',
     +      ACCESS='SEQUENTIAL', FORM='FORMATTED')
      SUM(5)=0.0
      DO 130 I=1,1533
        READ (1,1000) Z(I), S(I), INTEN3OB(I)
 130  CONTINUE
      DO 140 I=1534,3066
        READ (2,1000) Z(I), S(I), INTEN3OB(I)
 140  CONTINUE
      DO 150 I=1,3066
        SUM(5)=SUM(5)+INTEN3OB(I)
 150  CONTINUE
```

```
      TOTAL(5)=SUM(5)*0.0001006260
      CLOSE (UNIT=1, STATUS='KEEP')
      CLOSE (UNIT=2, STATUS='KEEP')
C
C     BAND 6
C
      OPEN (UNIT =1, FILE = 'wt5b6.dat', STATUS = 'OLD',
     +      ACCESS='SEQUENTIAL', FORM='FORMATTED')
      OPEN (UNIT =2, FILE = 'wt6b6.dat', STATUS = 'OLD',
     +      ACCESS='SEQUENTIAL', FORM='FORMATTED')
      SUM(6)=0.0
      DO 160 I=1,1533
        READ (1,1000) Z(I), S(I), INTEN3OB(I)
  160 CONTINUE
      DO 170 I=1534,3066
        READ (2,1000) Z(I), S(I), INTEN3OB(I)
  170 CONTINUE
      DO 180 I=1,3066
        SUM(6)=SUM(6)+INTEN3OB(I)
  180 CONTINUE
      TOTAL(6)=SUM(6)*0.0001006260
      CLOSE (UNIT=1, STATUS='KEEP')
      CLOSE (UNIT=2, STATUS='KEEP')
C
C     BAND 7
C
      OPEN (UNIT =1, FILE = 'wt5b7.dat', STATUS = 'OLD',
     +      ACCESS='SEQUENTIAL', FORM='FORMATTED')
      OPEN (UNIT =2, FILE = 'wt6b7.dat', STATUS = 'OLD',
     +      ACCESS='SEQUENTIAL', FORM='FORMATTED')
      SUM(7)=0.0
      DO 190 I=1,1533
        READ (1,1000) Z(I), S(I), INTEN3OB(I)
  190 CONTINUE
      DO 200 I=1534,3066
        READ (2,1000) Z(I), S(I), INTEN3OB(I)
  200 CONTINUE
      DO 210 I=1,3066
        SUM(7)=SUM(7)+INTEN3OB(I)
  210 CONTINUE
      TOTAL(7)=SUM(7)*0.0001006260
      CLOSE (UNIT=1, STATUS='KEEP')
      CLOSE (UNIT=2, STATUS='KEEP')
C
C     BAND 8
C
      OPEN (UNIT =1, FILE = 'wt5b8.dat', STATUS = 'OLD',
     +      ACCESS='SEQUENTIAL', FORM='FORMATTED')
      OPEN (UNIT =2, FILE = 'wt6b8.dat', STATUS = 'OLD',
     +      ACCESS='SEQUENTIAL', FORM='FORMATTED')
      SUM(8)=0.0
      DO 220 I=1,1533
        READ (1,1000) Z(I), S(I), INTEN3OB(I)
  220 CONTINUE
      DO 230 I=1534,3066
        READ (2,1000) Z(I), S(I), INTEN3OB(I)
  230 CONTINUE
      DO 240 I=1,3066
        SUM(8)=SUM(8)+INTEN3OB(I)
  240 CONTINUE
      TOTAL(8)=SUM(8)*0.0001006260
      CLOSE (UNIT=1, STATUS='KEEP')
      CLOSE (UNIT=2, STATUS='KEEP')
C
```

```
C   BAND 9
C
    OPEN (UNIT =1, FILE = 'wt5b9.dat', STATUS = 'OLD',
   +      ACCESS='SEQUENTIAL', FORM='FORMATTED')
    OPEN (UNIT =2, FILE = 'wt6b9.dat', STATUS = 'OLD',
   +      ACCESS='SEQUENTIAL', FORM='FORMATTED')
    SUM(9)=0.0
    DO 250 I=1,1533
      READ (1,1000) Z(I), S(I), INTEN3OB(I)
250   CONTINUE
    DO 260 I=1534,3066
      READ (2,1000) Z(I), S(I), INTEN3OB(I)
260   CONTINUE
    DO 270 I=1,3066
      SUM(9)=SUM(9)+INTEN3OB(I)
270   CONTINUE
    TOTAL(9)=SUM(9)*0.0001006260
    CLOSE (UNIT=1, STATUS='KEEP')
    CLOSE (UNIT=2, STATUS='KEEP')
C
C   BAND 10
C
    OPEN (UNIT =1, FILE = 'wt5b10.dat', STATUS = 'OLD',
   +      ACCESS='SEQUENTIAL', FORM='FORMATTED')
    OPEN (UNIT =2, FILE = 'wt6b10.dat', STATUS = 'OLD',
   +      ACCESS='SEQUENTIAL', FORM='FORMATTED')
    SUM(10)=0.0
    DO 280 I=1,1533
      READ (1,1000) Z(I), S(I), INTEN3OB(I)
280   CONTINUE
    DO 290 I=1534,3066
      READ (2,1000) Z(I), S(I), INTEN3OB(I)
290   CONTINUE
    DO 300 I=1,3066
      SUM(10)=SUM(10)+INTEN3OB(I)
300  CONTINUE
    TOTAL(10)=SUM(10)*0.0001006260
    CLOSE (UNIT=1, STATUS='KEEP')
    CLOSE (UNIT=2, STATUS='KEEP')
C
C   BAND 11
C
    OPEN (UNIT =1, FILE = 'wt5b11.dat', STATUS = 'OLD',
   +      ACCESS='SEQUENTIAL', FORM='FORMATTED')
    OPEN (UNIT =2, FILE = 'wt6b11.dat', STATUS = 'OLD',
   +      ACCESS='SEQUENTIAL', FORM='FORMATTED')
    SUM(11)=0.0
    DO 310 I=1,1533
      READ (1,1000) Z(I), S(I), INTEN3OB(I)
310   CONTINUE
    DO 320 I=1534,3066
      READ (2,1000) Z(I), S(I), INTEN3OB(I)
320   CONTINUE
    DO 330 I=1,3066
      SUM(11)=SUM(11)+INTEN3OB(I)
330   CONTINUE
    TOTAL(11)=SUM(11)*0.0001006260
    CLOSE (UNIT=1, STATUS='KEEP')
    CLOSE (UNIT=2, STATUS='KEEP')
C
C   BAND 12
C
    OPEN (UNIT =1, FILE = 'wt5b12.dat', STATUS = 'OLD',
   +      ACCESS='SEQUENTIAL', FORM='FORMATTED')
```

```
      OPEN (UNIT =2, FILE = 'wt6b12.dat', STATUS = 'OLD',
     +     ACCESS='SEQUENTIAL', FORM='FORMATTED')
      SUM(12)=0.0
      DO 340 I=1,1533
        READ (1,1000) Z(I), S(I), INTEN3OB(I)
  340 CONTINUE
      DO 350 I=1534,3066
        READ (2,1000) Z(I), S(I), INTEN3OB(I)
  350 CONTINUE
      DO 360 I=1,3066
        SUM(12)=SUM(12)+INTEN3OB(I)
  360 CONTINUE
      TOTAL(12)=SUM(12)*0.000001006260
      CLOSE (UNIT=1, STATUS='KEEP')
      CLOSE (UNIT=2, STATUS='KEEP')
C
C   BAND 13
C
      OPEN (UNIT =1, FILE = 'wt5b13.dat', STATUS = 'OLD',
     +     ACCESS='SEQUENTIAL', FORM='FORMATTED')
      OPEN (UNIT =2, FILE = 'wt6b13.dat', STATUS = 'OLD',
     +     ACCESS='SEQUENTIAL', FORM='FORMATTED')
      SUM(13)=0.0
      DO 370 I=1,1533
        READ (1,1000) Z(I), S(I), INTEN3OB(I)
  370 CONTINUE
      DO 380 I=1534,3066
        READ (2,1000) Z(I), S(I), INTEN3OB(I)
  380 CONTINUE
      DO 390 I=1,3066
        SUM(13)=SUM(13)+INTEN3OB(I)
  390 CONTINUE
      TOTAL(13)=SUM(13)*0.000001006260
      CLOSE (UNIT=1, STATUS='KEEP')
      CLOSE (UNIT=2, STATUS='KEEP')
 1000 FORMAT (1X,3G12.6)
C
C   OUTPUT DATA
C
      OPEN (UNIT=3, FILE='totalpwr.dat', FORM='FORMATTED',
     +     STATUS='NEW')
      WRITE (3,2000)
      DO 2100 I=1,13
        WRITE (3,2200) I, TOTAL(I)
 2100 CONTINUE
 2000 FORMAT ('TANK CONDITION FULL: TAPES 5 AND 6; ROWS 1-42')
 2200 FORMAT (3X,'POWER RADIATED BAND ',I2,' IS ', G12.6,'WATTS.')
      CLOSE (UNIT=3, STATUS='KEEP')
      END
```

APPENDIX B
PROGRAM VERIFICATION

This Appendix illustrates the checks used to verify the programming algorithms in Appendix A. It lists a portion of the complex pressure data for the inner and outer planes of circumferential row one from frequency bin 1966 for the tank empty condition. Bin 1966 corresponds to 15 kHz. It then lists the acoustic intensity as calculated by a spreadsheet program and the acoustic intensity as computed by the program PROCESS.F in Appendix A. As can be seen by the intensities tablulated in Table B.1, these independent procedures provided the same results.

Intensity calculations are based on equation 2.8:

$$I_r \approx \frac{1}{2\omega\rho_o\Delta r}\mathrm{Im}[p_1 p_2^*]$$

For frequency bin 1966 and the experimental conditions described in the body of the thesis, the following values apply:

ω=94,243.5 rad/sec
ρ_o=983.75 kg/m^3
Δr=0.006 meters

These values were used in the spreadsheet calculations to compute acoustic intensity. The units for pressure are Pascals. The units for acoustic intensity are Watts/m^2.

As another check on the data, the acoustic intensity magnitude for a freefield plane wave is calculated. This intensity is based on the approximation [15]:

$$I = \frac{<p^2>}{\rho_o c}$$

and is expected to be slightly greater than the "actual" nearfield value computed. For the plane wave intensities presented in Table B.1, $<p^2>$ is based on the average pressure at the midplane (from equation 2.5):

$$p \approx \frac{1}{2}(p_1 + p_2)$$

Again, the other values are based on the experimental conditions:

ρ_o=983.75 kg/m^3

c = 1475 m/sec (Tank water at 17.9°C)

Table B.1 Program Verification Data

Z	Inner plane		Outer Plane		Calculated Intensity	Computed Intensity	Plane Wave Intensity
	Real P1	Imag P1	Real P2	Imag P2			
-36.00	-13.2321	-1.67449	-12.8799	-4.54199	-3.4635E-05	-3.4635E-05	1.2408E-04
-35.00	-14.1635	-0.04722	-10.5686	-5.85801	-7.4128E-05	-7.4128E-05	1.1135E-04
-34.00	-9.25365	-3.14129	-8.78924	-4.72049	-1.4446E-05	-1.4446E-05	6.6710E-05
-33.00	-3.80159	-4.93322	-3.27868	-4.90039	-2.2065E-06	-2.2065E-06	2.5287E-05
-32.00	0.61027	-5.24253	3.3911	-7.46611	-1.1884E-05	-1.1884E-05	3.0572E-05
-31.00	5.76668	-5.55313	6.08846	-5.98311	6.2260E-07	6.2255E-07	4.7124E-05
-30.00	6.72051	-4.65721	6.77444	-4.2906	-2.4403E-06	-2.4403E-06	4.5152E-05
-29.00	7.45589	-3.22586	9.41027	-4.04148	-2.0078E-07	-2.0074E-07	5.8086E-05
-28.00	5.68809	-3.97036	7.9568	-2.46212	-1.5807E-05	-1.5808E-05	3.9190E-05
-27.00	4.59266	-2.98953	5.5902	-2.52509	-4.5977E-06	-4.5977E-06	2.3095E-05
-26.00	3.98743	-3.92129	2.76533	-1.55915	-4.1586E-06	-4.1586E-06	1.3026E-05
-25.00	0.646823	-7.35229	2.6479	-4.59799	-1.4825E-05	-1.4825E-05	2.6464E-05

Table B.1 Program Verification Data Continued

Z	Inner plane		Outer Plane		Calculated	Computed	Plane Wave
	Real P1	Imag P1	Real P2	Imag P2	Intensity	Intensity	Intensity
-24.00	0.986519	-8.88323	4.24174	-6.19663	-2.8374E-05	-2.8374E-05	4.3870E-05
-23.00	2.52886	-6.38308	2.41966	-5.02579	-2.4586E-06	-2.4586E-06	2.6634E-05
-22.00	0.367171	-1.54735	1.9656	-2.43877	-1.9289E-06	-1.9289E-06	3.6736E-06
-21.00	-1.15236	-5.16369	-0.34690	-4.79081	-3.3522E-06	-3.3522E-06	1.7453E-05
-20.00	-2.21889	-2.03787	1.43416	-5.85272	-1.4300E-05	-1.4300E-05	1.0829E-05
-19.00	-3.10151	-3.92611	-1.8865	-3.16814	-2.1747E-06	-2.1747E-06	1.2952E-05
-18.00	-2.6115	-5.19605	-0.87340	-5.54765	-8.9429E-06	-8.9429E-06	2.1970E-05
-17.00	-0.94645	-6.35722	-0.47048	-6.98676	-3.2553E-06	-3.2553E-06	3.1011E-05
-16.00	-0.75002	-4.2347	-0.28433	-3.86173	-1.5211E-06	-1.5211E-06	1.1474E-05
-15.00	-0.94378	-1.99392	-1.57381	-5.565	-1.9003E-06	-1.9003E-06	1.0932E-05
-14.00	-1.02827	2.23194	0.882804	-3.41634	-1.3865E-06	-1.3865E-06	2.4523E-07
-13.00	-1.49523	1.39493	1.59873	0.194197	2.2655E-06	2.2655E-06	4.3675E-07

Table B.1 Program Verification Data Continued

Z	Inner plane		Outer Plane		Calculated Intensity	Computed Intensity	Plane Wave Intensity
	Real P1	Imag P1	Real P2	Imag P2			
-12.00	-1.24133	1.2866	0.356446	-1.11782	-8.3500E-07	-8.3500E-07	1.3976E-07
-11.00	-1.42648	1.5399	-1.61549	1.15045	-7.6095E-07	-7.6095E-07	2.8402E-06
-10.00	-3.02889	-0.00695	-1.33535	0.363528	9.9804E-07	9.9804E-07	3.3021E-06
-9.00	-2.55371	1.79068	-2.11305	2.26957	1.8085E-06	1.8085E-06	6.5898E-06
-8.00	-1.32671	5.42179	-1.11252	1.52115	-3.6077E-06	-3.6077E-06	9.3264E-06
-7.00	-1.26725	5.19918	0.54076	4.09478	7.1912E-06	7.1913E-06	1.4967E-05
-6.00	-0.37235	2.50327	-1.9732	1.5631	-3.9166E-06	-3.9166E-06	3.7952E-06
-5.00	-1.57778	1.76413	-0.30823	4.69163	6.1648E-06	6.1648E-06	7.7901E-06
-4.00	-1.63597	3.97665	-1.8627	0.14768	-6.4408E-06	-6.4408E-06	5.0375E-06
-3.00	-3.11906	3.30855	-1.03778	-0.90136	-5.6132E-06	-5.6132E-06	3.9738E-06
-2.00	-0.86323	1.10139	-3.60938	-0.27443	-3.7861E-06	-3.7861E-06	3.5629E-06
-1.00	-3.45573	-2.97146	-3.00454	1.63439	1.3101E-05	1.3101E-05	7.4955E-06
0.00	-2.5483	-0.88316	-2.21477	-3.01414	-5.1458E-06	-5.1458E-06	6.5229E-06